2012

Center-of-gravity estimation of an aircraft solely using traditional aircraft measurement sensors

Andrew Komendat

Center-of-Gravity Estimation of an Aircraft Solely Using Traditional Aircraft Measurement Sensors

by

Andrew J. Komendat

Thesis submitted to the Faculty of the Rochester Institute of Technology in partial fulfillment of the requirements for the degree of

Master of Science

in Mechanical Engineering

Approved by:

_____

Dr. Agamemnon Crassidis
Thesis Adviser, Advisory Committee, Department of Mechanical Engineering

_____

Dr. Jason Kolodziej
Advisory Committee, Department of Mechanical Engineering

_____

Dr. Wayne Walter
Advisory Committee, Department of Mechanical Engineering

_____

Dr. Edward Hensel
Department Head, Department Rep, Department of Mechanical Engineering

ACKNOWLEDGMENTS

I would like to thank the faculty and staff members of the Mechanical Engineering Department at the Rochester Institute of Technology. Their desire to challenge and inspire their students has taught me everything I know. In particular I'd like to thank my adviser Dr. Agamemnon for his patience and guidance throughout this endeavor, as well as committee members Dr. Jason Kolodziej, Dr. Wayne Walter, and Dr. Edward Hensel for their continued support. Most importantly I'd like to thank my family and friends for shaping me into the person I am today. Without their unwavering love and care I would most certainly not have come this far. May the unknown of the future match the joys of past and present.

"A person who never made a mistake never tried anything new."

-Albert Einstein

ABSTRACT

Center-of-Gravity Estimation of an Aircraft Solely Using Standard Aircraft Measurement Sensors

Andrew J. Komendat

Supervising Professor: Dr. Agamemnon Crassidis

In this work, a novel algorithm for estimating aircraft center-of-gravity location based solely on traditional aircraft measurements is investigated. The algorithm uses known physics-based kinematic relationships between aircraft states for the estimation process and requires only traditional sensor measurements typically employed by aircraft. Three models are used in the algorithm development: one based on using attitude measurements, the second based on using air data measurements, and the third based on using navigation type measurements. Estimation of the aircraft's aerodynamic parameters is not required in the new approach. However, sensor error such as accelerometer bias effects are estimated in the algorithm process. A high performance aircraft simulation model is used to test the feasibility of the approach. In all individual and combined model simulations center-of-gravity was estimated with a high degree of accuracy. In addition, flight test data is used to verify the effectiveness of the algorithm in localizing the center-of-gravity successfully.

Table of Contents

LIST OF TABLES

LIST OF FIGURES

NOMENCLATURE

X, Y, Z	:	Primary, Secondary, and Tertiary Earth-Fixed Coordinate System Axis
i, **j**, **k**	:	Primary, Secondary, and Tertiary Earth-Fixed Unit Vectors
ϕ, θ, ψ	:	Bank, Elevation and Heading Euler Angles
p, q, r	:	Roll, Pitch, and Yaw Angular Rates
u, v, w	:	Primary, Secondary, and Tertiary Body-Fixed Velocities
$\boldsymbol{\omega}$	:	Vehicle Angular Velocity Vector
$\boldsymbol{\alpha}$	:	Vehicle Angular Acceleration Vector
m	:	Vehicle Mass
s	:	Vehicle Position Vector
v	:	Vehicle Velocity Vector
a	:	Vehicle Acceleration Vector
j	:	Vehicle Jerk Vector
GPS	:	Global Positioning System
INS	:	Inertial Navigation System
CG	:	Center-of-Gravity
α	:	Angle-of-Attack
β	:	Sideslip Angle
V	:	Total Velocity
g	:	Acceleration Due to Gravity (9.81 m/s^2)
n_x, n_y, n_z	:	Primary, Secondary, and Tertiary Acceleration Components (in gee's)
F_x, F_y, F_z	:	Primary, Secondary, and Tertiary Force Components
x_b, y_b, z_b	:	Primary, Secondary, and Tertiary Body-Fixed Coordinate System Axis
L, M, N	:	Primary, Secondary, and Tertiary Moments
H	:	Angular Momentum Vector
r	:	Center-of-Gravity Location Offset Vector
I	:	Mass Moment of Inertia Matrix
$\mathbf{v}_c$	:	Velocity of the Center-of-Gravity Vector
$\mathbf{a}_c$	:	Acceleration of the Center-of-Gravity Vector

CHAPTER 1: INTRODUCTION

1.1: BACKGROUND

Accurate estimates of center-of-gravity are critical in aircraft operation to ensure the safety of passengers and efficient aircraft use. Center-of-gravity location vastly affects aircraft stability and effectiveness of overall aircraft control. Poor loading of an airframe can result in uncontrollable or undesired maneuverability of an aircraft. Estimates of center-of-gravity are also utilized in airframe fatigue calculations. Current approaches rely on manually recording alterations to vehicle's loading factors. In many cases assumptions are required for fuel vehicle burn curves as well. The task is typically time-consuming, laborious and inaccurate yielding highly conservative estimates for stress factors. Also, errors are highly problematic for human based estimates and therefore often require redundancy further complicating the process. Improved estimates allow for the relaxation of such conservative estimates and lengthen the life of the vehicle. Center-of-gravity shifts regularly occur in flight based of movement of passengers, fuel burn, deployment of cargo or weapons, undesired shifting of luggage, etc. As such, there's a need to estimate center-of-gravity location throughout the entire flight regime to ensure significant changes are not seen in center-of-gravity location.

Current methods utilized for center-of-gravity estimation in flight are focused around development of a highly detailed aircraft model.[1-3] These models become extremely complicated and require steady level flight to achieve accuracy. Conventional aircraft inputs such as flight surface orientations as well as atmospheric conditions are incorporated in the model. Development of this is quite costly requiring extensive testing time and data storage, and does not account for extreme or unpredictable changes in aerodynamics that may occur. Rarely in flight are truly trim and level flight conditions observed for a period of time given turbulence and autopilot corrections. Overall this approach introduces unnecessary cost and uncertainty to a critical aircraft parameter.

Another common approach used in flight operation involves manual calculations and fuel burn curves. The manual uses weighted averages of vehicle components to locate center-of-gravity accounting for cargo distribution.[4] However, significant uncertainty and conservatism introduce the opportunity for and the likely occurrence of human error. Changes in center-of-gravity location in flight based on cargo shifting or deployment are more difficult to account for and require additional efforts during each flight from ground or aircraft crew.

1.2: Innovation and Motivation for Current Work

In the technology available for aircraft operation an opportunity was observed. The study performed here focuses on the development of a physics-based approach to in flight center-of-gravity estimation. The proposed algorithm exploits known rigid body dynamics relationships with commonly available sensors and measurements to estimate center-of-gravity. The concept is not dependent on the type of rigid body involved and would theoretically estimate center-of-gravity location for any type of rigid body aircraft motion. The algorithm proposed uses an optimization approach for translation of accelerometer measurements at a known sensor location on the body to an estimated location and compares them to nominal expected conditions observed at the center-of-gravity of the aircraft. Other available sensors such as attitude estimates, GPS or INS information, or air data measurements can be the source of comparison in the optimization approach.

The advantage of the innovative technology for center-of-gravity estimation is the purely dynamics and physics-based approach. Estimates are theoretically independent of all aerodynamics or forcing on the vehicle and can generate and improve autonomously. The automatic approach removes the opportunity for human error found in manual calculation approaches and removes the necessity for expensive models and can provide near real-time estimates of center-of-gravity in the dynamic aircraft world. Thought must be given to the accuracy of measurements obtained and the conditions encountered by the vehicle during the flight regime.

The most significant requirements or limitation for the algorithm includes the necessity for the body to be rigid, a constant center-of-gravity location across the period of information collection, and the existence of dynamic conditions. Relationships for accelerometer transformations to estimated center-of-gravity locations can only be utilized if the body is truly rigid, particularly between the center-of-gravity and sensor locations. Relative motion or flexure between the two locations will introduce accelerations to sensors that are not representative of the body as a whole. A significant shift in center-of-gravity location throughout the estimation collection period will result in different aircraft reactions to forcing. The estimation routine can only be incorporated if the body reacted identically to rotational effects throughout the data collection period. Finally, during the collection period rotation effects must be observed in a three dimensional level. The algorithm is based on rotational effects inherent to rotations about the center-of-gravity as well as translational accelerations. If no accelerations due to rotational effects are observed, acceleration conditions will be identical at all points on the rigid body and optimization of the center-of-gravity location cannot be performed. However, this can only occur for completely steady-state flight in which case the center-of-gravity location is not

necessarily needed. Any perturbation from this point would require pilot input and introduce dynamic conditions to the system.

The advantages of the approach outlined will be demonstrated in a simulation environment using an aircraft simulation sensor collection and true measurements from previous aircraft operation. Simulink® and Matlab® will be the software programs of choice to incorporate simulations and flight data, including the introduction of realistic sensor biases and noise where applicable. The performance of the technology developed will be shown as follows:

1. Design and implementation of three models (Attitude Model, Air Data Model, and GPS and INS Model) used in the algorithm for center-of-gravity estimation using perfect sensor measurements and derivatives available from the aircraft simulation.
2. Incorporate and address commonly observed biases and noise associated with available sensors.
3. Demonstrate performance of each algorithm in an array of aircraft flight conditions, assessing the performance of the technology at varying conditions.
4. Analyze and quantify the effectiveness of the center-of-gravity estimation algorithm.

CHAPTER 2: SENSOR CONSISTENCY

2.1: COORDINATE SYSTEM DEFINITION

A number of coordinate systems are available and commonly used to describe the orientation and other parameters of an aircraft. The primary coordinate system of interest for studies described here is the body-fixed coordinate system. The body-fixed coordinate frame is fixed to and rotates with the aircraft body. The x-axis, defined as x_b, is taken positive forward through the front of the vehicle, the y-axis, defined y_b, is taken positive out the right wing of the vehicle, and the z-axis, defined as z_b, is taken as positive downwards through the bottom of the aircraft. The orientation of the body-fixed coordinate system is depicted in Fig. 1.

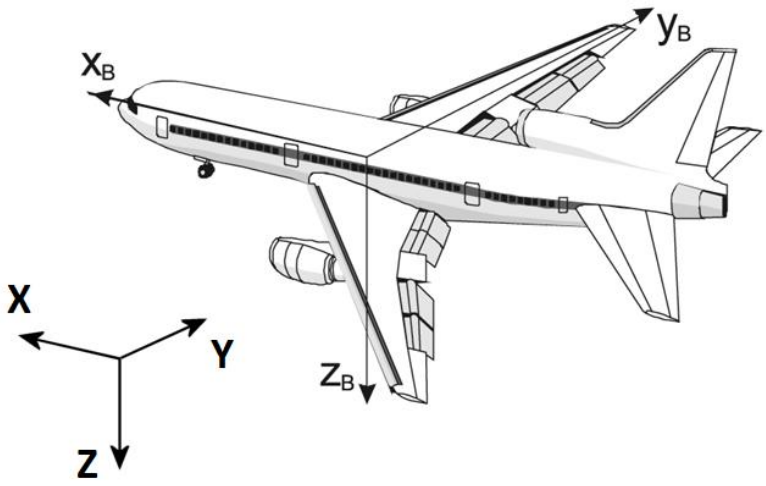

FIGURE 1: AIRCRAFT COORDINATE SYSTEM

To associate the motion of the vehicle to positioning with respect to Earth, a secondary coordinate system must be defined; the Earth-fixed coordinate system. The Earth-fixed coordinate system uses the "flat Earth" assumption and assumes the Earth is fixed. The Earth-fixed coordinate system is also shown in Fig. 1. The x-axis is defined as X is true North, the y-axis is defined as Y points due East, and the z-axis is defined as Z points inward toward the center of the Earth.[5]

2.2: PARAMETER DEFINITION

The association between orientation of the body-fixed coordinate system and Earth-fixed coordinate system can be observed through the use of Euler angles. Euler angles are described as angular rotations about the Earth-fixed coordinate system to achieve orientation of the body-fixed system. Rotations about the x-axis, defined as ϕ, indicate roll, about the y-axis,

defined as θ, indicate pitch, and about the z-axis, defined as ψ, indicate yaw. Table 1 summarizes the notation incorporated in this report with respect to the coordinate system of reference for position, velocity, acceleration, jerk, angle, and angular rate.[5]

	Primary Axis		Secondary Axis		Tertiary Axis	
	Earth	Body	Earth	Body	Earth	Body
Designation	X_E	X_b	Y_E	Y_b	Z_E	Z_b
Position	S_x	s_x	S_y	s_y	S_z	s_z
Velocity	V_x	u	V_y	v	V_z	w
Acceleration	A_x	a_x	A_y	a_y	A_z	a_z
Jerk	J_x	j_x	J_y	j_y	J_z	j_z
Angle	ϕ_E	ϕ_b	θ_E	θ_b	ψ_E	ψ_b
Angular Rate	$\dot{\phi}$	p	$\dot{\theta}$	q	$\dot{\psi}$	r

TABLE 1: PARAMETER COORDINATE NOTATION

2.3: EULER MODEL

The first step in data processing for the measurements required involves determination of truth signals. The most difficult signals to incorporate, particularly when derivatives and integrals are required, are rotational rates and aircraft attitude measurements. Issues involving the use of rotational measurements are solved using the Euler Model.

The order in which rotations are applied to the vehicle affects the final orientation of the aircraft; hence a rotation convention must be maintained when using Euler angles. The conventional 3-2-1 order for aircraft will be used. To relate the body-fixed coordinate system to the Earth-fixed coordinate system the axes start in the same orientation and are first rotated by ψ about the z-axis. The second rotation is about the y-axis by θ. Finally, the third rotation is by ϕ about the x-axis.[5] This is demonstrated by Fig. 2. Such a correlation is required to track position and velocity of the body in an Earth-fixed reference frame.

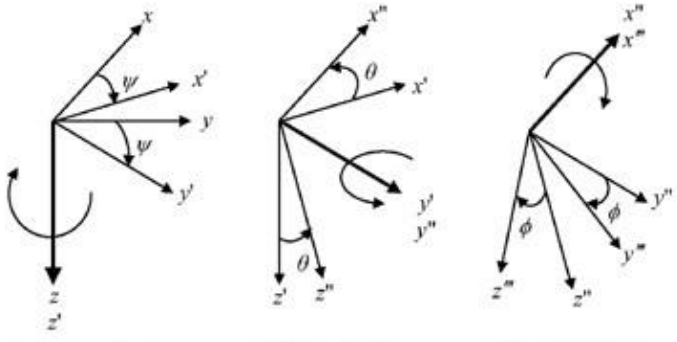

FIGURE 2: EULER ROTATION ORDER

This definition can be used to translate velocities in the body-fixed frame to the Earth-fixed frame and vice versa. Using the Euler angles and components in each direction, relationships between the reference frames based on pure orientation can be obtained. Equation 1 through Eq. 3 show intermediate relationships of the rotation process, resulting in the final relationship shown in Eq. 4.[5] To simplify the expressions, $\sin\theta$ will be represented by S_θ and $\cos\theta$ represented by C_θ.

$$\frac{dx}{dt} = u_1 C_\psi - v_1 S_\psi \tag{1}$$

$$\frac{dy}{dt} = u_1 S_\psi + v_1 C_\psi$$

$$\frac{dz}{dt} = w_1$$

$$u_1 = u_2 C_\theta + w_2 S_\theta \tag{2}$$

$$v_1 = v_2$$

$$w_1 = -u_2 S_\theta + w_2 C_\theta$$

$$u_2 = u \tag{3}$$

$$v_2 = v C_\phi - w S_\phi$$

$$w_2 = v S_\phi + w C_\phi$$

$$\begin{bmatrix} \frac{dx}{dt} \\ \frac{dy}{dt} \\ \frac{dz}{dt} \end{bmatrix} = \begin{bmatrix} C_\psi C_\theta & -S_\psi C_\phi + C_\psi S_\theta S_\phi & S_\psi S_\phi + C_\psi S_\theta C_\phi \\ S_\psi C_\theta & C_\psi C_\phi + S_\psi S_\theta S_\phi & -C_\psi S_\phi + S_\psi S_\theta C_\phi \\ -S_\theta & C_\theta S_\phi & C_\theta C_\phi \end{bmatrix} \begin{bmatrix} u \\ v \\ w \end{bmatrix} \tag{4}$$

Integration of the Earth-fixed reference frame velocities results in position in the Earth fixed frame. The relationship derived can be used in conjunction with GPS and INS devices. Additionally, using the rotation convention described, a relationship of Euler rotational rates to body rotational rates can be obtained. Equation 5 and Eq. 6 below describe the transformation states from body rotational rates to Euler rotational rates. Integration of the Euler derivatives

results in calculation of the Euler angles which can be used to minimize and eliminate biases and errors in measurements of attitude estimation devices.

$$\begin{bmatrix} p \\ q \\ r \end{bmatrix} = \begin{bmatrix} 1 & 0 & -S_\theta \\ 0 & C_\phi & C_\theta S_\phi \\ 0 & -S_\phi & C_\theta C_\phi \end{bmatrix} \begin{bmatrix} \dot{\phi} \\ \dot{\theta} \\ \dot{\psi} \end{bmatrix} \tag{5}$$

$$\begin{bmatrix} \dot{\phi} \\ \dot{\theta} \\ \dot{\psi} \end{bmatrix} = \begin{bmatrix} 1 & S_\phi \tan\theta & C_\phi \tan\theta \\ 0 & C_\phi & -S_\phi \\ 0 & S_\phi \sec\theta & C_\phi \sec\theta \end{bmatrix} \begin{bmatrix} p \\ q \\ r \end{bmatrix} \tag{6}$$

The Euler Model checks the consistency of the pitch rate, roll rate, yaw rate, pitch angle, and bank angle measurements (although it is not required, heading angle measurements may also be checked). The Euler Model is also used to determine state initial conditions, sensors biases, and sensor scale factors for the aircraft's pitch rate, roll rate, yaw rate, pitch angle, and bank angle sensors.

A detailed description of the Euler Model is given by Eq. 6 through Eq. 8. The model consists of three components: an initial condition model described by Eq. 7, a dynamical system state component described by Eq. 6, and an output measurement model described by Eq. 8. The output measurement model is compared to the flight data measurement to form the minimization cost function value. The subscripts $(\ )_m$ are the aircraft measured responses, $(\ )_z$ are the computed output responses, $(\ )_b$ are the measurement biases, and $(\ )_0$ are the state initial conditions. Aircraft angular acceleration measurements ($\dot{p}$, $\dot{q}$, and $\dot{r}$) are the forcing input to the Euler Model and are required. If these measurements are not available, they may be generated by using a forward/backward derivative type filter (ex. Butterworth filter).[6]

$$
\begin{aligned}
p(0) = {} & [p_m(0) - p_b + p_0]\cos(\theta_p)\cos(\psi_p) \\
& + [q_m(0) - q_b + q_0]\cos(\theta_p)\sin(\psi_p) \\
& - [r_m(0) - r_b + r_0]\sin(\theta_p)
\end{aligned} \tag{7}
$$

$$
\begin{aligned}
q(0) = {} & [p_m(0) - p_b + p_0](\cos(\psi_q)\sin(\theta_q)\sin(\phi_q) \\
& - \sin(\psi_q)\cos(\phi_q)) \\
& + [q_m(0) - q_b + q_0](\sin(\psi_q)\sin(\theta_q)\sin(\phi_q) \\
& + \cos(\psi_q)\cos(\phi_q)) \\
& + [r_m(0) - r_b + r_0]\sin(\phi_q)\cos(\theta_q)
\end{aligned}
$$

$$
\begin{aligned}
p(0) = {} & [p_m(0) - p_b + p_0](\cos(\psi_r)\sin(\theta_r)\cos(\phi_r) \\
& + \sin(\psi_r)\sin(\phi_r)) \\
& + [q_m(0) - q_b + q_0](\sin(\psi_r)\sin(\theta_r)\cos(\phi_r) \\
& - \cos(\psi_r)\sin(\phi_r)) \\
& + [r_m(0) - r_b + r_0]\cos(\phi_r)\cos(\theta_r)
\end{aligned}
$$

$$\theta(0) = \theta_m(0) - \theta_b + \theta_0$$

$$\phi(0) = \phi_m(0) - \phi_b + \phi_0$$

$$\psi(0) = \psi_m(0) - \psi_b + \psi_0$$

$$
\begin{aligned}
p_z = {} & [p + p_b]\cos(\theta_p)\cos(\psi_p) + [q + q_b]\cos(\theta_p)\sin(\psi_p) \\
& - [r + r_b]\sin(\theta_p)
\end{aligned} \tag{8}
$$

$$
\begin{aligned}
q_z = {} & [p + p_b](\cos(\psi_q)\sin(\theta_q)\sin(\phi_q) - \sin(\psi_q)\cos(\phi_q)) \\
& + [q + q_b](\sin(\psi_q)\sin(\theta_q)\sin(\phi_q) \\
& + \cos(\psi_q)\cos(\phi_q)) + [r + r_b]\sin(\phi_q)\cos(\theta_q)
\end{aligned}
$$

$$
\begin{aligned}
r_z = {} & [p + p_b](\cos(\psi_r)\sin(\theta_r)\cos(\phi_r) + \sin(\psi_r)\sin(\phi_r)) \\
& + [q + q_b](\sin(\psi_r)\sin(\theta_r)\cos(\phi_r) \\
& - \cos(\psi_r)\sin(\phi_r)) + [r + r_b]\cos(\phi_r)\cos(\theta_r)
\end{aligned}
$$

$$\theta_z = \theta + \theta_b$$

$$\phi_z = \phi + \phi_b$$

$$\psi_z = \psi + \psi_b$$

Here the variables $\phi_i, \theta_i, \psi_i \} \quad i = p, q, r$ are the rate gyro sensor instrument misalignment Euler angles off the vehicle reference axes.[6-8] For the studies performed here and the flight data incorporated, all instrument axes are aligned with the body primary axes.

The Euler Model is run prior to processing of any realistic flight data. The concept is to create a truth for attitude estimates and rotational rates through comparison of various onboard sensors. The algorithm involved includes an optimization routine for estimating rate gyro biases and uses those to create an attitude estimate that is free of dependence on center-of-gravity location, a critical point in the center-of-gravity estimation algorithm to prevent circular calculations and improve accuracy.

CHAPTER 3: THEORETICAL DEVELOPMENT OF THE CENTER-OF-GRAVITY ALGORITHM

3.1: FLIGHT DYNAMICS

3.1.1: FORCE EQUATIONS

A concept used in the algorithm described is Newton's second law. Newton's law simply states that the sum of all forces acting on an object is equal to the time rate of change of linear momentum of the body.[5,9-11] In problems involving Earth, the Earth-fixed reference frame can be used as the inertial reference frame. Newton's law can be expressed in both vector and component notation as shown in Eq. 9 and Eq. 10.

$$\sum \boldsymbol{F} = \frac{d}{dt}(m\boldsymbol{v}) \tag{9}$$

$$F_x = \frac{d}{dt}(mu) \tag{10}$$

$$F_y = \frac{d}{dt}(mv)$$

$$F_z = \frac{d}{dt}(mw)$$

By breaking the body into elemental masses and forces, Eq. 9 can be rewritten as Eq. 11 where δm is the mass of the arbitrary element and $\delta \boldsymbol{F}$ is the force exerted on the element. Additionally, the velocity of the element can be shown by Eq. 12, a summation of the velocity of the center of mass $\boldsymbol{v}_c$and velocity of the particle with respect to the center of mass.

$$\boldsymbol{F} = \sum \delta \boldsymbol{F} = \frac{d}{dt}\sum (\boldsymbol{v})\delta m \tag{11}$$

$$\boldsymbol{v} = \boldsymbol{v}_c + \frac{d\boldsymbol{r}}{dt} \tag{12}$$

Assuming the mass of the vehicle is constant and knowing that the summation $\sum r\ \delta m$ is equal to zero, combining Eq. 11 and Eq. 12 result in Eq. 13 as follows.

$$\boldsymbol{F} = m\frac{d\boldsymbol{v}_c}{dt} \tag{13}$$

It can be shown that for any rotating rigid body, the derivative of an arbitrary vector **A** referring to a frame with an angular velocity $\boldsymbol{\omega}$ can be represented with the following identity.

$$\left.\frac{d\boldsymbol{A}}{dt}\right|_I = \left.\frac{d\boldsymbol{A}}{dt}\right|_B = \boldsymbol{\omega}\ x\ \boldsymbol{A} \tag{14}$$

Here the subscript I represents the inertial coordinate frame and B the body coordinate frame. Using this identity and substituting in for $\boldsymbol{v}_c$ Eq. 15 is found.

$$\boldsymbol{F} = m\left.\frac{d\boldsymbol{v}_c}{dt}\right|_B + m(\boldsymbol{\omega}\ x\ \boldsymbol{v}_c) \tag{15}$$

Provided the constant center-of-gravity and mass assumption is valid this equation can be implemented using known aircraft parameters. Substituting in body angular rates and velocities and breaking into vector components the following relationships are obtained.[5,12]

$$F_x = m(\dot{u} + qw - rv) \tag{16}$$

$$F_y = m(\dot{v} + ru - pw)$$

$$F_z = m(\dot{w} + pv - qu)$$

Here the parameters F_x, F_y, and F_z indicate forcing in each of the body frame coordinate axes. These forces incorporate thrust, aerodynamic forces, and effects of gravity on the air vehicle. As previously discussed, these forces driving translational movements on the body can be replaced as functions of acceleration at the center-of-gravity location combined with gravitational effects. The result is revealed in Eq. 17 and Eq. 18.

$$\boldsymbol{F} = m\boldsymbol{a}_c \tag{17}$$

$$\dot{u} = a_{x,CG} - qw + rv \tag{18}$$

$$\dot{v} = a_{y,CG} - ru + pw$$

$$\dot{w} = a_{z,CG} - pv + qu$$

Knowing measurements of body velocities and rotational rates at the center-of-gravity location, as well as previously determined estimates of center-of-gravity acceleration on the vehicle, an estimate of the derivative of body axes velocities can be found. Through the integration of Eq. 18 body velocity estimates can be obtained. The expression can be used later to determine other parameters for a comparison to measurements observed on the vehicle.

3.1.2: Moment Equations

Similar to the equations for force on an aircraft, moment equations can be developed. The second law of motion for rotational moments can be described by Eq. 19.

$$\sum \boldsymbol{M} = \frac{d}{dt}(\boldsymbol{H}) \tag{19}$$

Through a similar breaking of elemental mass components the simplification shown in Eq. 20 can be derived.

$$\boldsymbol{H} = \sum \delta \boldsymbol{H} = \sum (\boldsymbol{r}\ x\ \boldsymbol{v}_c)\delta m + \sum [\boldsymbol{r}\ x\ (\boldsymbol{\omega}\ x\ \boldsymbol{r})]\delta m \tag{20}$$

Substituting for the dynamic forces encountered in flight, the following expressions can be determined. These equations are incorporated into the high performance vehicle simulation previously developed and used to prove algorithm performance. Aerodynamic parameters and properties are substituted in for all aircraft reactions, including L, M, and N the moment coefficients and components of **H**, the angular momentum of the system.

$$L = \dot{H}_x + qH_z - rH_y \tag{21}$$

$$M = \dot{H}_y + rH_x - pH_z$$

$$N = \dot{H}_z + pH_y - qH_x$$

Making a final substitution for moment coefficients and picking the proper body axes for moment equation incorporation using symmetry of the aircraft, a final equation is obtained. Where applicable, the non-zero components of the mass moment of inertia matrix were included. Eq. 22 reveals the final expression for moment equations.[5,12]

$$L = I_x\dot{p} - I_{xz}\dot{r} + qr(I_z - I_y) - I_{xz}pq \tag{22}$$

$$M = I_y\dot{q} + rp(I_x - I_z) + I_z(p^2 - r^2)$$

$$N = -I_{xz}\dot{p} - I_z\dot{r} + pq\left(I_y - I_x\right) + I_{xz}qr$$

3.1.3: Body Angular Velocities, Euler Angle Rates, and Directional Transformations

Relationships relating orientation and position of the airframe in reference to the Earth-fixed reference frame and body-fixed coordinate frame were derived as part of the Euler Model previously described in section 2.3. The expressions are the key to relating accelerometer information with rate gyro and attitude measurements from airframe sensors. They allow for

the creation of estimated aircraft parameters based on the inherent physical relationships present on the rigid body under consideration.

3.1.4: Summary of Flight Dynamics Equations

As a result of the derivations performed here, equations describing the motion and orientation of an aircraft have been developed. These physical relationships will be used twice in the completion of the work being done here. First, the equations will be implemented into the high performance aircraft simulation previously created to produce sensor data. In this application aerodynamic coefficients based on aircraft performance were estimated and control inputs were designed to operate the aircraft in a realistic fashion. Through inclusion of realistic sensor biases and noise as well as inclusion of sensor locations, a realistic data collection is found. The second implementation of the equations derived is in the center-of-gravity estimation algorithm. Here rather than involving the highly detailed aerodynamic model, expressions relating estimated parameters will be used and replace these conditions. Optimization will effectively result in the estimation of these aerodynamic parameters cumulatively.

Equation 23 through Eq. 27 respectively summarize the force equations, moment equations, angular velocity equations, Euler angle rate equations, and directional transformation equations used in this study.[5,9-12]

$$\dot{u} = a_{x,CG} - qw + rv \tag{23}$$

$$\dot{v} = a_{y,CG} - ru + pw$$

$$\dot{w} = a_{z,CG} - pv + qu$$

$$L = I_x\dot{p} - I_{xz}\dot{r} + qr(I_z - I_y) - I_{xz}pq \tag{24}$$

$$M = I_y\dot{q} + rp(I_x - I_z) + I_z(p^2 - r^2)$$

$$N = -I_{xz}\dot{p} - I_z\dot{r} + pq\left(I_y - I_x\right) + I_{xz}qr$$

$$\begin{bmatrix} p \\ q \\ r \end{bmatrix} = \begin{bmatrix} 1 & 0 & -S_\theta \\ 0 & C_\phi & C_\theta S_\phi \\ 0 & -S_\phi & C_\theta C_\phi \end{bmatrix} \begin{bmatrix} \dot{\phi} \\ \dot{\theta} \\ \dot{\psi} \end{bmatrix} \tag{25}$$

$$\begin{bmatrix}\dot{\phi}\\ \dot{\theta}\\ \dot{\psi}\end{bmatrix}=\begin{bmatrix}1 & S_\phi \tan\theta & C_\phi \tan\theta\\ 0 & C_\phi & -S_\phi\\ 0 & S_\phi \sec\theta & C_\phi \sec\theta\end{bmatrix}\begin{bmatrix}p\\ q\\ r\end{bmatrix} \tag{26}$$

$$\begin{bmatrix}\frac{dx}{dt}\\ \frac{dy}{dt}\\ \frac{dz}{dt}\end{bmatrix}=\begin{bmatrix}C_\psi C_\theta & -S_\psi C_\phi + C_\psi S_\theta S_\phi & S_\psi S_\phi + C_\psi S_\theta C_\phi\\ S_\psi C_\theta & C_\psi C_\phi + S_\psi S_\theta S_\phi & -C_\psi S_\phi + S_\psi S_\theta C_\phi\\ -S_\theta & C_\theta S_\phi & C_\theta C_\phi\end{bmatrix}\begin{bmatrix}u\\ v\\ w\end{bmatrix} \tag{27}$$

3.2: Transformation of Sensor Locations

The most critical correlation in physics utilized in this algorithm is the use of rigid body relative motion. It is known that rigid bodies rotate about their center of mass. It is important to note that often bodies will move in a fashion where rotation is not about the center-of-gravity and rather an arbitrary point. Here the distinction is made to describe the motion of a body as a combination of translation of the body at the center-of-gravity from forcing and gravitational effects combined with rotation about the center-of-gravity caused by moments on the body. Additionally it can be shown that knowing center of mass location and rotation rates, conditions for acceleration at any point on the rigid body can be determined.[12] The proposed algorithm requires the transformation of acceleration and jerk conditions from the measurement suite to an estimated center-of-gravity location. The calculation begins initially from the equation for relative velocity motion described in Eq. 28.

$$\boldsymbol{v}_B = \boldsymbol{v}_A + \boldsymbol{\omega}\, x\, \boldsymbol{r}_{B/A} \tag{28}$$

From here we see that the velocity at a given point B can be described by the condition of velocity at point A relative to the coordinate system plus the cross product of rotational rate and position of point B with respect to point A. Conventionally a term for relative motion between the two points in the rotating reference frame (body-fixed coordinate frame) would be included but is removed here on the rigid body assumption. The derivative of Eq. 28 with respect to time yields Eq. 29 shown below.

$$\boldsymbol{a}_B = \boldsymbol{a}_A - \boldsymbol{\alpha}\, x\, \boldsymbol{r}_{B/A} + \boldsymbol{\omega}\, x\, \left(\boldsymbol{\omega}\, x\, \boldsymbol{r}_{B/A}\right) \tag{29}$$

Taking the derivative again results in the transformation equation for jerk of a rigid body. Jerk is the rate of change of acceleration of a body. The derivatives taken here introduce a new set of independent equations required for the first algorithm in center-of-gravity estimation. Performing this operation, Eq. 30 is obtained.[12]

$$\boldsymbol{j}_B = \boldsymbol{j}_A - \boldsymbol{\omega}\, x\, [\boldsymbol{\omega}\, x\, (\boldsymbol{\omega}\, x\, \boldsymbol{r}) + (\boldsymbol{\alpha}\, x\, \boldsymbol{r})] - 2\boldsymbol{\alpha}\, x\, (\boldsymbol{\omega}\, x\, \boldsymbol{r}) - \dot{\boldsymbol{\alpha}}\, x\, \boldsymbol{r} \tag{30}$$

These equations for rigid body motion can be extended for application in aircraft use. Equation 8 is applicable for an air vehicle where the Earth-fixed frame serves as the global reference frame and the body-fixed reference frame as the rotating frame. The rotational velocity of the body is observed through the p, q, and r rotational rates, and offsets from point A being the distance from the center-of-gravity location to sensor locations. The orientation of the airframe and tri-axial accelerometer axis are assumed the same. More complicated expressions for acceleration translations with rotations have been produced but are unnecessary here. Substituting in these parameters for relative acceleration Eq. 31 is obtained.[13]

$$a_{x,s} = a_{x,CG} - (r^2 + q^2)x + (pq - \dot{r})y + (pr + \dot{q})z \tag{31}$$

$$a_{y,s} = a_{y,CG} + (pq + \dot{r})x - (p^2 + r^2)y + (qr - \dot{p})z$$

$$a_{z,s} = a_{z,CG} + (pr - \dot{q})x + (qr + \dot{p})y - (p^2 + q^2)z$$

It is observed that operation without the existence of rotation of the body will result in identical acceleration conditions at the sensor and center-of-gravity locations. The inactive case is expected as without rotation the body acts as a particle. Such would be the case for any offset from the center-of-gravity location. When this is the case, changing the center-of-gravity estimate will not affect the error associated with the algorithm and estimates cannot be improved upon.

As shown previously in Eq. 30, taking the derivative of acceleration of the rigid body results in a relationship for jerk of the body. Equation 32 shown below indicates the relationship between jerk at the center-of-gravity and at a given location on the rigid body based on rotation rates and offsets.[13]

$$j_{x,s} = j_{x,CG} - q * (\dot{q} * x - \dot{p} * y + p * (p * z - r * x) + q * (q * z - r * y)) + r * (\dot{p} * z - \dot{r} * x + p * (p * y - q * x) - r * (q * z - r * y)) + \ddot{q} * z - \ddot{r} * y + 2 * \dot{q} * (p * y - q * x) + 2 * \dot{r} * (p * z - r * x) \quad (32)$$

$$j_{y,s} = j_{y,CG} + p * (\dot{q} * x - \dot{p} * y + p * (p * z - r * x) + q * (q * z - r * y)) - \ddot{p} * z + \ddot{r} * x + r * (\dot{q} * z - \dot{r} * y + q * (p * y - q * x) + r * (p * z - r * x)) - 2 * \dot{p} * (p * y - q * x) + 2 * \dot{r} * (q * z - r * y)$$

$$j_{z,s} = j_{z,CG} - p * (\dot{p} * z - \dot{r} * x + p * (p * y - q * x) - r * (q * z - r * y)) + \ddot{p} * y - \ddot{q} * x - q * (\dot{q} * z - \dot{r} * y + q * (p * y - q * x) + r * (p * z - r * x)) - 2 * \dot{p} * (p * z - r * x) - 2 * \dot{q} * (q * z - r * y)$$

These equations serve as the primary modes for translating acceleration and jerk conditions to the estimated center-of-gravity location. Jerk conditions at the sensor location are obtained by taking the derivative of the accelerometer signal, and are used only in the first center-of-gravity estimation approach. Once again these relationships are only valid for a rigid body and cannot be used when significant flexure is observed between the sensor and center-of-gravity locations.

3.3: Center-of-Gravity Attitude Model

The first method investigated for center-of-gravity estimation is the Attitude Model. The Attitude Model concept was developed as the most ideal method for center-of-gravity estimation due to the relaxation of necessity for additional sensors beyond accelerometer, rate gyro, and attitude information.

3.3.1: Imposed Loading Definition

One attribute of aircraft dynamics that will be utilized to determine the center-of-gravity is the definition of imposed loading and acceleration at the center-of-gravity location. Imposed loading is defined as the sum of all external loading on an aircraft including aerodynamic forces and thrust. These imposed loading forces combined with the effects of gravity provide the basis for translational motion of the vehicle.[14-21] Measured acceleration at the center-of-gravity

location can be described by the sum of the gravitation field vector, using Euler angle attitude relationships, and imposed loading and can be seen in Eq. 33.

$$\boldsymbol{a}_{CG} = \begin{bmatrix} a_x \\ a_y \\ a_z \end{bmatrix}_{CG} = \begin{bmatrix} a_{x,imposed} \\ a_{y,imposed} \\ a_{z,imposed} \end{bmatrix} + \begin{bmatrix} -\sin\theta \\ \cos\theta \sin\phi \\ \cos\theta \cos\phi \end{bmatrix} \tag{33}$$

Taking the first derivative of Eq. 33 reveals a condition for the jerk condition at the center-of-gravity based on imposed loading and the gravitational field vector. The relationship derived will be used in the first center-of-gravity estimation algorithm as part of the method to estimate imposed loading. Equation 34, shown below, describes the relationship for imposed loading, the gravitational field vector, and jerk at the center-of-gravity location.

$$\begin{aligned} \boldsymbol{j}_{CG} = \begin{bmatrix} j_x \\ j_y \\ j_z \end{bmatrix}_{CG} &= \begin{bmatrix} \dot{a}_x \\ \dot{a}_y \\ \dot{a}_z \end{bmatrix}_{CG} \\ &= \begin{bmatrix} \dot{a}_{x,imposed} \\ \dot{a}_{y,imposed} \\ \dot{a}_{z,imposed} \end{bmatrix} + \begin{bmatrix} -\dot{\theta}\cos\theta \\ -\dot{\theta}\sin\theta\sin\phi + \dot{\phi}\cos\theta\cos\phi \\ -\dot{\theta}\sin\theta\cos\phi - \dot{\phi}\cos\theta\sin\phi \end{bmatrix} \end{aligned} \tag{34}$$

The equation derivative provides the additional set of equations required to make the problem set fully defined for the first algorithm. Imposed loading encapsulates all the applied aerodynamic and thrust forces related to the vehicle frame. An accurate estimate of imposed loading can be used to determine aircraft orientation by localizing the gravitational field vector.

3.3.2: Concept and Schematic

The Attitude Model is designed to require the least number of sensors through signal manipulation including additional derivatives and integrals. The added equations that make the algorithm properly defined are the calculation of jerk to determine imposed loading estimate. The added set of equations requires additional differentiation of signals in non-real-time which again can introduce inherent error for noisy signals. The schematic for the Attitude Model is show in Fig. 3.

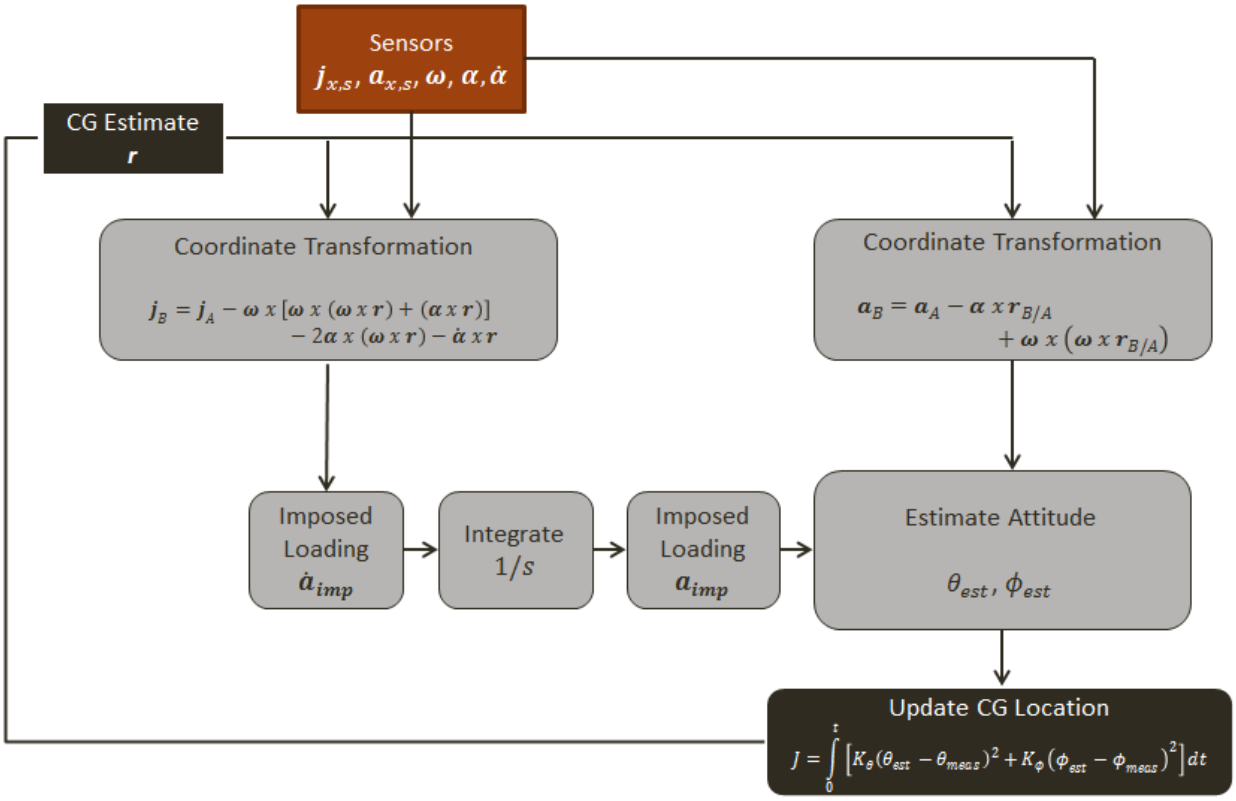

FIGURE 3: ATTITUDE MODEL SCHEMATIC

The first step of the Attitude Model involves transformation of the sensor readings, both true measurements and processed signals, of acceleration and jerk to the estimated center-of-gravity location. For the first step of the optimization routine the translation distance is purely a guess and should be improved upon by the algorithm in future iterations. Using Eq. 31 and Eq. 32, this operation can be performed. The result is a condition for acceleration and jerk at the estimated center-of-gravity location.

The second step for the Attitude Model requires subtracting the gravitational field vector effects from the center-of-gravity jerk condition. Using Eq. 34, an estimate of the derivative of imposed loading can be obtained as seen in Eq. 35. Integration of this produces an estimate of imposed loading.[14,15]

$$\begin{bmatrix} \dot{a}_{x,imposed} \\ \dot{a}_{y,imposed} \\ \dot{a}_{z,imposed} \end{bmatrix} = \begin{bmatrix} j_x \\ j_y \\ j_z \end{bmatrix}_{CG} + \begin{bmatrix} \dot{\theta}\cos\theta \\ \dot{\theta}\sin\theta\sin\phi - \dot{\phi}\cos\theta\cos\phi \\ \dot{\theta}\sin\theta\cos\phi + \dot{\phi}\cos\theta\sin\phi \end{bmatrix} \tag{35}$$

The calculation of imposed loading on the body can then be used in Eq. 35, leaving the equation apparently fully defined. However, solving for new attitude estimates allows for the introduction of an error signal to the algorithm. An accurate center-of-gravity estimate would

produce an attitude estimate equal to the real attitude estimate, but significant deviation from this location will provide an error and room for improvement. Equation 33 can be rearranged to find Eq. 36 and Eq. 37 shown below.

$$\theta_{est} = \tan^{-1}\left[\frac{-a_{x,CG} - \left(\frac{a_{x,imposed}}{g}\right)}{a_{z,CG} - \left(\frac{a_{z,imposed}}{g}\right)}\right] \tag{36}$$

$$\phi_{est} = \tan^{-1}\left[\frac{-a_{y,CG} - \left(\frac{a_{y,imposed}}{g}\right)}{a_{z,CG} - \left(\frac{a_{z,imposed}}{g}\right)}\right] \tag{37}$$

These attitude estimates can be used as a comparison to measured attitude parameters using an optimization routine. A Matlab® function 'fmincon' allows for constrained optimization within reasonable bounds to potentially speed up the localization process. The function will iterate to improve center-of-gravity location estimates until a minimum cost is found. The cost function used is a sum of squared differences of the signals and is shown in Eq. 38. The cost function provides the baseline for the next iteration, and new estimates can then be fed back to find new parameter estimates.

$$J = \int_0^t \left[K_\theta(\theta_{est} - \theta_{meas})^2 + K_\phi(\phi_{est} - \phi_{meas})^2\right]dt \tag{38}$$

3.3.3: Addressing Biases in Measurements

Biases in accelerometers are inherent to all realistic sensor systems and must be accounted for. Particularly in cases where measurements are integrated steady biases in measurements compound into significant errors and must be addressed. In the Attitude Model, accelerometer measurements are not integrated as they will be in later models and do not introduce such problems. Jerk terms are derivatives of the accelerometer signals that remove the effect of these biases. As such, accelerometer biases are difficult and unnecessary to predict in the Attitude Model and are not included in the optimization routine.

3.4: Center-of-Gravity Air Data Model

3.4.1: Air Data Parameters

Air data information can be an additional sensor and measurement with which to compare estimates from center-of-gravity estimation. Proper manipulation of acceleration and rotational measurements on the aircraft can yield estimates of air data for the given flight condition. Air

data measurements consist of three parameters: total airspeed, angle-of-attack, and sideslip angle.

The premise of the model is that typically these sensors are not co-located with the center-of-gravity of the aircraft. Therefore, errors can be formed with a model developing estimates of these measurements to localize the center-of-gravity location. The center-of-gravity referenced estimates resulting from the propagation of model can be transformed to the sensor locations using known kinematic relationships for comparison. A description of the Air Data Model is given by Eq. 39 through Eq. 42. The Air Data Model equations are complete meaning no small angle assumptions were made. The model consists of four components: an initial condition model described by Eq. 39, a linear accelerometer sensor transformation model described by Eq. 40 that transforms the location of the linear accelerometer sensor to the center-of-gravity reference point, a dynamical system state component described by Eq. 41, and an output measurement model described by Eq. 42. The output measurement model is compared to the flight data measurement to form the minimization cost function value. The subscripts $(\,)_m$ are the aircraft measured responses, $(\,)_z$ are the computed output responses, $(\,)_b$ are the measurement biases, and $(\,)_0$ are the state initial conditions.[5,17]

$$V(0) = \left\{\left[(V_m(0) - V_b + V_0)\cos\left(\frac{\alpha_m(0)}{\alpha_z} - \alpha_b + \alpha_0\right)\cos\left(\frac{\beta_m(0)}{\beta_z} - \beta_b + \beta_0\right) - q(z_{cg} - z_V) + r(y_{cg} - y_V)\right]^2 + \left[(V_m(0) - V_b + V_0)\sin\left(\frac{\beta_m(0)}{\beta_z} - \beta_b + \beta_0\right) - r(x_{cg} - x_V) + p(z_{cg} - z_V)\right]^2 + \left[(V_m(0) - V_b + V_0)\sin\left(\frac{\alpha_m(0)}{\alpha_z} - \alpha_b + \alpha_0\right)\cos\left(\frac{\beta_m(0)}{\beta_z} - \beta_b + \beta_0\right) - p(y_{cg} - y_V) + q(x_{cg} - x_V)\right]^2\right\}^{\frac{1}{2}} \tag{39}$$

$$\alpha(0) = \tan^{-1}\left[\frac{(V_m(0)-V_b+V_0)\sin\left(\frac{\alpha_m(0)}{\alpha_z}-\alpha_b+\alpha_0\right)\cos\left(\frac{\beta_m(0)}{\beta_z}-\beta_b+\beta_0\right)-p(y_{cg}-y_\alpha)+q(x_{cg}-x_\alpha)}{(V_m(0)-V_b+V_0)\cos\left(\frac{\alpha_m(0)}{\alpha_z}-\alpha_b+\alpha_0\right)\cos\left(\frac{\beta_m(0)}{\beta_z}-\beta_b+\beta_0\right)-q(z_{cg}-z_\alpha)+r(y_{cg}-y_\alpha)}\right]$$

$$\beta(0) = \sin^{-1}\left[\frac{(V_m(0)-V_b+V_0)\sin\left(\frac{\beta_m(0)}{\beta_z}-\beta_b+\beta_0\right)-r\left(x_{cg}-x_\beta\right)+p\left(z_{cg}-z_\beta\right)}{(V_m(0)-V_b+V_0)}\right]$$

$$n_x = n_x - n_x + \Big[(r^2 + q^2)\big(x_{cg} - x_{nx}\big)^2 + (pq - \dot{r})\big(y_{cg} - y_{nx}\big)^2 + (pr + \dot{q})\big(z_{cg} - z_{nx}\big)^2\Big]/g \quad (40)$$

$$n_y = n_y - n_y - \Big[(pq + \dot{r})\big(x_{cg} - x_{ny}\big)^2 - (p^2 + r^2)\big(y_{cg} - y_{ny}\big)^2 + (qr - \dot{p})\big(z_{cg} - z_{ny}\big)^2\Big]/g$$

$$n_z = n_z - n_z + \Big[(pr - \dot{q})\big(x_{cg} - x_{nz}\big)^2 + (qr + \dot{p})\big(y_{cg} - y_{nz}\big)^2 - (p^2 + q^2)\big(z_{cg} - z_{nz}\big)^2\Big]/g$$

$$\dot{V} = g\big[(n_x \cos\alpha + n_x \sin\alpha)\cos\beta + n_y \sin\beta + \sin\beta\cos\theta\sin\phi - (\cos\alpha\sin\theta - \sin\alpha\cos\theta\cos\phi)\cos\beta\big] \quad (41)$$

$$\dot{\alpha} = q - (p\cos\alpha + r\sin\alpha)\tan\beta + \frac{g[n_z\cos\alpha - n_x\sin\alpha]}{V\cos\beta} + \frac{g}{V\cos\beta}(\cos\theta\cos\phi\cos\alpha + \sin\theta\sin\alpha)$$

$$\dot{\beta} = \frac{gn_y\cos\beta - g(n_x\cos\alpha + n_z\sin\alpha)\sin\beta}{V} + p\sin\alpha - r\cos\alpha + \frac{g}{V}[\cos\beta\cos\theta\sin\phi - \sin\beta\,(\cos\theta\cos\phi\sin\alpha - \sin\theta\cos\alpha)]$$

$$V_z = \Big\{\big[V\cos\alpha\cos\beta + q\big(z_{cg} - z_V\big) - r\big(y_{cg} - y_V\big)\big]^2 + \big[V\sin(\beta) + r\big(x_{cg} - x_V\big) - p\big(z_{cg} - z_V\big)\big]^2 + \big[V\sin(\alpha)\cos(\beta) + p\big(y_{cg} - y_V\big) - q\big(x_{cg} - x_V\big)\big]^2\Big\}^{\frac{1}{2}} + V_b \quad (42)$$

$$\alpha_z = \tan^{-1}\left[\frac{V\sin(\alpha)\cos(\beta) + p\big(y_{cg} - y_\alpha\big) - q\big(x_{cg} - x_\alpha\big)}{V\cos(\alpha)\cos(\beta) + q\big(z_{cg} - z_\alpha\big) - r\big(y_{cg} - y_\alpha\big)}\right] + \alpha_b$$

$$\beta_z = \sin^{-1}\left[\frac{V\sin(\beta) + r\big(x_{cg} - x_\beta\big) - p\big(z_{cg} - z_\beta\big)}{V}\right] + \beta_b$$

3.4.2: Concept and Schematic

The Air Data Model shares most similarity with the GPS and INS Model in terms of structure. Air data measurement devices can only measure relative wind velocities and do not always properly correlate to total velocities when significant wind is present. As such, consideration of wind velocity must be given. The schematic for the Air Data Model can be found in Fig. 4.

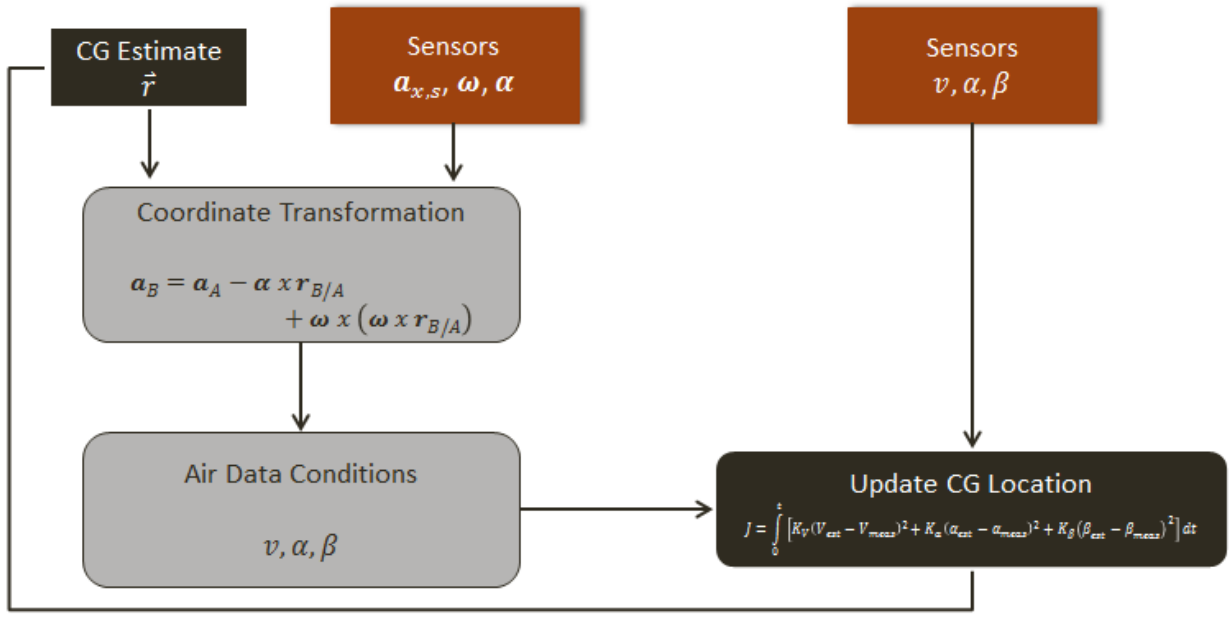

FIGURE 4: AIR DATA MODEL SCHEMATIC

As shown in the previous model, Eq. 31 provides the first step towards center-of-gravity estimation, the translation of the sensor acceleration. Following this the aircraft body-fixed coordinate system velocities must again be determined using Eq. 23. The Air Data Model then uses Eq. 39 through Eq. 42 to create an estimate for air data parameters. These new estimates provide the basis for comparison in the cost function to real measurements. The cost function used for the Air Data Model is shown in Eq. 43, and is iterated upon to minimize the cost and error in air data parameters.

$$J = \int_0^t [K_V(V_{est} - V_{meas})^2 + K_\alpha(\alpha_{est} - \alpha_{meas})^2 + K_\beta(\beta_{est} - \beta_{meas})^2]dt \tag{43}$$

3.4.3: Addressing Biases in Measurements

Biases are inherent to most measurement devices available. To improve center-of-gravity estimates biases must be accounted for in the calculation. Rate gyro biases are assumed to be predetermined and eliminated by the Euler Model available as described in section 2.3. Accelerometer biases can be estimated and removed by adding variables to the estimation routine. Bias estimation is included by adding initial estimates to the initialization of the algorithm and subtracting the bias estimates from the corresponding accelerometer signal.

Determination of the accelerometer biases in the Air Data Model is critical due to the use of the measurements. Subsequent calculations involving accelerometer measurements will be

integrated, compounding errors from steady errors in measurements. For this reason, accelerometer biases must be addressed and removed from measurement systems.

3.5: Center-of-Gravity GPS and INS Model

3.5.1: Concept and Schematic

When GPS and INS measurements are consistently available and accurate, this algorithm provides potential to be the most accurate of all center-of-gravity estimation models. The added information to fully define this approach is the introduction of GPS and INS measurements as a comparison in the cost function. Combining the INS and GPS information for accurate position and velocity information in the Earth-fixed coordinate frame is critical for estimation accuracy. The derivative of position to velocity allows for six signals available for cost analysis inclusion. The schematic for the GPS and INS center-of-gravity estimation is shown in Fig. 5.

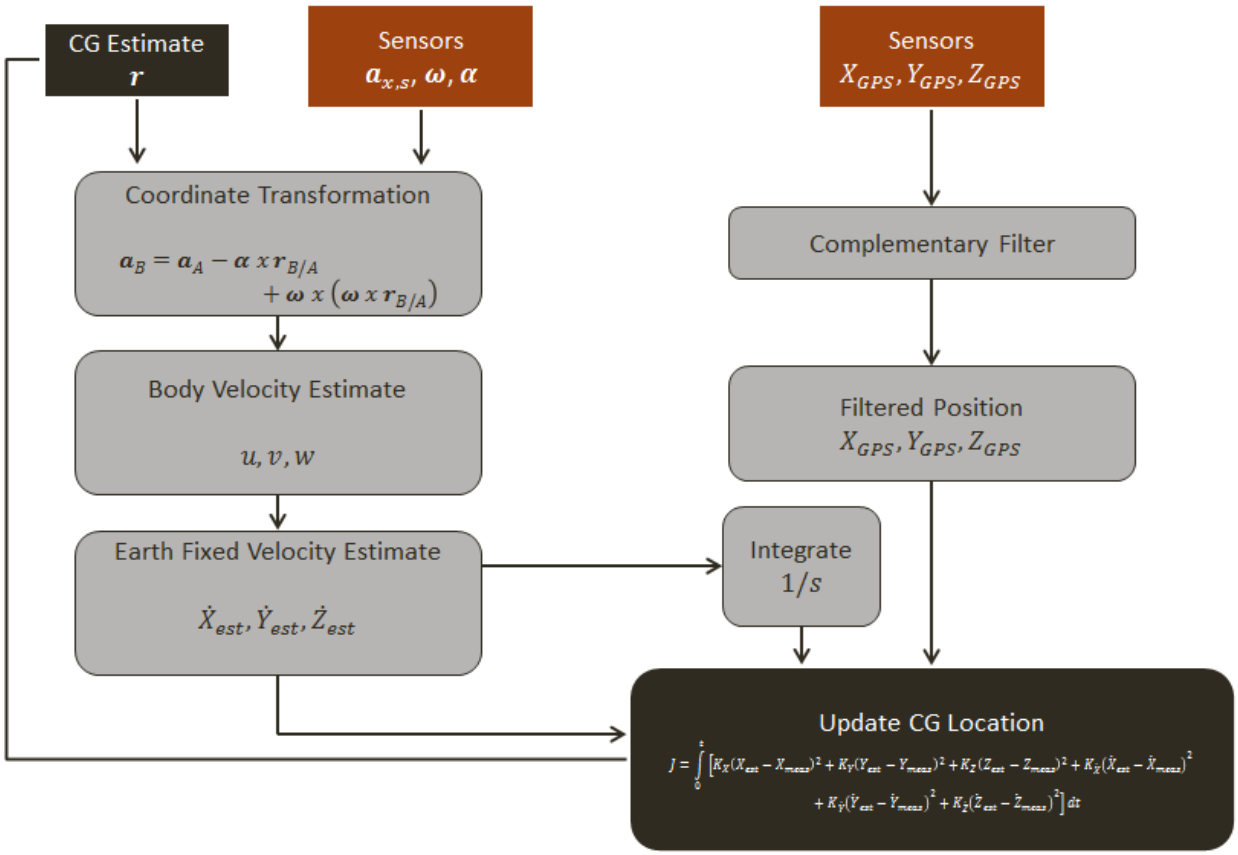

FIGURE 5: GPS AND INS MODEL SCHEMATIC

The GPS and INS Model initializes once again with estimates for position of the center-of-gravity. Again, the accelerometer readings are transformed to the estimated center-of-gravity

location where other parameters can be estimated. The next step here involves the calculation of velocity in the body-fixed coordinate frame. The relationship for this was developed in Eq. 23. Integration then results in calculation of the velocity of the aircraft in the body-fixed coordinate frame.

The next step requires the transformation of velocity in the body-fixed frame to the Earth-fixed coordinate frame. The relationship for transformation between body-fixed and Earth-fixed coordinate axes is found in Eq. 27. The resulting parameters describe velocity of the vehicle in the Earth-fixed frame.

Integration of the velocities in the Earth-fixed coordinate frame along with accurate information of the initial Earth-fixed frame position provides six independent signals for inclusion in the final cost function; velocity and position in each axis. The cost function used in the GPS and INS Model is shown in Eq. 44.

$$J = \int_0^t \Big[K_X (X_{est} - X_{meas})^2 + K_Y (Y_{est} - Y_{meas})^2 + K_Z (Z_{est} - Z_{meas})^2 + K_{\dot{X}} \left(\dot{X}_{est} - \dot{X}_{meas}\right)^2 + K_{\dot{Y}} \left(\dot{Y}_{est} - \dot{Y}_{meas}\right)^2 + K_{\dot{Z}} \left(\dot{Z}_{est} - \dot{Z}_{meas}\right)^2 \Big] dt \tag{44}$$

3.5.2: Addressing Biases in Measurements

Biases are inherent to most measurement devices available. To improve center-of-gravity estimates biases must be accounted for in the calculation. Rate gyro biases are assumed to be predetermined and eliminated by the Euler model previously described in section 2.3. Accelerometer biases can be estimated and removed by adding variables to the estimation routine. Bias estimation is included by adding initial estimates to the initialization of the algorithm and subtracting the bias estimates from the corresponding accelerometer signal.

Determination of the accelerometer biases in the Air Data Model is critical due to the use of the measurements. Subsequent calculations involving accelerometer measurements will be integrated, compounding errors from steady errors in measurements. For this reason, accelerometer biases must be addressed and removed from measurement systems.

3.6: Optimization Routine

The models each outlined as components in the center-of-gravity estimation routine consist of a handful of Matlab® and Simulink® codes. Each follows a similar overall structure and is operated in a similar manner for simulation purposes.

The algorithm starts with an initial run script or m-file. The file contains all the truth definitions, loads previously collected data, and defines all the necessary initial conditions. Flags for models incorporated, constraints in optimization, and numerous other options are included there. The final step of the script is the application of the 'fmincon' function, an optimization routine where the function called produces the cost for weighting in the determination of optimal solutions. In this user created optimization function, the Simulink® diagram used for center-of-gravity estimation is called upon. The function saves the iterative estimates for specified parameters, then processes the required aircraft parameter estimates for the flight conditions specified to create new error signals and conditions. The Simulink® diagrams contain the described equations for transformation equations for sensor locations, flight dynamics equations as applicable, and parameter estimates as called upon by the individual models. The new estimates are then weighted as defined and passed into the final cost output.

The optimization function used is a constrained function in which bounds on parameter estimates are placed, preventing unreasonable estimates to speed up simulation time in the occurrence of extreme parameter estimate dynamics. In the simulations performed bounds were never exceeded indicating the function is effective at reaching final values without an excessive number of iterations. The function is incorporated using the active-set algorithm, which uses a Sequential Quadratic Programming (SQP) method. In this method at each iteration, a Quadratic Programming (QP) subproblem is solved, which is created using an approximation of the Hessian of the Lagrangian function with a quasi-Newton updating method. This method for generating new iteration measurements is considered an improvement over conventional trust-region-reflective iterative solvers because a merit function is used in the line search for solving the subproblem rather than the interior reflective Newton method which linearizes the complicated problem set.

CHAPTER 4: SIMULATION RESULTS

4.1: ATTITUDE MODEL RESULTS – LARGE INPUT

The performance of the Attitude Model is proven through simulation in Matlab®. The measurement inputs for the aircraft were determined using a previously developed aircraft simulation of a highly dynamic high performance military type vehicle. Control inputs include throttle setting, horizontal tail, trailing edge flaperons, and a rudder control surface setting. To display the success of the algorithm, the control inputs were varied using sinusoidal inputs across the collection period to ensure robustness of the algorithm design. The units for all responses are standard for each plot included in the results: input control surfaces are in degrees, body velocity terms are in feet per second, Euler angles are in degrees, rotational rates are in degrees per second, center-of-gravity location estimates are in feet, accelerometer measurements are in feet per second squared, air data angles are in degrees, and GPS and INS locations are in feet. The response of the aircraft to the control inputs is displayed in Fig. 6 shown below.

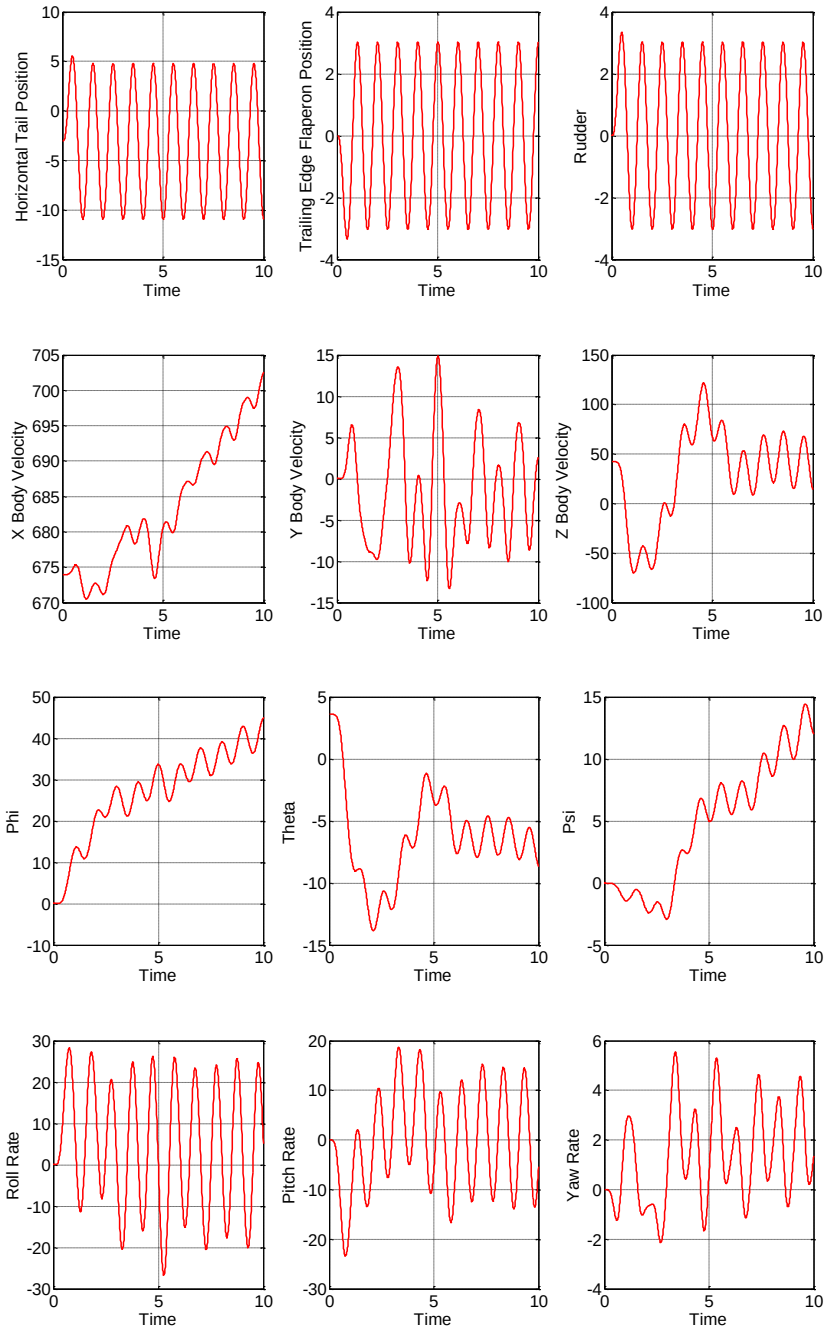

FIGURE 6: ATTITUDE MODEL AIRCRAFT INPUT AND RESPONSE

Figure 6 shown portrays the ten second response of the vehicle to highly dynamic sinusoidal inputs to the control surfaces. These control inputs vary more than typical changes in control inputs, and if the algorithm can handle this dynamic of a platform then solving for all dynamic conditions shall be plausible.

The algorithm then operates using the information provided from the simulation. Measurement signals for body rotational rates, air data, GPS and INS information, and attitude estimates can be obtained directly from devices including the attitude estimation device. Accelerometer readings at specified sensor locations within the aircraft are processed in the algorithm using simulated center-of-gravity conditions. These measurements are then manipulated using the calculations described previously. The following summarizes the resulting estimates and errors obtained from the attitude estimation algorithm using simulated high performance vehicle. Note that the error described is an error between estimates and actual center-of-gravity values and is not reflective of a percent error.

Parameter	Initial Estimate	Estimated Value	Actual Value	Error
X CG Location Estimate	20	26.9621	26.8731	0.089
Y CG Location Estimate	1	0.0085	0	0.0085
Z CG Location Estimate	5	7.1696	7.54072	-0.37112
N_x Bias	0	-	0	-
N_y Bias	0	-	0	-
N_z Bias	0	-	0	-

TABLE 2: ATTITUDE ALGOTIHM RESULTS SUMMARY

As shown the algorithm provided highly accurate estimates for each axis of center-of-gravity estimation. Biases in accelerometers were also estimated with a great degree of accuracy. Figure 7 shown below displays the progression of the estimates for the x, y, and z axes during optimization.

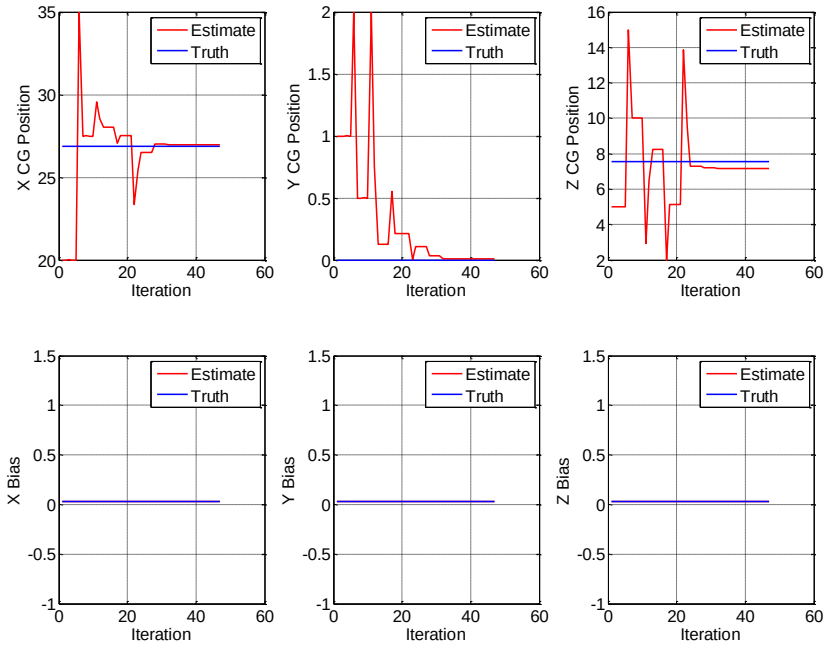

FIGURE 7: ATTITUDE MODEL ITERATION IMPROVEMENT

Here the center-of-gravity estimate is shown following each iteration in the optimization routine. Estimates go through improvement and regression cycles inherent to optimization techniques. To ensure accurate estimates are obtained, comparison of real measurements to estimated values can be depicted. It's important that in the simulation results the 'truth' signals are available from the aircraft simulation and indicate actual conditions. Measurements incorporated to the algorithm differ from the truth signals due to the introduction of realistic Gaussian white noise and filtering techniques. Forwards and backwards filtering is incorporated to remove time delays inherent to filtering techniques such as those incorporated which eliminate high frequency noise patterns such as those typically observed in sensors. Truth signals in real data collection are not attainable, but are included here to display accuracy of parameter estimation from the algorithm. Figure 8 through Fig. 11 below show the comparison of numerous key parameters utilized during center-of-gravity estimation.

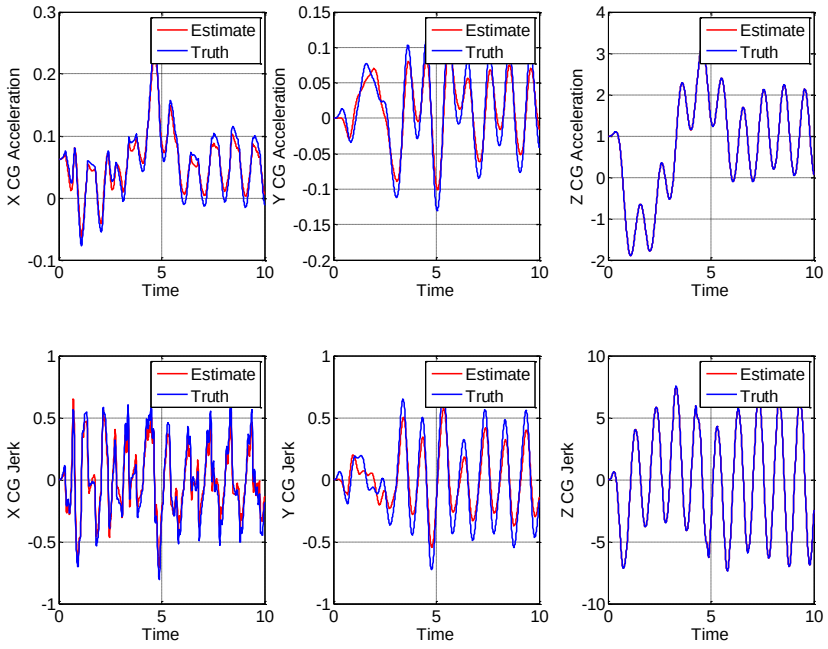

FIGURE 8: ATTITUDE MODEL ACCELERATION AND JERK COMPARISON

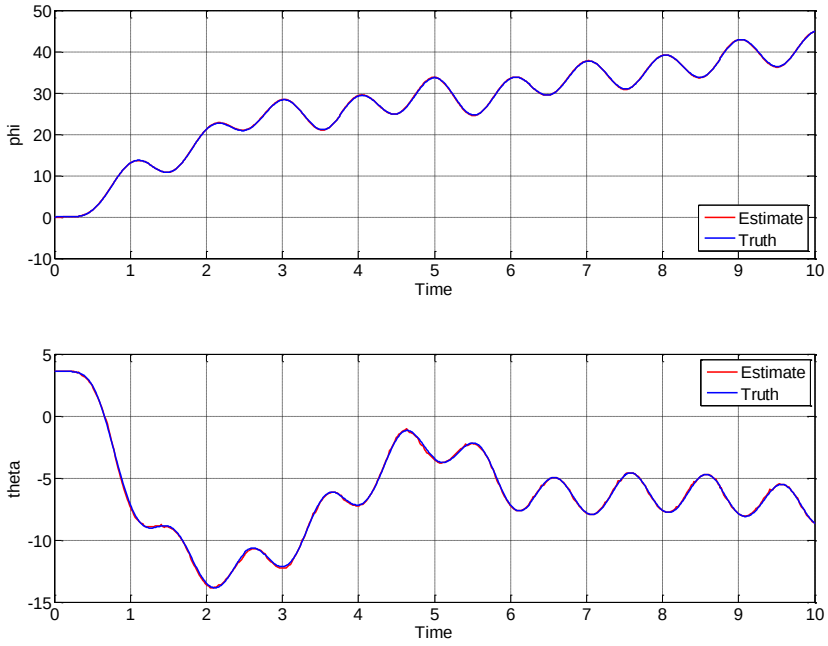

FIGURE 9: ATTITUDE MODEL ATTITUDE COMPARISON

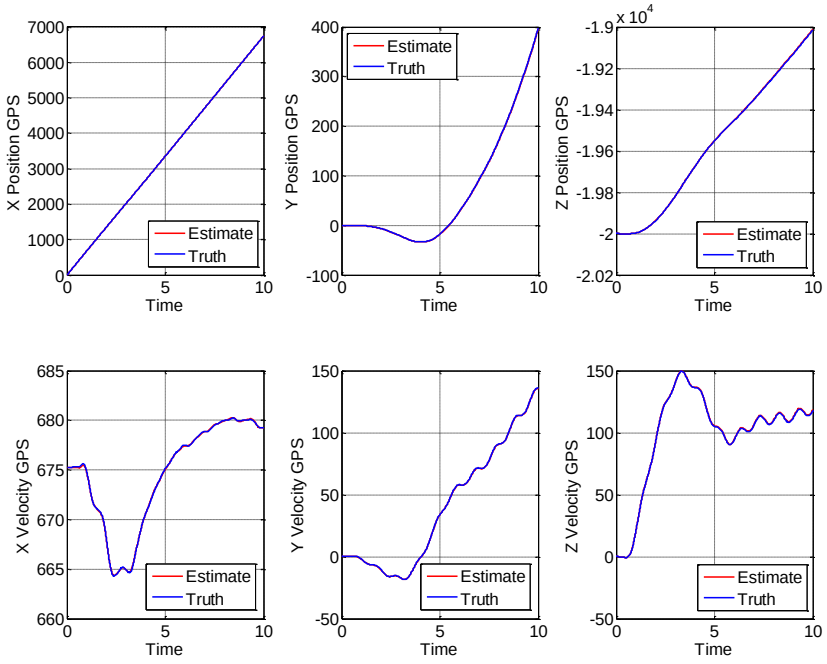

FIGURE 10: ATTITUDE MODEL POSITION AND VELOCITY COMPARISON

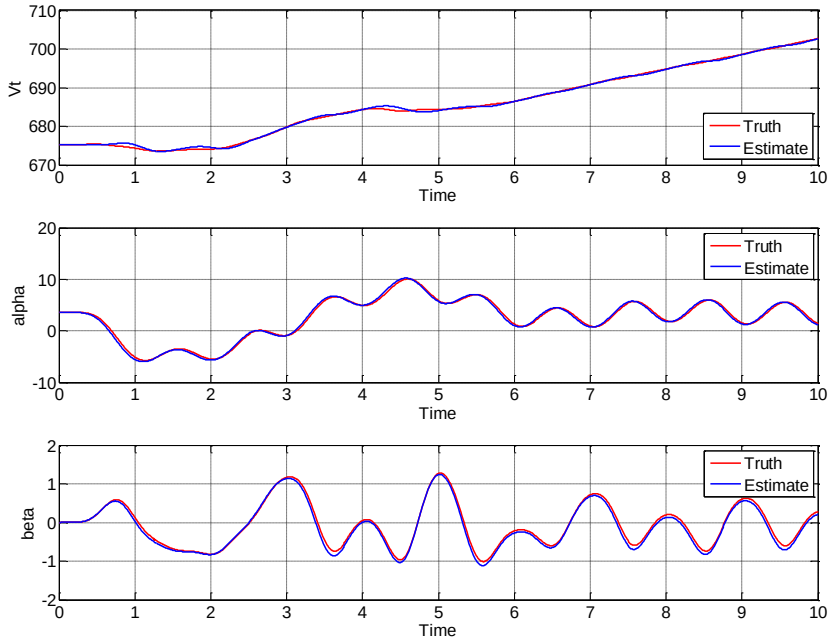

FIGURE 11: ATTITUDE MODEL AIR DATA COMPARISON

Each comparison plot indicates adequate accuracy between estimates of parameters of the vehicle and actual values or measurements from simulation. Note that the Attitude Model only uses the error between attitude estimates phi and theta towards calculating the cost for optimization purposes. Incorporation of other parameters to the cost function may allow for more accurate estimates and reduce any potential error in center-of-gravity estimates due to sensor errors or malfunctions.

4.2: Attitude Model Results – Small Input

The algorithm is again processed using a smaller control input magnitude. The test is done to observe the algorithm's ability to operate in less dynamic conditions. The control inputs and aircraft responses are shown in Fig. 12.

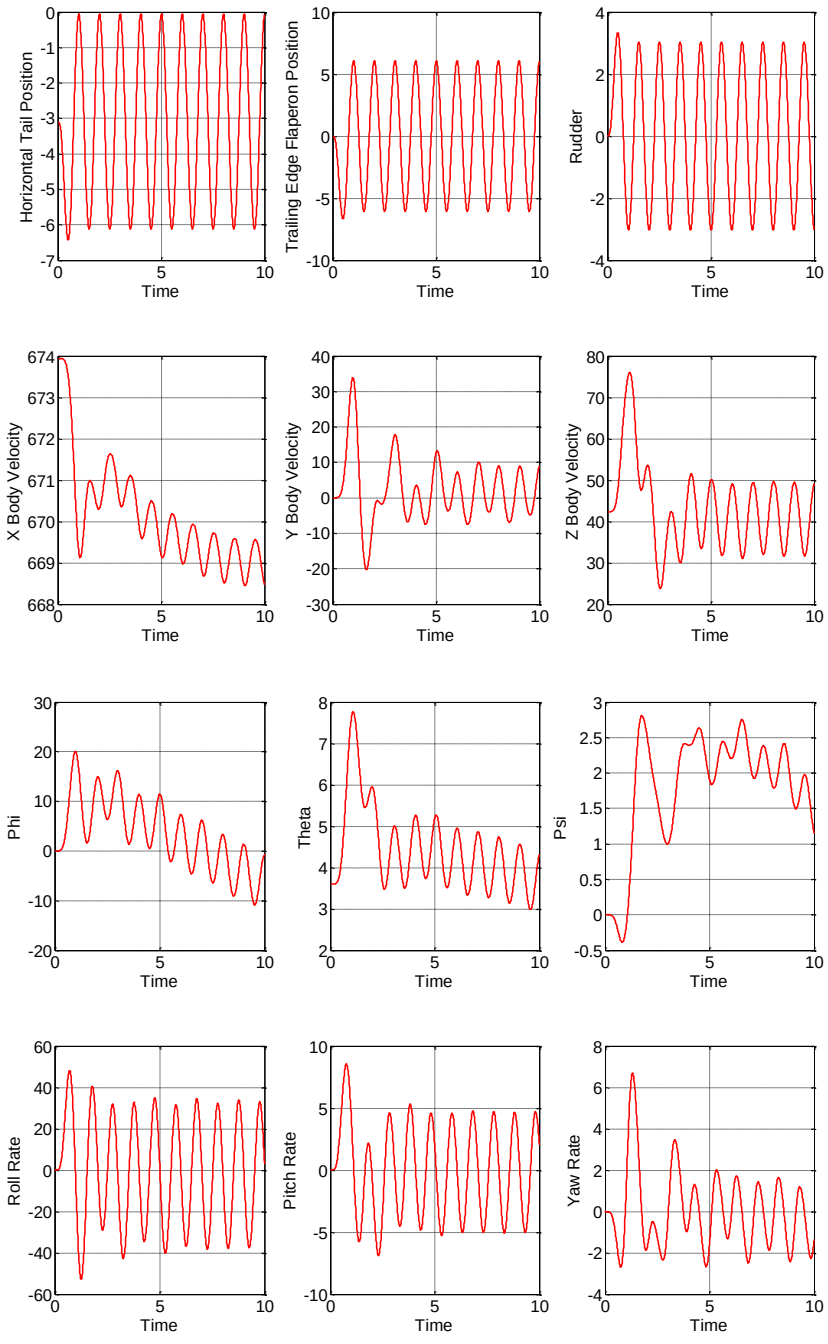

FIGURE 12: ATTITUDE MODEL SMALL INPUT AIRCRAFT RESPONSE

In comparison to the control inputs and aircraft response observed for the large inputs seen in Fig. 6, significantly less dynamics are seen. The results may be typical of standard flight conditions when no significant maneuvers are performed. Table 3 shows the results of the algorithm processed using these reduced inputs.

Parameter	Initial Estimate	Estimated Value	Actual Value	Error
X CG Location Estimate	20	26.9954	26.8731	0.1223
Y CG Location Estimate	1	0.1994	0	0.1994
Z CG Location Estimate	5	7.0848	7.5407	-0.4559
N_x Bias	0	-	0	-
N_y Bias	0	-	0	-
N_z Bias	0	-	0	-

TABLE 3: ATTITUDE MODEL SMALL INPUT RESULTS SUMMARY

Here the results for center-of-gravity location closely correlate with those of large inputs to the vehicle. Accelerometer biases for the Attitude Model were not estimated in this analysis. The Attitude Model is minimally dependent on biases observed in the accelerometers due to the use of derivatives of measurements in the algorithm. The dependence will vary later as the other two models rely on taking integrals of these signals and related parameters which propagate errors. Figure 13 shows the changes in estimates during the optimization routine.

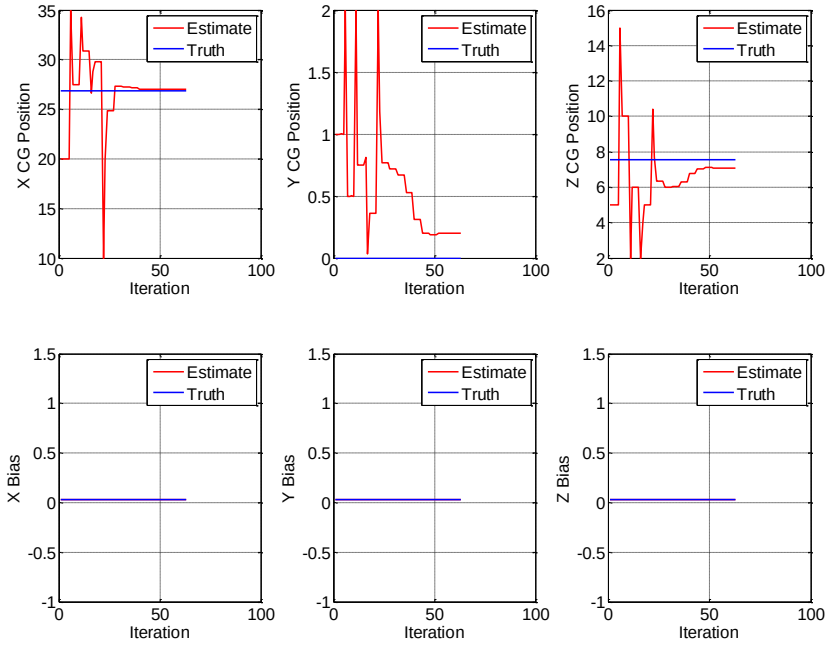

FIGURE 13: ATTITUDE MODEL SMALL INPUT ITERATION IMPROVEMENT

The changes throughout optimization are similar to those in other analyses. Once again, no bias estimation is performed and as so no changes to those estimates are seen. Figure 14 through Fig. 17 display the correlation between estimates and other key parameters used in the optimization routine.

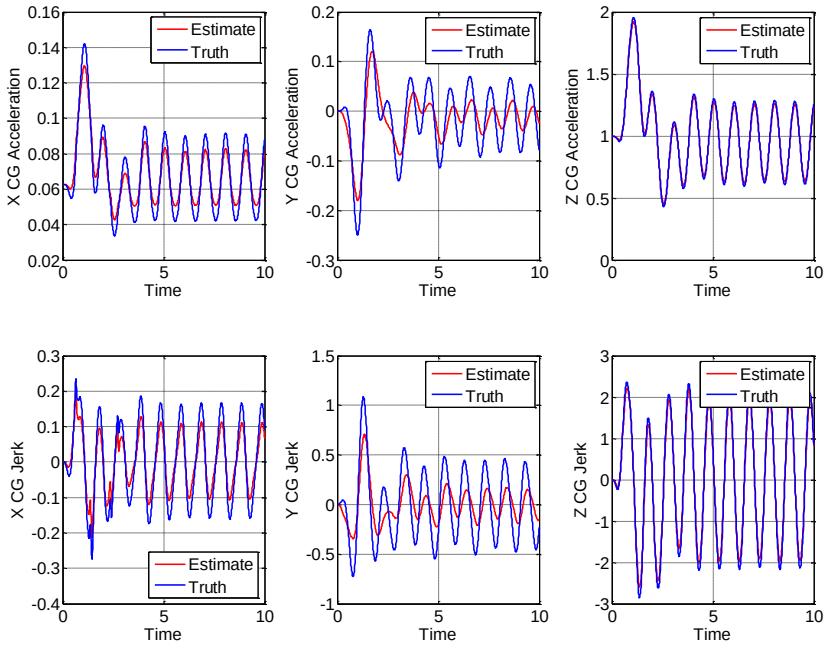

FIGURE 14: ATTITUDE MODEL SMALL INPUT ACCELERATION AND JERK COMPARISON

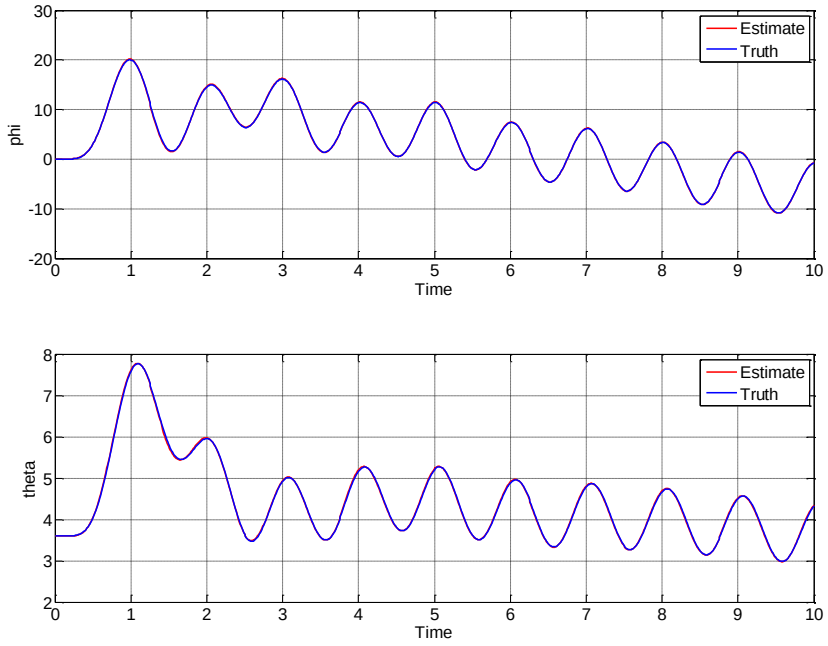

FIGURE 15: ATTITUDE MODEL SMALL INPUT ATTITUDE COMPARISON

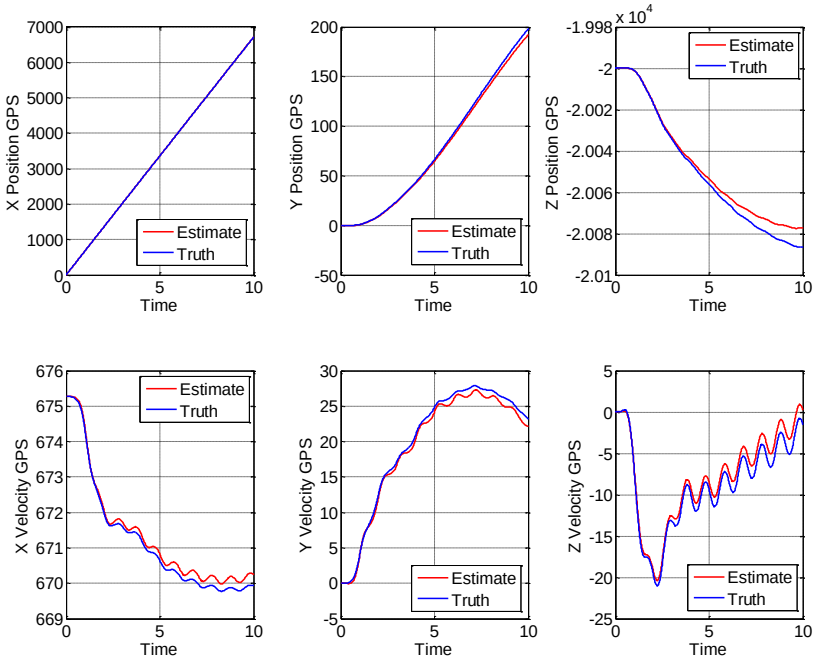

FIGURE 16: ATTITUDE MODEL SMALL INPUT POSITION AND VELOCITY COMPARISON

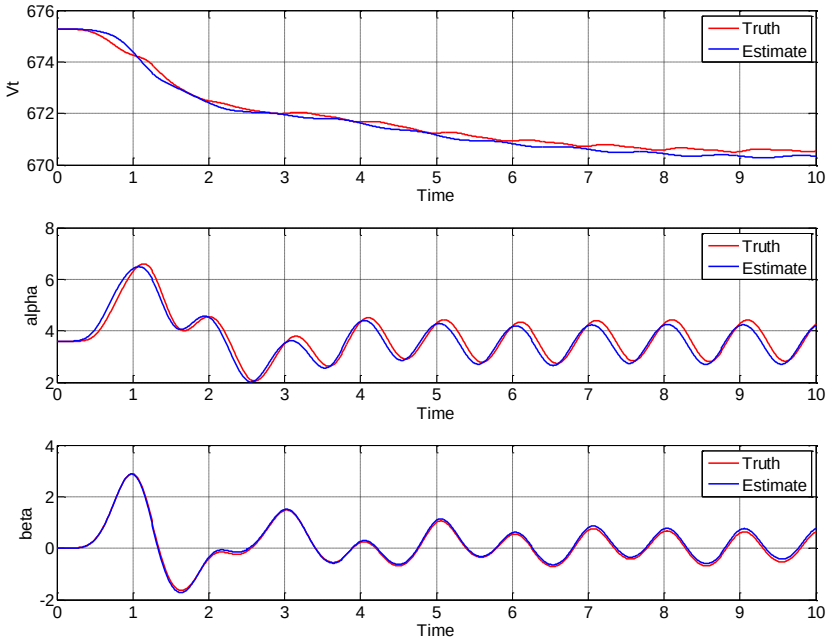

FIGURE 17: ATTITUDE MODEL SMALL INPUT AIR DATA COMPARISON

As expected each of the key parameters, particularly the attitude estimates, indicate excellent coordination with sensor measurements or simulation outputs. The model has proven to be effective at estimating the center-of-gravity without highly dynamic conditions.

4.3: AIR DATA MODEL RESULTS – LARGE INPUT

The second method for center-of-gravity estimation involves comparison of estimated parameters to available air data. Information required for this includes the total airspeed as well as an alpha and beta measurements giving the fully defined relative wind vector. Calculations based on estimated center-of-gravity location can be performed to create air data estimates.

Identical control inputs and models used in the attitude and GPS and INS model were applied to the air data model. Once again the inputs and aircraft response is highly dynamic and seen in Fig. 6. Here estimates of air data parameters including total velocity, alpha, and beta angles are used for comparison and to penalize the cost function in the optimization routine. Table 4 summarizes the resulting estimates and errors obtained from the air data estimation algorithm using simulated high performance vehicle inputs.

Parameter	Initial Estimate	Estimated Value	Actual Value	Error
X CG Location Estimate	20	26.8707	26.8731	-0.0024
Y CG Location Estimate	1	0	0	0
Z CG Location Estimate	5	7.5984	7.5407	0.0577
N_x Bias	0.04	0.03	0.03	0
N_y Bias	0.04	0.03	0.03	0
N_z Bias	0.04	0.0304	0.03	0.0004

TABLE 4: AIR DATA MODEL RESULTS SUMMARY

Once again, an accurate estimate of center-of-gravity location and accelerometer biases are obtained. Here again less integration and derivative operations are required for the calculations, and thus less numerical error may be expected.

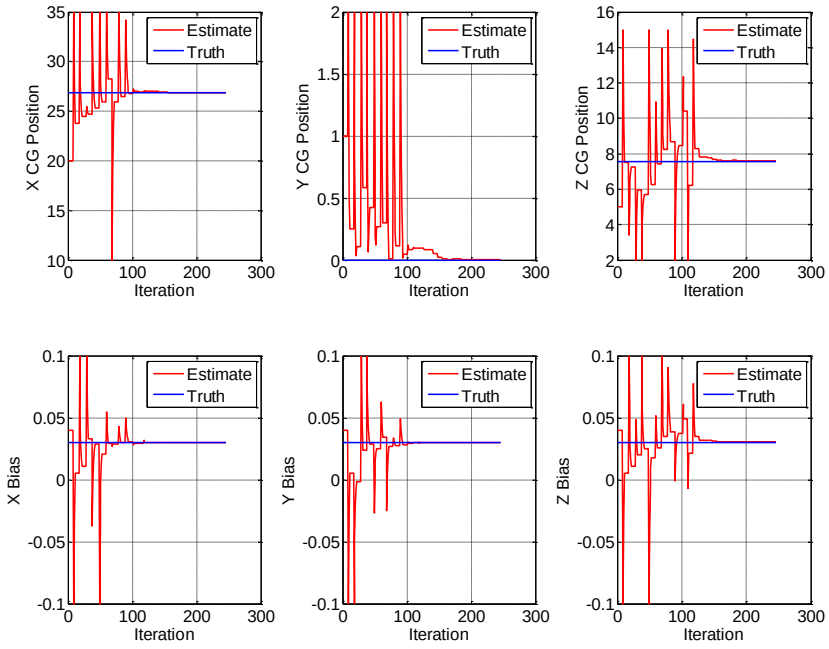

FIGURE 18: AIR DATA MODEL ITERATION IMPROVEMENT

Once again the algorithm has a chattering of accuracy before a final estimate is obtained. Estimates go through improvement and regression cycles inherent to optimization techniques. To ensure accurate estimates are obtained, comparison of real measurements to estimated values can be depicted. Figure 19 through Fig. 22 below show the comparison of numerous key parameters utilized during center-of-gravity estimation.

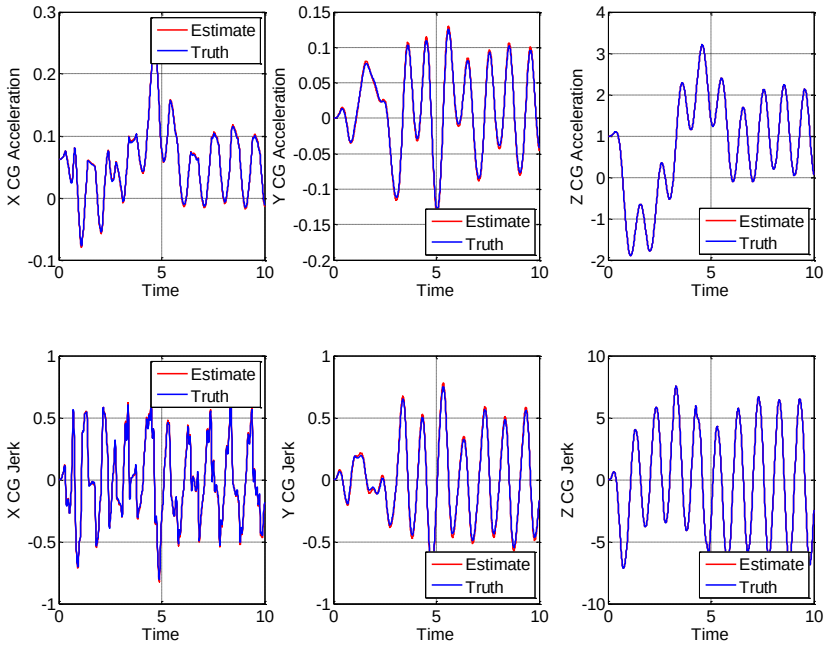

FIGURE 19: AIR DATA MODEL ACCELERATION AND JERK COMPARISON

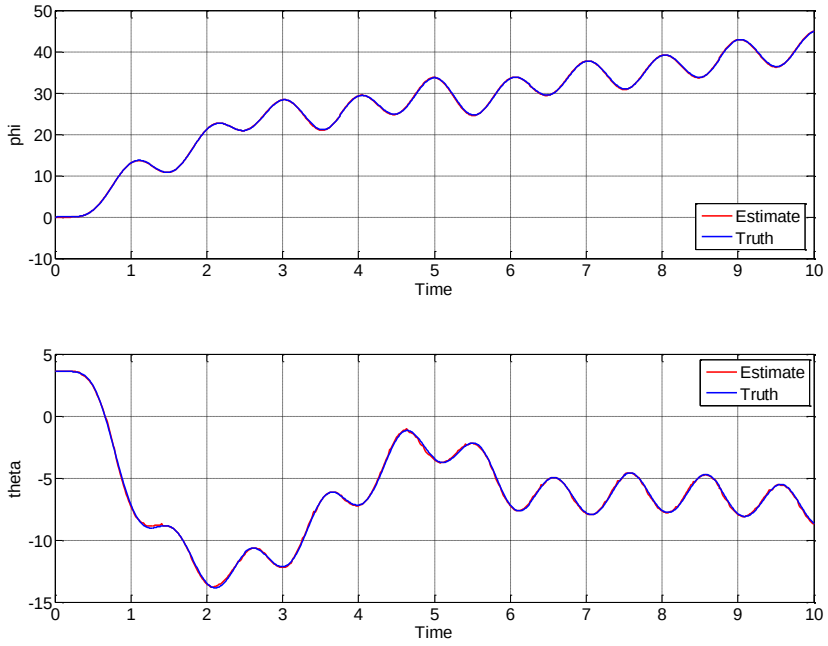

FIGURE 20: AIR DATA MODEL ATTITUDE COMPARISON

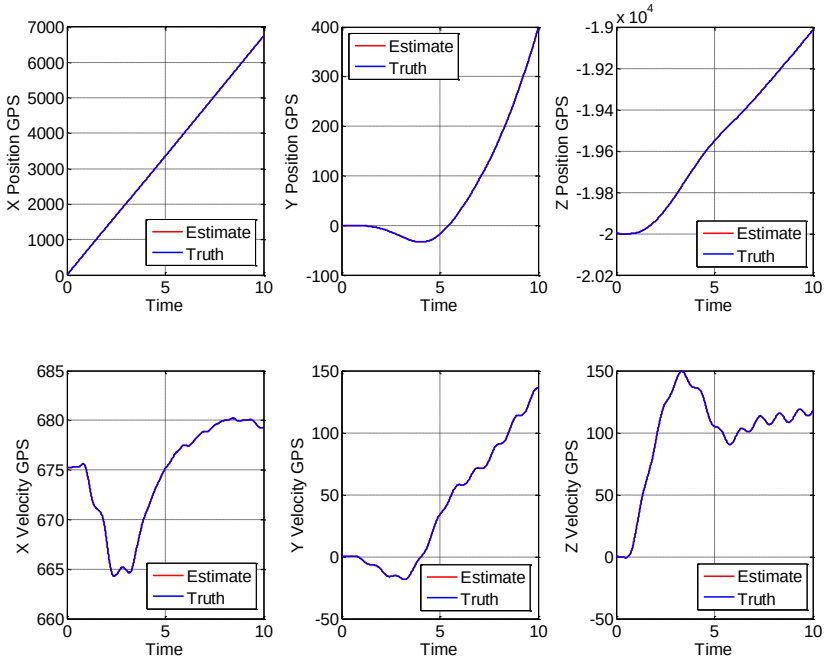

FIGURE 21: AIR DATA MODEL POSITION AND VELOCITY COMPARISON

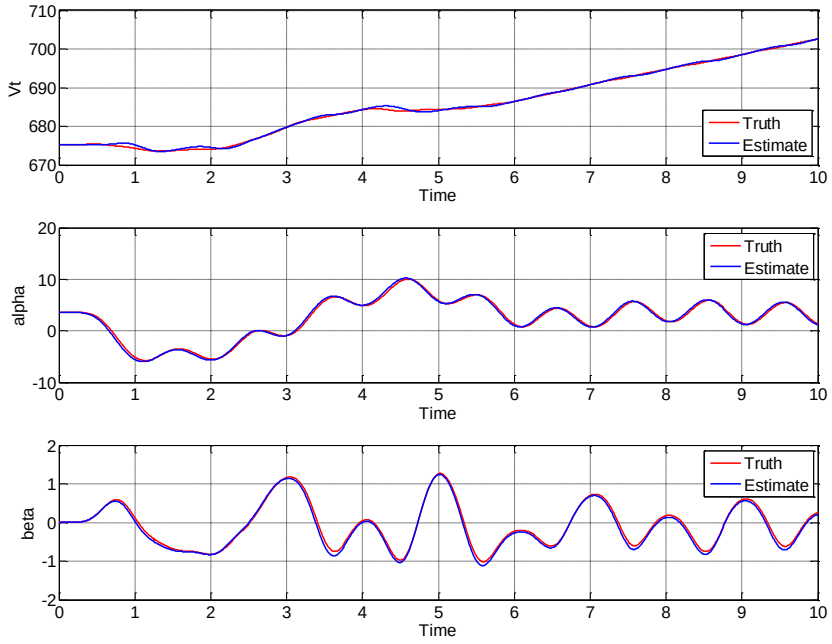

FIGURE 22: AIR DATA MODEL AIR DATA COMPARISON

Each comparison plot indicates adequate accuracy between estimates of parameters of the vehicle and actual values or measurements. Note that for the Air Data Model only total velocity, alpha, and beta angle estimates count towards calculating the cost for optimization purposes. Incorporation of other parameters to the cost function may allow for more accurate estimates and reduce potential error in center-of-gravity estimates due to sensor errors or malfunctions.

4.4: AIR DATA MODEL RESULTS – SMALL INPUT

The second model individually analyzed, the Air Data Model, is also investigated using the less dynamic conditions. The inputs are seen in Fig. 12 which then indicates a less extreme aircraft response to the given controls. The results of this simulation are found in Table 5.

Parameter	Initial Estimate	Estimated Value	Actual Value	Error
X CG Location Estimate	20	26.8486	26.8731	-0.0245
Y CG Location Estimate	1	0.0033	0	0.0033
Z CG Location Estimate	5	7.5407	7.5407	0
N_x Bias	0.04	0.03	0.03	0
N_y Bias	0.04	0.03	0.03	0
N_z Bias	0.04	0.03	0.03	0

TABLE 5: AIR DATA MODEL SMALL INPUT RESULTS SUMMARY

The results show great response to the lowered aircraft inputs as was the case in the first two models. It's noted that each algorithm displays similar characteristics in terms of the more and less accurate estimates for center-of-gravity location and accelerometer biases. The tracking of these estimates is depicted in Fig. 23.

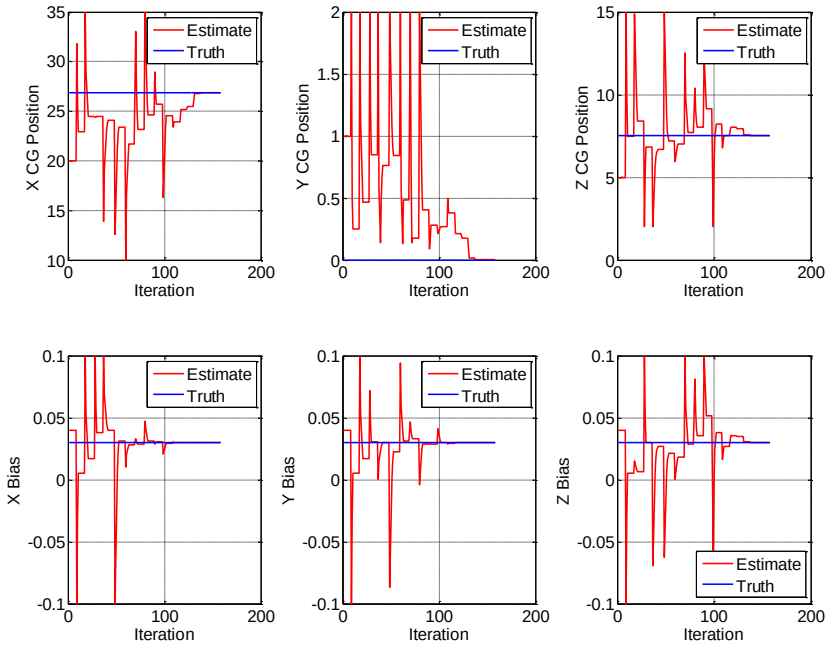

FIGURE 23: AIR DATA MODEL SMALL INPUT ITERATION IMPROVEMENT

The expected tracking and iteration improvements are observed. As a double-check, several key parameters and comparisons to their corresponding estimates are shown in Fig. 24 through Fig. 27.

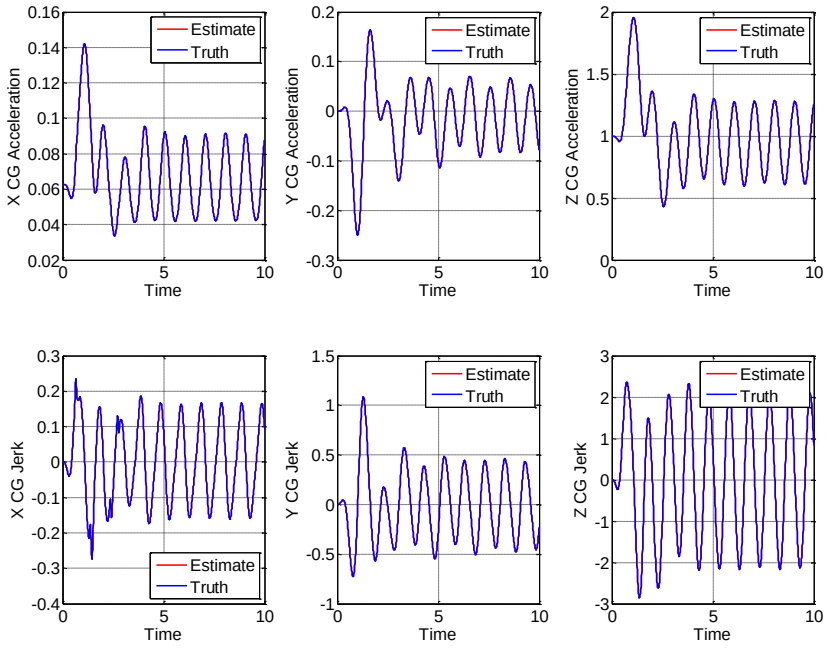

FIGURE 24: AIR DATA MODEL SMALL INPUT ACCELERATION AND JERK COMPARISON

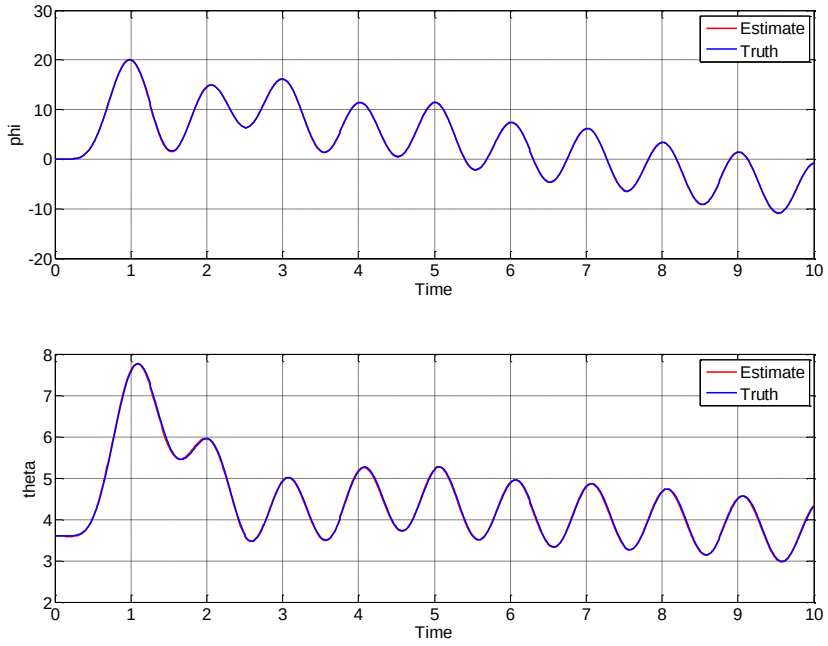

FIGURE 25: AIR DATA MODEL SMALL INPUT ATTITUDE COMPARISON

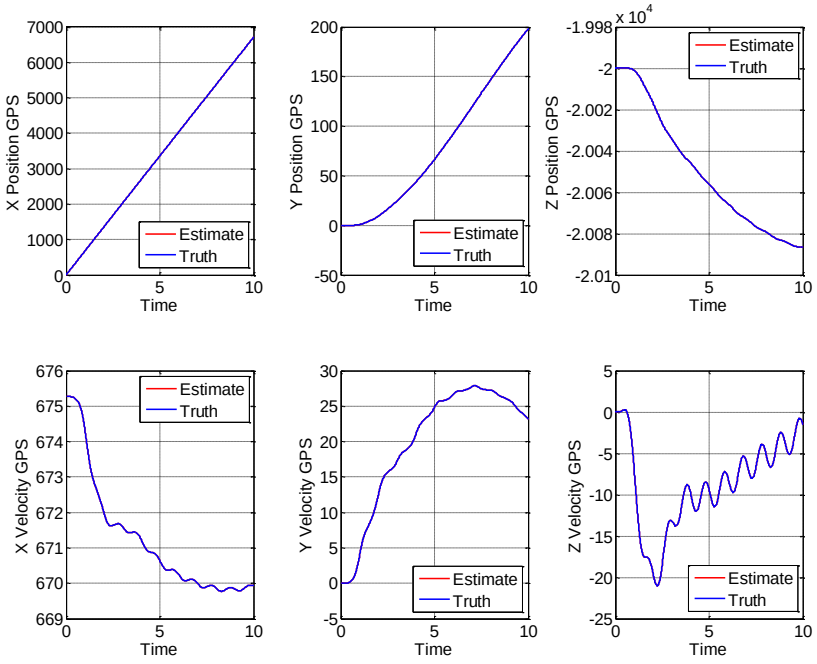

FIGURE 26: AIR DATA MODEL SMALL INPUT POSITION AND VELOCITY COMPARISON

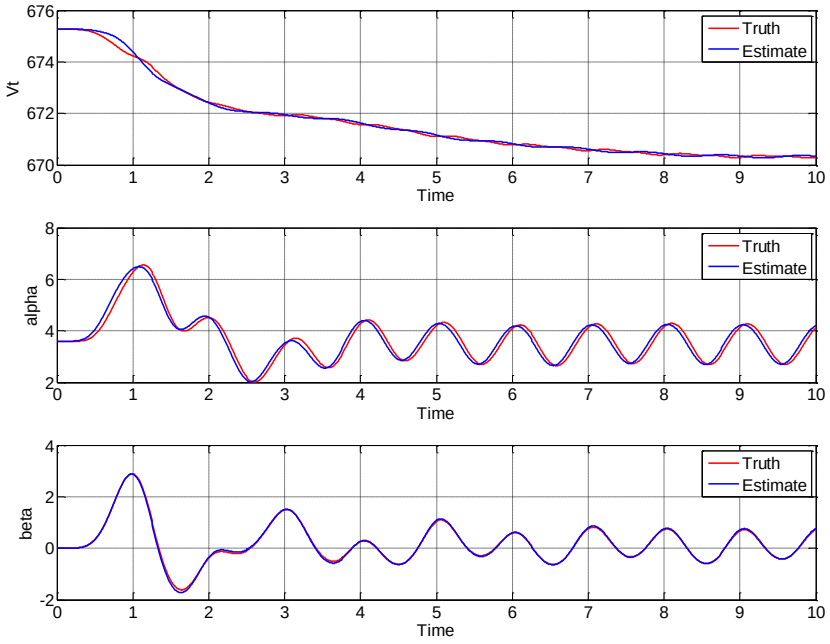

FIGURE 27: AIR DATA MODEL SMALL INPUT AIR DATA COMPARISON

The parameters each appear to correlate as expected with the air data parameters being the driving force behind changes and improvement in iterations. Each of the three models display adequate performance using the small input response measurements.

4.5: GPS AND INS MODEL RESULTS – LARGE INPUT

A third approach to center-of-gravity estimation involves comparison of estimated vehicle travel to Global Positioning System (GPS) and Inertial Navigation System (INS) information. The use of GPS and INS information in all methods of center-of-gravity estimation is not desired due regular loss of signal in some scenarios. Situations and locations exist that do not allow GPS technology and block GPS sensors. Accurate inertial systems are quite expensive and are not available on all commercial and military aircraft. The use of this algorithm is restricted to vehicles and data collection periods where reliable GPS and INS information are available.

Identical control inputs and models used in the attitude model were applied to the GPS and INS model. Once again the inputs and aircraft response are highly dynamic and seen in Fig. 6. Here estimates of position and velocity in the Earth-fixed coordinate system are used for comparison and to penalize the cost function in the optimization routine. Table 6 summarizes the resulting estimates and errors obtained from the GPS and INS estimation algorithm using simulated high performance vehicle inputs.

Parameter	Initial Estimate	Estimated Value	Actual Value	Error
X CG Location Estimate	20	26.8655	26.8731	-0.0076
Y CG Location Estimate	1	0	0	0
Z CG Location Estimate	5	7.5407	7.5407	0
N_x Bias	0.04	0.03	0.03	0
N_y Bias	0.04	0.03	0.03	0
N_z Bias	0.04	0.03	0.03	0

TABLE 6: GPS AND INS MODEL RESULTS SUMMARY

Here an improvement in center-of-gravity estimation is observed. The GPS and INS Model involves less numerical derivatives and integrals which inherently introduces added error to a calculation. Additionally, six parameters are used to create error signals rather than just two in the Attitude Model which provides an opportunity for higher accuracy. Figure 28 shows the change in center-of-gravity location with each iteration.

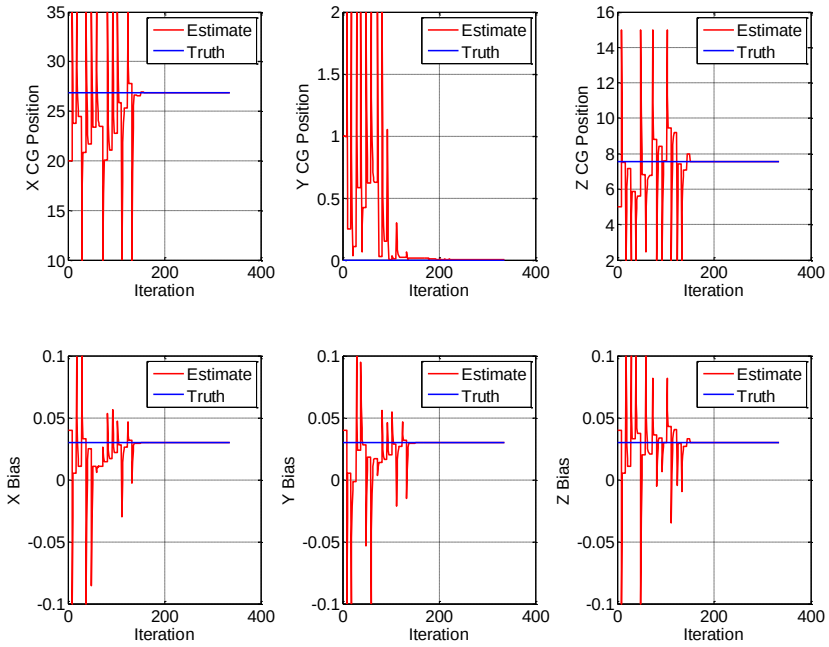

FIGURE 28: GPS AND INS MODEL ITERATION IMPROVEMENT

Once again the algorithm has a chattering of accuracy before a final estimate is obtained. Estimates go through improvement and regression cycles inherent to optimization techniques. To ensure accurate estimates are obtained, comparison of real measurements to estimated values can be depicted. Figure 29 through Fig. 32 below show the comparison of numerous key parameters utilized during the center-of-gravity estimation.

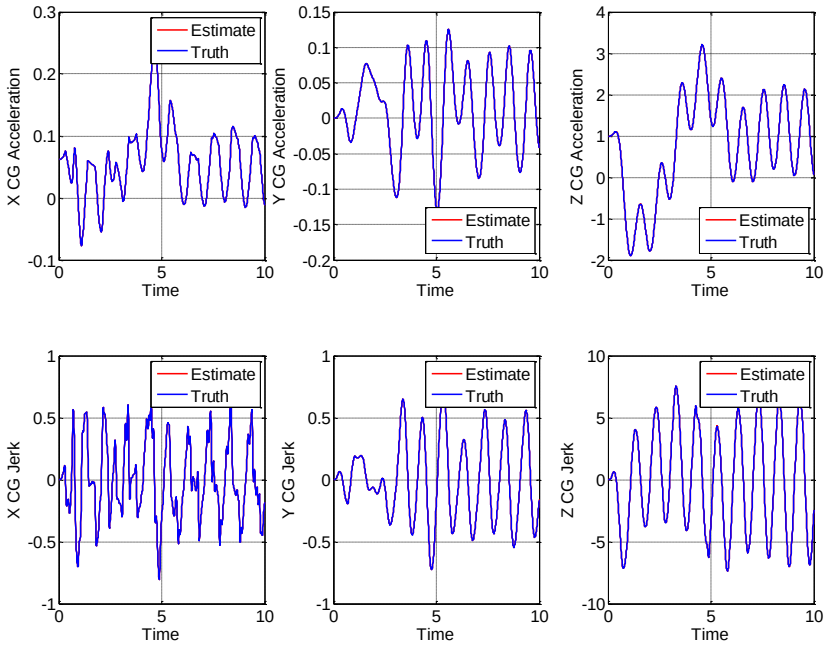

FIGURE 29: GPS AND INS MODEL ACCELERATION AND JERK COMPARISON

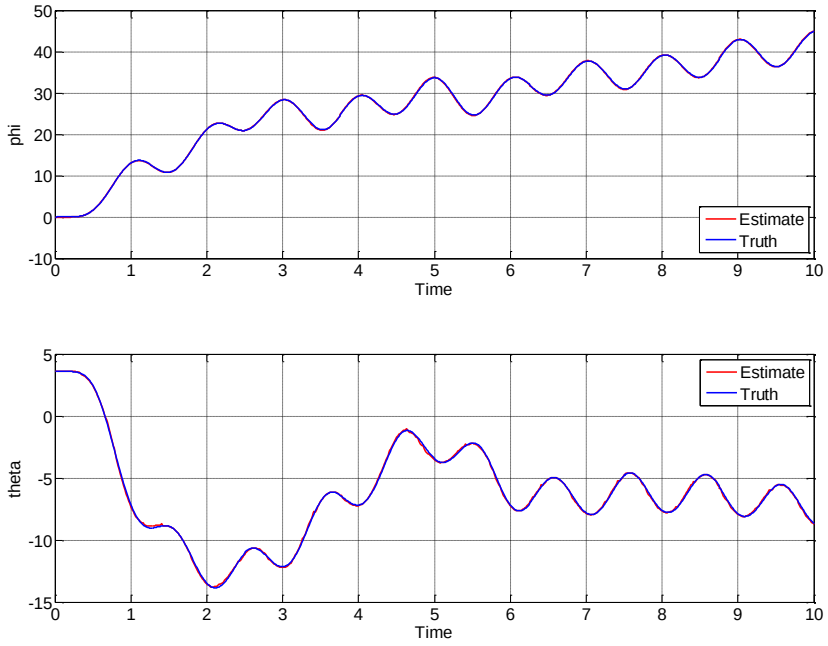

FIGURE 30: GPS AND INS MODEL ATTITUDE COMPARISON

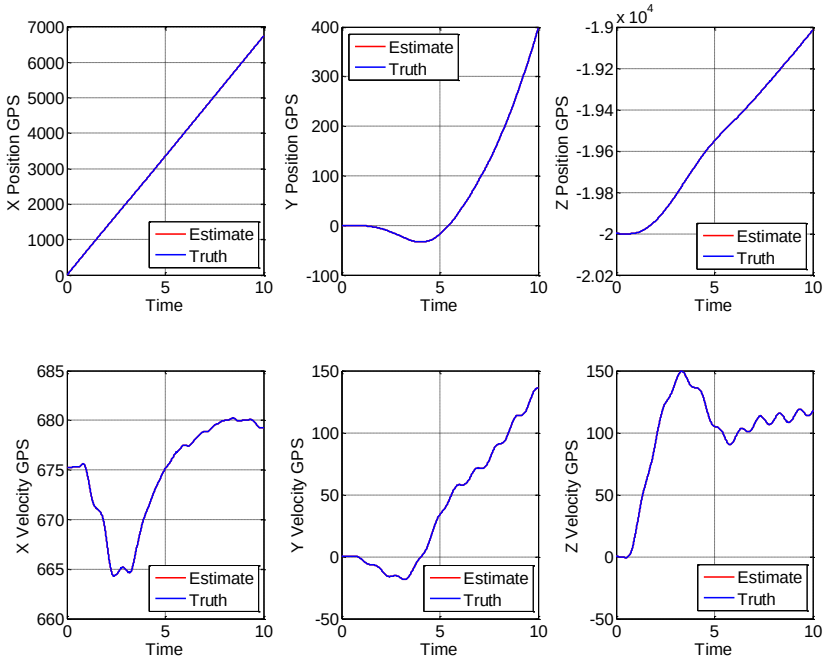

FIGURE 31: GPS AND INS MODEL POSITION AND VELOCITY COMPARISON

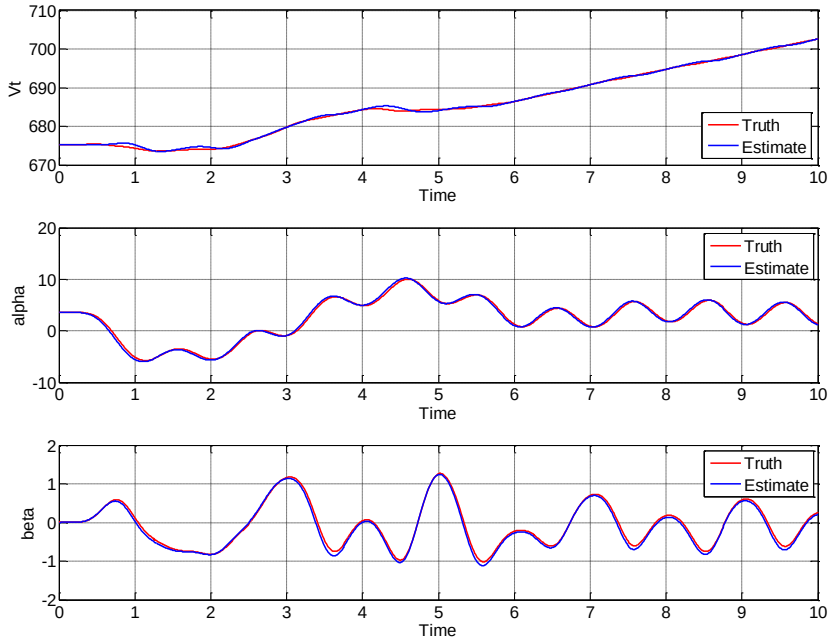

FIGURE 32: GPS AND INS MODEL AIR DATA COMPARISON

Each comparison plot indicates adequate accuracy between estimates of parameters of the vehicle and actual values or measurements. Note that for the GPS and INS Model only error between Earth-fixed position and velocity estimates count towards calculating the cost for optimization purposes. Incorporation of other parameters to the cost function may allow for more accurate estimates and reduce potential error in center-of-gravity estimates due to sensor errors or malfunctions. It should be noted again that GPS and INS information is not always available due to technologies that block GPS communications and unusual geographic locations. Reliance solely on the GPS and INS Model can be problematic in that respect.

4.6: GPS AND INS MODEL RESULTS – SMALL INPUT

The GPS and INS Model is tested using the small input aircraft response previously used. Figure 12 displays the control inputs and aircraft response to the less dynamic simulation. The function is performed to prove algorithm performance under less rigorous conditions. Table 7 shows the results from the simulation.

Parameter	Initial Estimate	Estimated Value	Actual Value	Error
X CG Location Estimate	20	26.8634	26.8731	-0.0097
Y CG Location Estimate	1	0.0024	0	0.0024
Z CG Location Estimate	5	7.5403	7.5407	-0.0004
N_x Bias	0.04	0.03	0.03	0
N_y Bias	0.04	0.03	0.03	0
N_z Bias	0.04	0.03	0.03	0

TABLE 7: GPS AND INS MODEL SMALL INPUT RESULTS SUMMARY

The results from simulation indicate excellent correlation as expected. The algorithm under investigation adequately performs under introduction to less dynamic conditions. The changes in center-of-gravity location estimate are shown in Fig. 33.

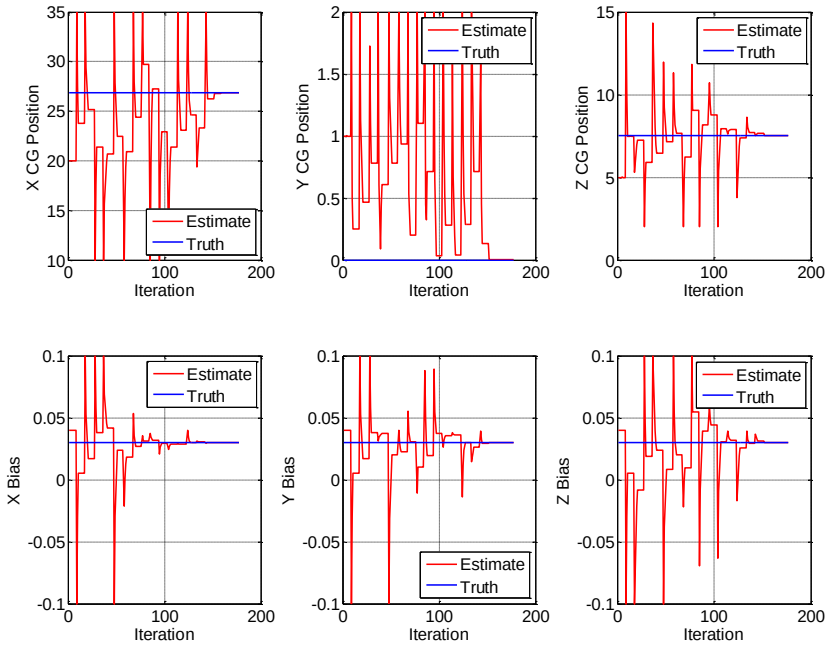

FIGURE 33: GPS AND INS MODEL SMALL INPUT ITERATION IMPROVEMENT

As expected chattering in estimates is seen during optimization, a characteristic of the optimization routine. To double check the validity of the solution obtained, Fig. 34 through Fig. 37 show the performance of key parameters and estimates using this new position.

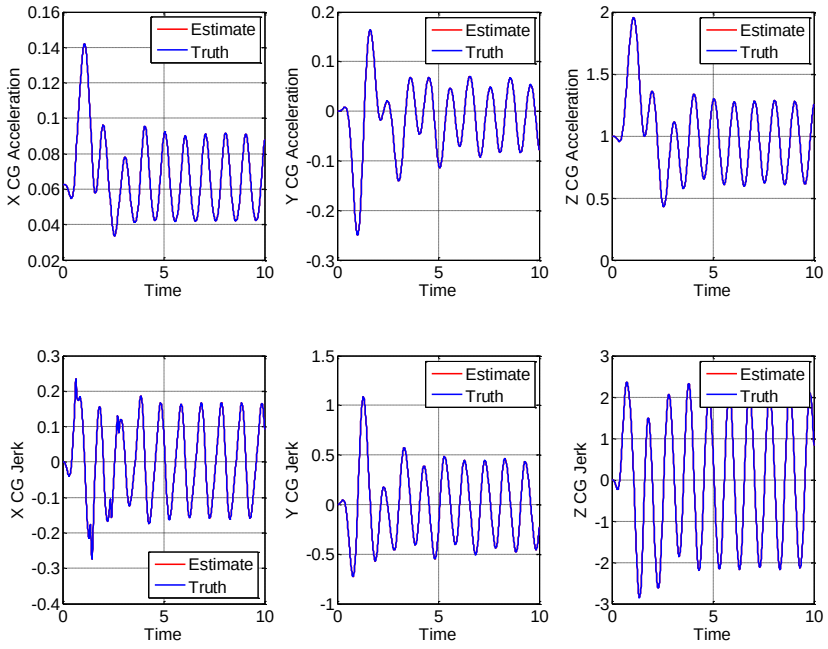

FIGURE 34: GPS AND INS MODEL SMALL INPUT ACCELERATION AND JERK COMPARISON

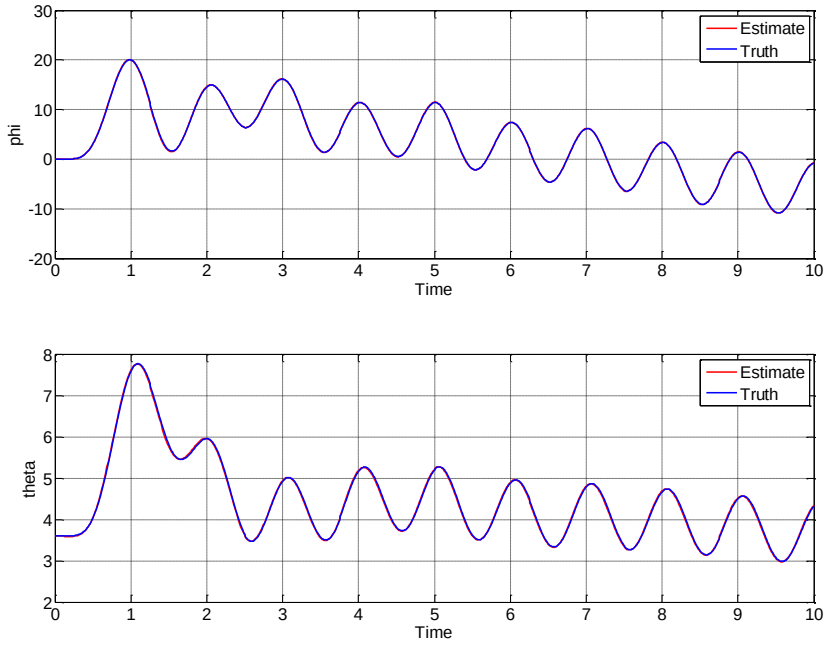

FIGURE 35: GPS AND INS MODEL SMALL INPUT ATTITUDE COMPARISON

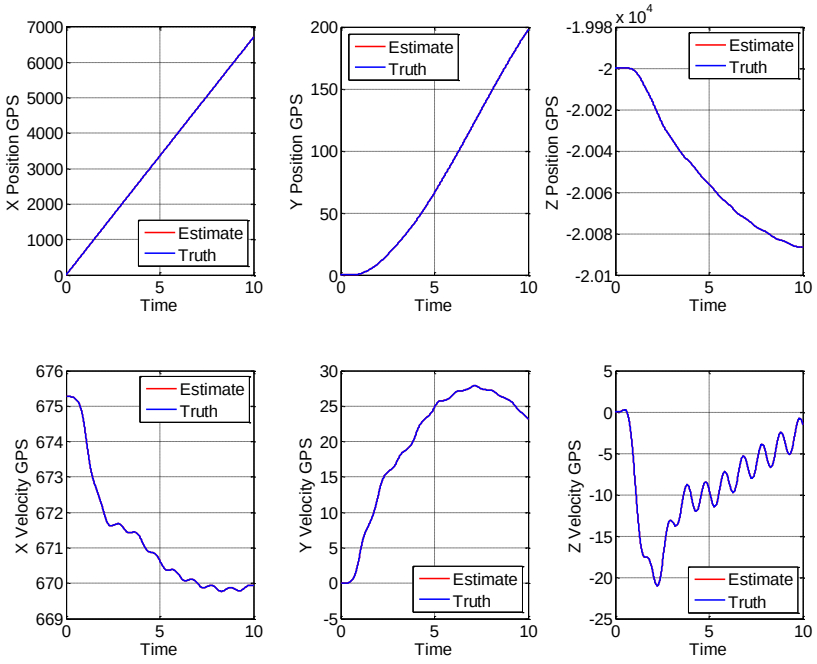

FIGURE 36: GPS AND INS MODEL SMALL INPUT POSITION AND VELOCITY COMPARISON

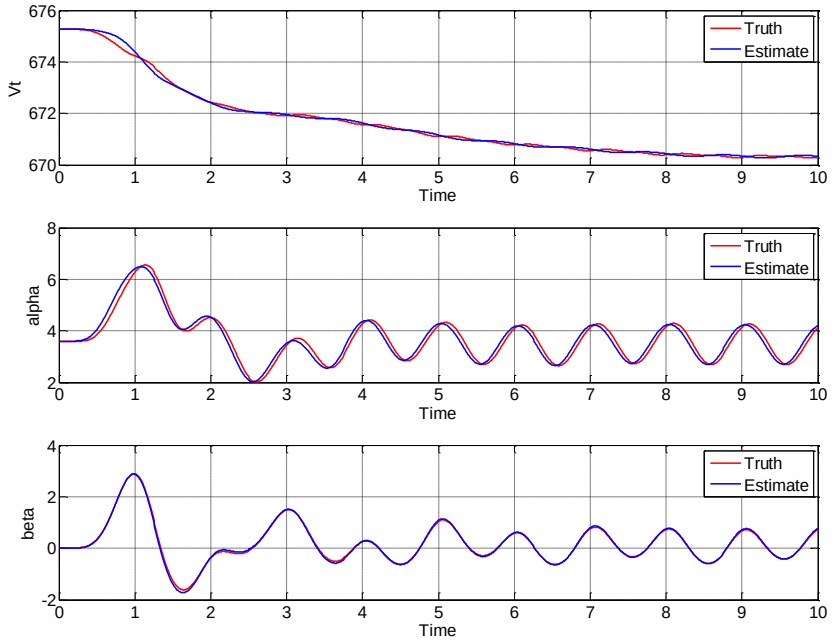

FIGURE 37: GPS AND INS MODEL SMALL INPUT AIR DATA COMPARISON

All the relevant parameters once again show great correlation and the performance of the algorithm is deemed successful at lower dynamic simulation cases. Here the position and velocity comparisons indicate the best correlation as they are the measurements used in cost function analysis.

4.7: Attitude and Air Data Model Results

The second model combination investigated is the Attitude Model and Air Data Models. Identical flight information obtained for the individual and first combined algorithm analysis is used. The results of the simulation are provided in Table 9. Tracking of the estimates during optimization is shown in Fig. 43.

Parameter	Initial Estimate	Estimated Value	Actual Value	Error
X CG Location Estimate	20	26.8688	26.8731	-0.0043
Y CG Location Estimate	1	0	0	0
Z CG Location Estimate	5	7.5069	7.5407	-0.0338
N_x Bias	0.04	0.03	0.03	0
N_y Bias	0.04	0.03	0.03	0
N_z Bias	0.04	0.0298	0.03	-0.0002

TABLE 8: ATTITUDE AND AIR DATA MODEL RESULTS SUMMARY

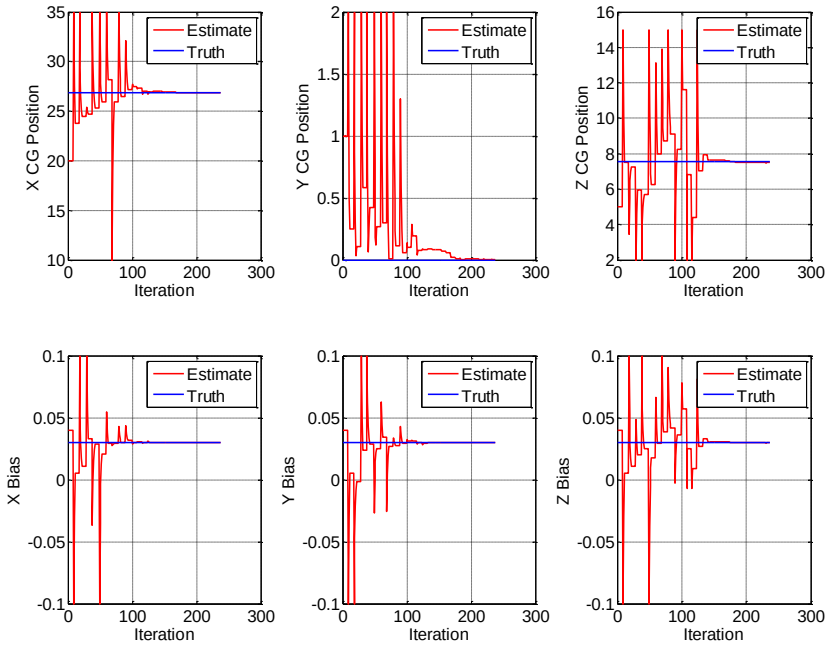

FIGURE 38: ATTITUDE AND AIR DATA MODEL ITERATION IMPROVEMENT

The results indicate consistent and accurate results for each estimated component as expected. Center-of-gravity location estimates are on par with previous analyses. Here a noticeably higher number of iterations were required for optimization settling. The increase could be an expected side effect of combining models in practice. The inclusion of additional terms to the error function results in not only more computations, but larger total cost magnitudes for the optimization routine which can require additional iterations for localizing the center-of-gravity. Figure 44 through Fig. 47 show the comparison of real and estimated parameters.

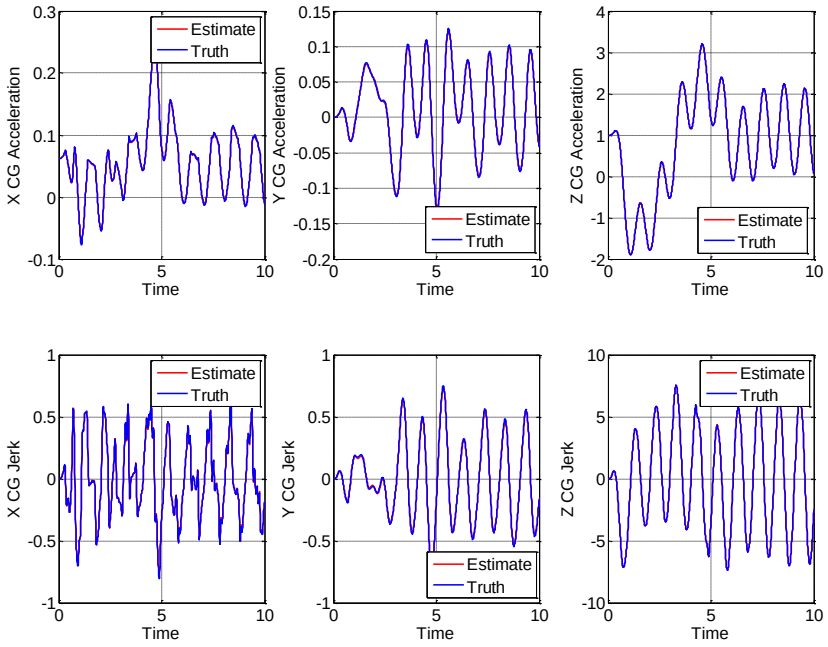

FIGURE 39: ATTITUDE AND AIR DATA MODEL ACCELERATION AND JERK COMPARISON

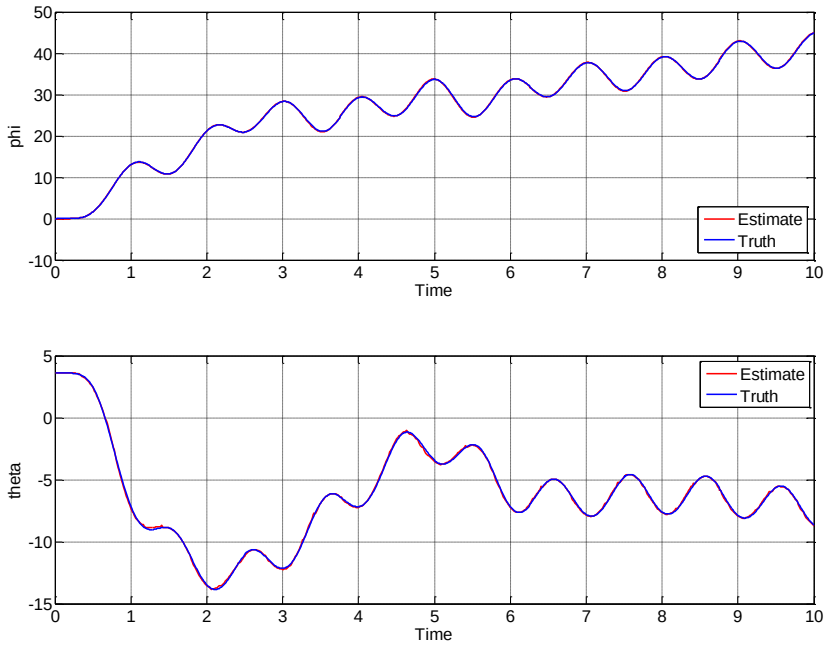

FIGURE 40: ATTITUDE AND AIR DATA MODEL ATTITUDE COMPARISON

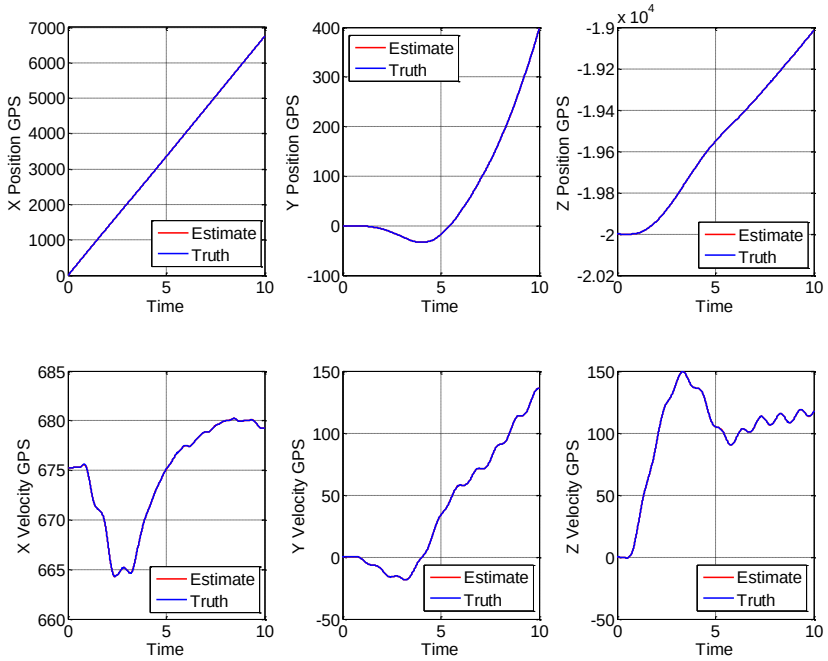

FIGURE 41: ATTITUDE AND AIR DATA MODEL POSITION AND VELOCITY COMPARISON

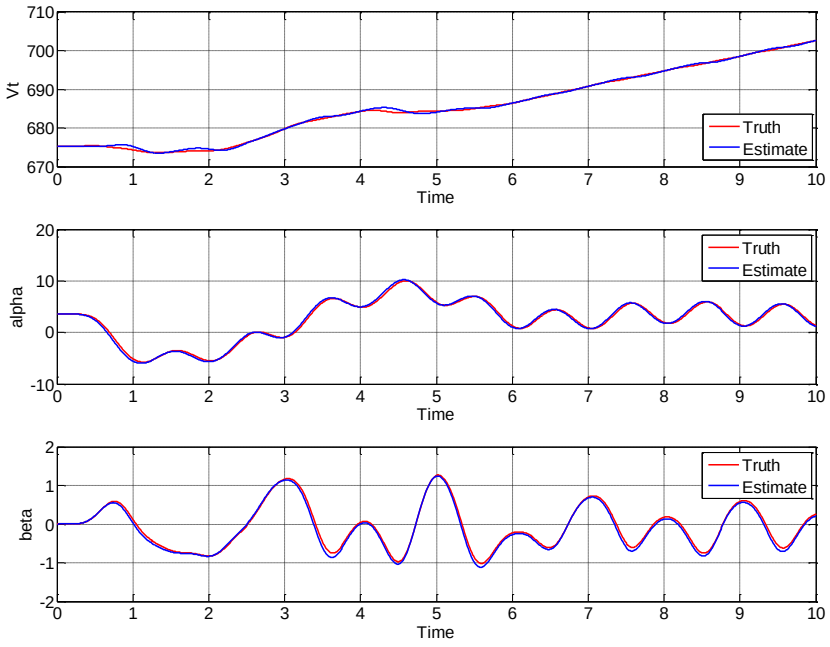

FIGURE 42: ATTITUDE AND AIR DATA MODEL AIR DATA COMPARISON

All parameters again indicate highly accurate estimates, particularly where the attitude and air data signals indicate excellent correlation. As expected, the combination of multiple models in the algorithm produces improved results for center-of-gravity estimation.

4.8: ATTITUDE AND GPS AND INS MODEL RESULTS

The benefits for developing multiple center-of-gravity estimation models lies not only in the varying conditions and sensor availability in an air vehicle, but also in the ability to combine models to produce potentially more accurate estimates. Through addition of their respective cost functions the models can be effectively used together. Though such an approach will increase complexity and computation time, it provides the capability of limiting the error caused by measurement device biases or noise, computational errors, or errant initial conditions.

The first combination investigated for model inclusion is the Attitude Model and GPS and INS Model. The combination of multiple models requires tuning of weighting factors placed on the error signals from each respective measurement. The requirement is apparent in the Air Data Model where the scale of certain measurements, particularly velocity, would dominate cost functions and become the driving factor in optimization. Weighting factors included here were intended to balance the emphasis of importance of each algorithm and error signal to the optimization technique.

The results of the first combined analysis are shown in Table 8. The results indicate improvement over the singular algorithm processing. The same data collection used for the three individual models is used again here for comparison.

Parameter	Initial Estimate	Estimated Value	Actual Value	Error
X CG Location Estimate	20	26.8656	26.8731	-0.0075
Y CG Location Estimate	1	0	0	0
Z CG Location Estimate	5	7.5403	7.5407	-0.0004
N_x Bias	0.04	0.03	0.03	0
N_y Bias	0.04	0.03	0.03	0
N_z Bias	0.04	0.03	0.03	0

TABLE 9: ATTITUDE AND GPS AND INS MODEL RESULTS SUMMARY

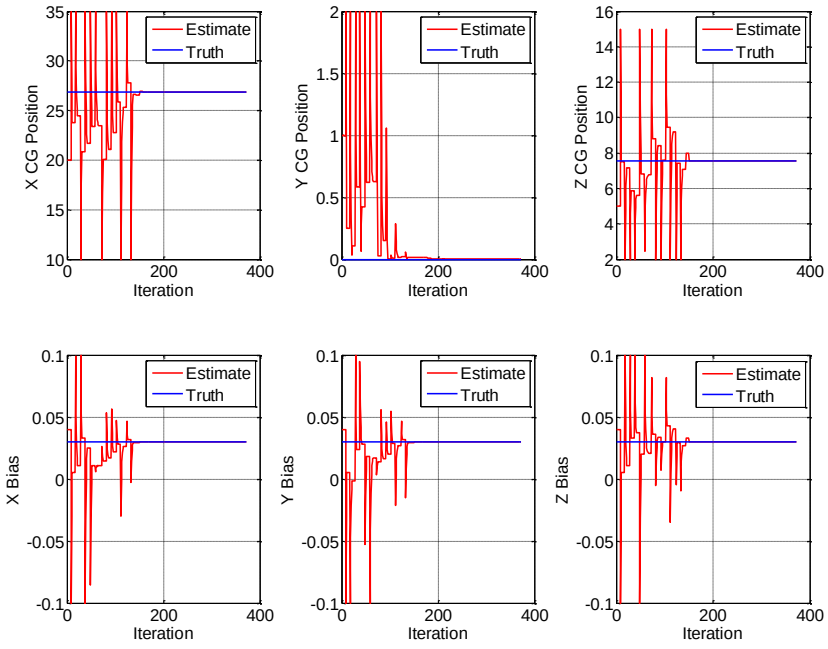

FIGURE 43: ATTITUDE AND GPS AND INS MODEL ITERATION IMPROVEMENT

Once again the algorithm has a chattering of accuracy before a final estimate is obtained. Estimates go through improvement and regression cycles inherent to optimization techniques. To ensure accurate estimates are obtained, comparison of real measurements to estimated values can be depicted. Figure 39 through Fig. 42 below show the comparison of numerous key parameters utilized during the center-of-gravity estimation.

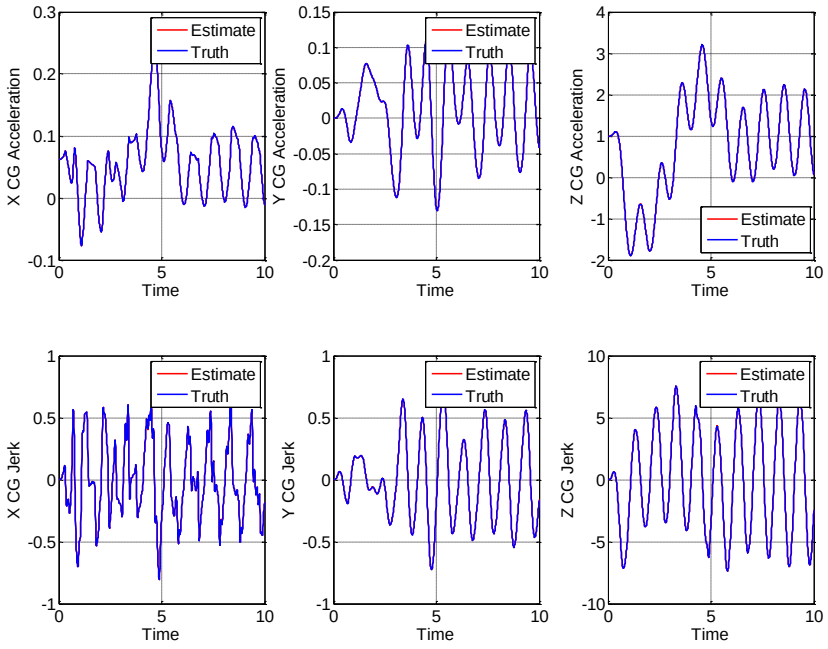

FIGURE 44: ATTITUDE AND GPS AND INS MODEL ACCELERATION AND JERK COMPARISON

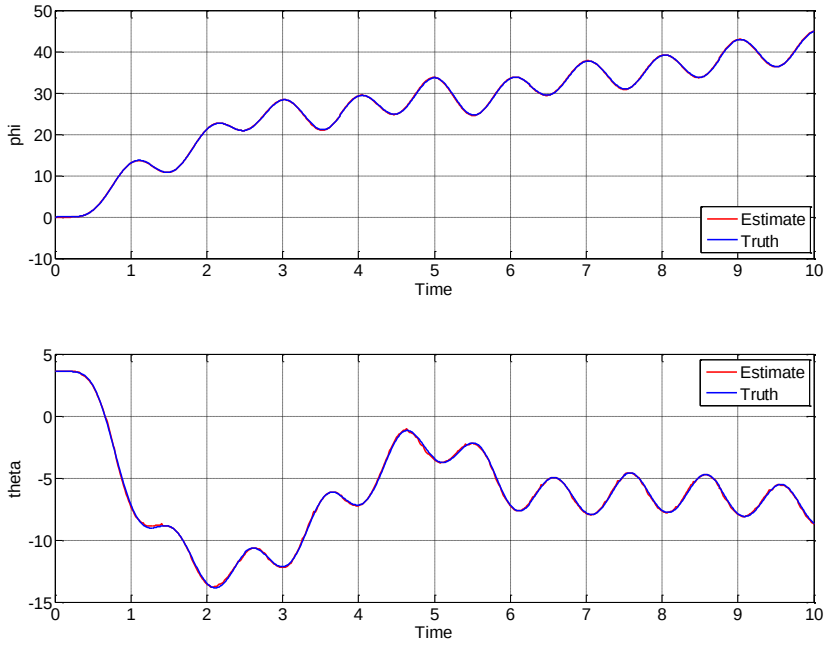

FIGURE 45: ATTITUDE AND GPS AND INS MODEL ATTITUDE COMPARISON

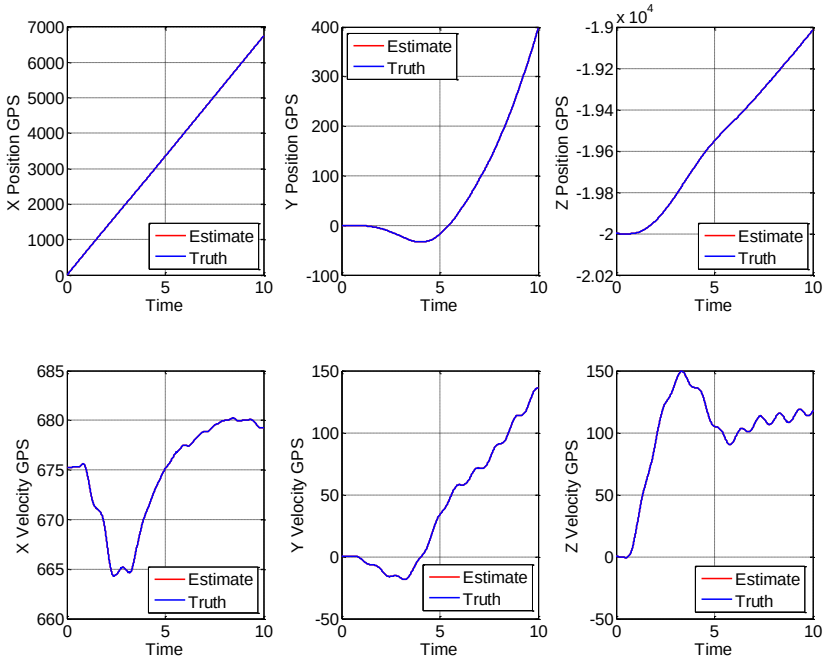

FIGURE 46: ATTITUDE AND GPS AND INS MODEL POSITION AND VELOCITY COMPARISON

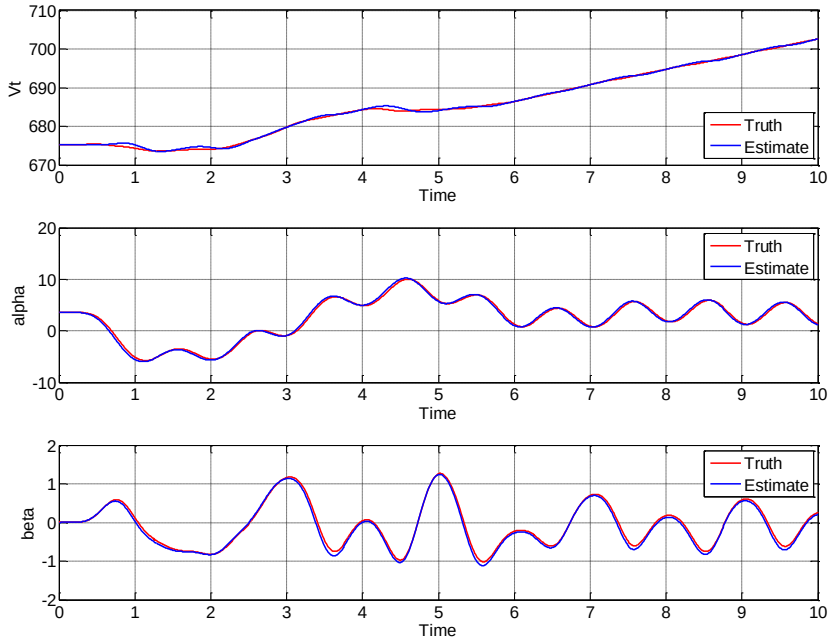

FIGURE 47: ATTITUDE AND GPS AND INS MODEL AIR DATA COMPARISON

Similar to the previous results all parameters show adequate correspondence to the actual parameter measurements from simulation. The combined algorithm is more robust however, due to the inclusion of more error signals to the evaluation. Due to the added sensor comparisons, errant signals in practice will have less impact on the final estimate than with a single algorithm.

4.9: ATTITUDE, GPS AND INS, AND AIR DATA MODEL RESULTS – LARGE INPUT

The end goal of the models proposed and tested is to utilize all three when measurement sensors are available for a highly robust and accurate center-of-gravity algorithm. The combination of all three requires the most computation in practice, but contains the possibility of minimizing the errors from inaccurate sensors. With tuned weighting of the error signals of each algorithm studied, center-of-gravity location and accelerometer biases were estimated. Table 10 and Fig. 48 show the results from the combined simulation using the simulation results depicted in Fig. 6.

Parameter	Initial Estimate	Estimated Value	Actual Value	Error
X CG Location Estimate	20	26.8679	26.8731	-0.0052
Y CG Location Estimate	1	0	0	0
Z CG Location Estimate	5	7.5401	7.5407	-0.0006
N_x Bias	0.04	0.03	0.03	0
N_y Bias	0.04	0.03	0.03	0
N_z Bias	0.04	0.03	0.03	0

TABLE 10: ATTITUDE, GPS AND INS, AND AIR DATA MODEL RESULTS SUMMARY

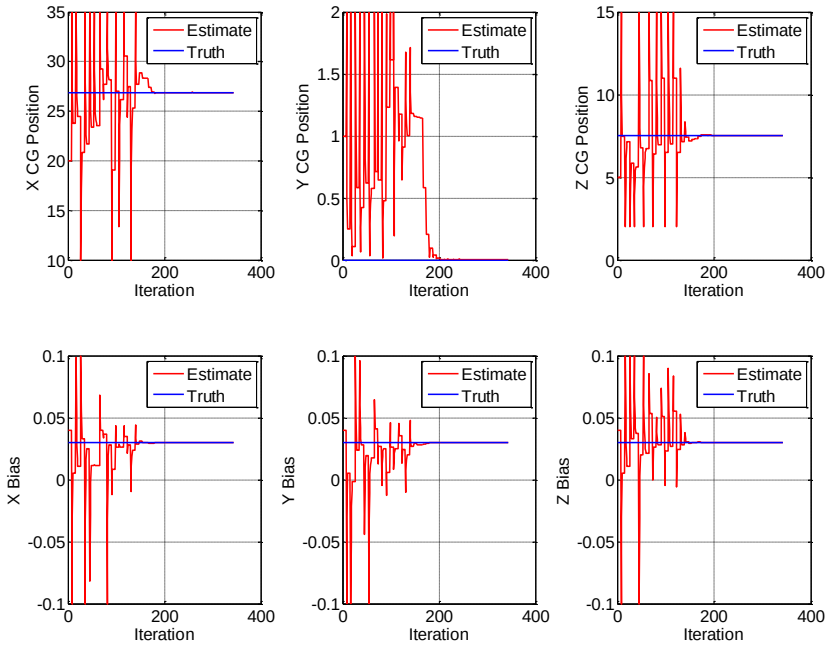

FIGURE 48: ATTITUDE, GPS AND INS, AND AIR DATA MODEL ITERATION IMPROVEMENT

Here the best balance of accuracy between each direction of center-of-gravity estimates and accelerometer biases is observed as anticipated. Again a higher number of iterations in the optimization routine were required. Though significantly more computations are needed for this algorithm, the best center-of-gravity estimation performance is observed. Figure 49 through Fig. 52 show the correlation of each parameter in comparison to estimates created through the algorithm.

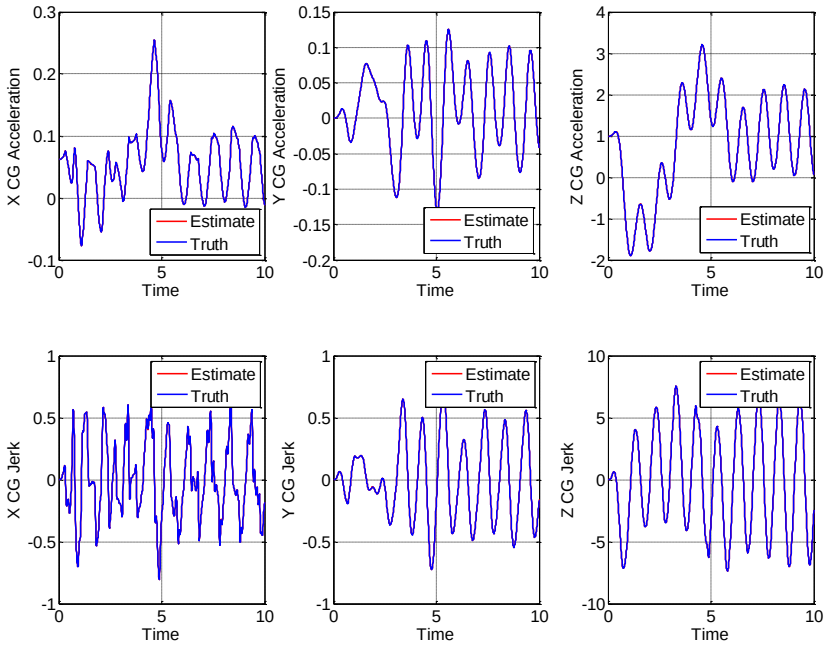

FIGURE 49: ATTITUDE, GPS AND INS, AND AIR DATA MODEL ACCELERATION AND JERK COMPARISON

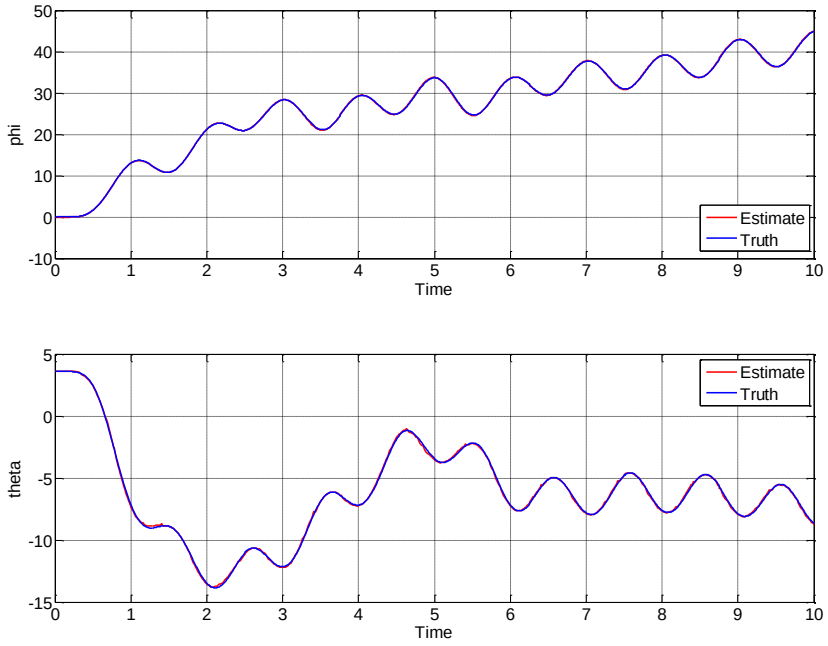

FIGURE 50: ATTITUDE, GPS AND INS, AND AIR DATA MODEL ATTITUDE COMPARISON

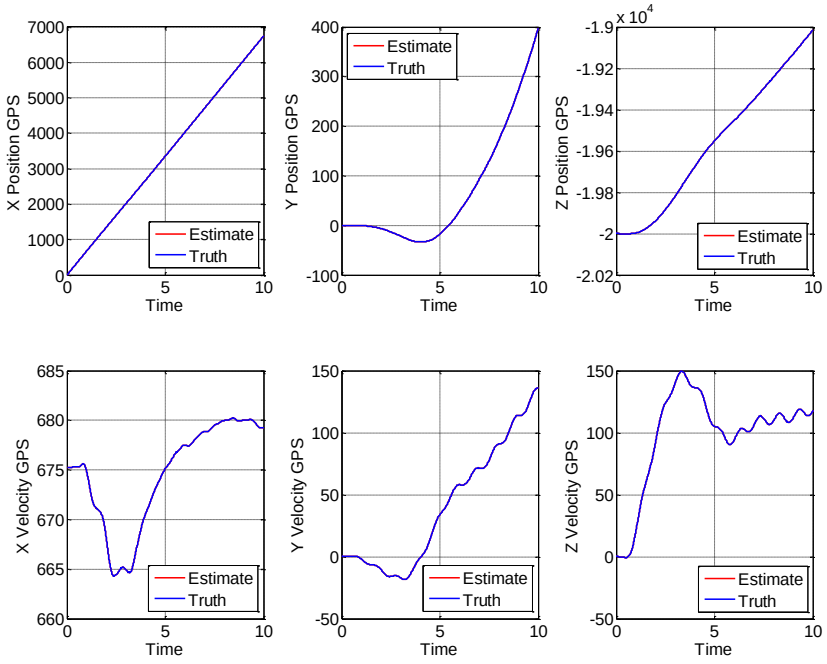

FIGURE 51: ATTITUDE, GPS AND INS, AND AIR DATA MODEL POSITION AND VELOCITY COMPARISON

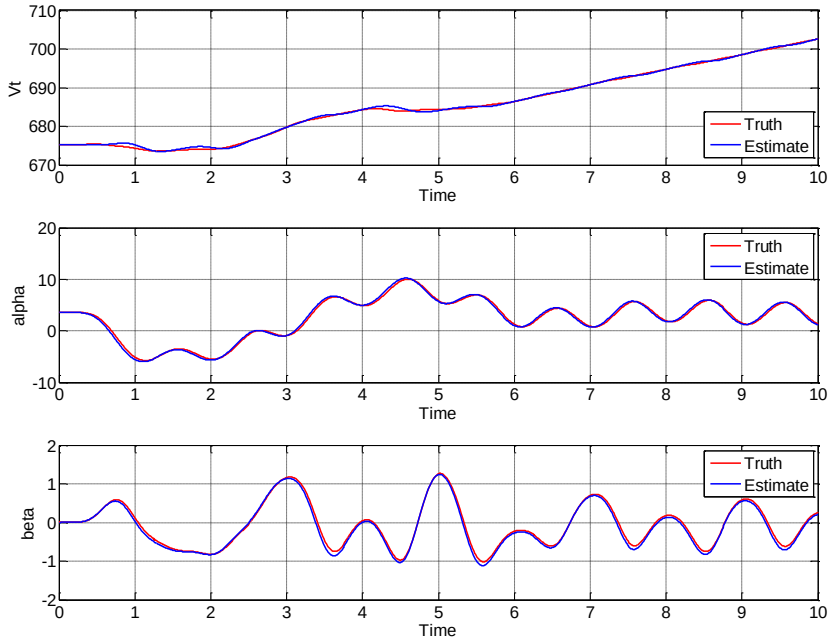

FIGURE 52: ATTITUDE, GPS AND INS, AND AIR DATA MODEL AIR DATA COMPARISON

Here all parameters tracked in simulation indicate excellent correspondence to real values collected from the simulation. The combined setup would be the ideal use of the information available, to incorporate all the commonly available sensors and information into a single, robust system.

4.10: Attitude, GPS and INS, and Air Data Model Results – Small Input

The combination of all three models into one algorithm is additionally tested using the smaller input data collection utilized in the three individual algorithm analyses. The aircraft inputs and responses are shown in Fig. 12. The results from this simulation are summarized in Table 11.

Parameter	Initial Estimate	Estimated Value	Actual Value	Error
X CG Location Estimate	20	26.8586	26.8731	-0.0145
Y CG Location Estimate	1	0.0024	0	0.0024
Z CG Location Estimate	5	7.5405	7.5407	-0.0002
N_x Bias	0.04	0.03	0.03	0
N_y Bias	0.04	0.03	0.03	0
N_z Bias	0.04	0.03	0.03	0

TABLE 11: ATTITUDE, GPS AND INS, AND AIR DATA MODEL SMALL INPUT RESULTS SUMMARY

As shown, the combined algorithm once again outperforms the used of the singular models overall. Each parameter is estimated with a high degree of accuracy. Figure 53 shows the changes to center-of-gravity and bias estimates throughout the optimization routine.

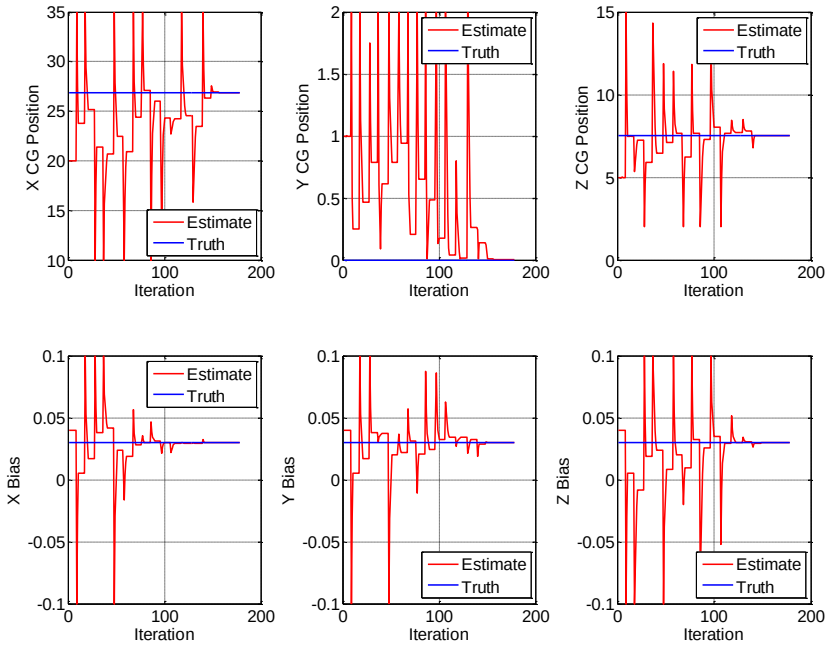

FIGURE 53: ATTITUDE, GPS AND INS, AND AIR DATA MODEL SMALL INPUT ITERATION IMPROVEMENT

Again a significantly higher number of iterations is required in comparison to earlier single algorithm operations. Each parameter can visually reach a highly accurate final estimate. To display the accuracy of the algorithm, Fig. 54 through Fig. 57 show the correspondence of estimated parameters to simulation values obtained including potential measurements.

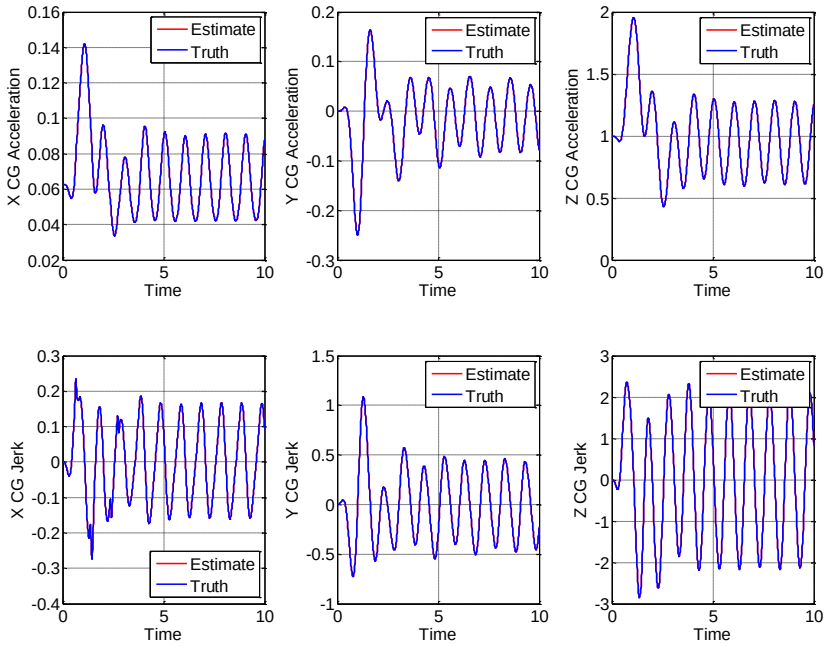

FIGURE 54: ATTITUDE, GPS AND INS, AND AIR DATA MODEL SMALL INPUT ACCELERATION AND JERK COMPARISON

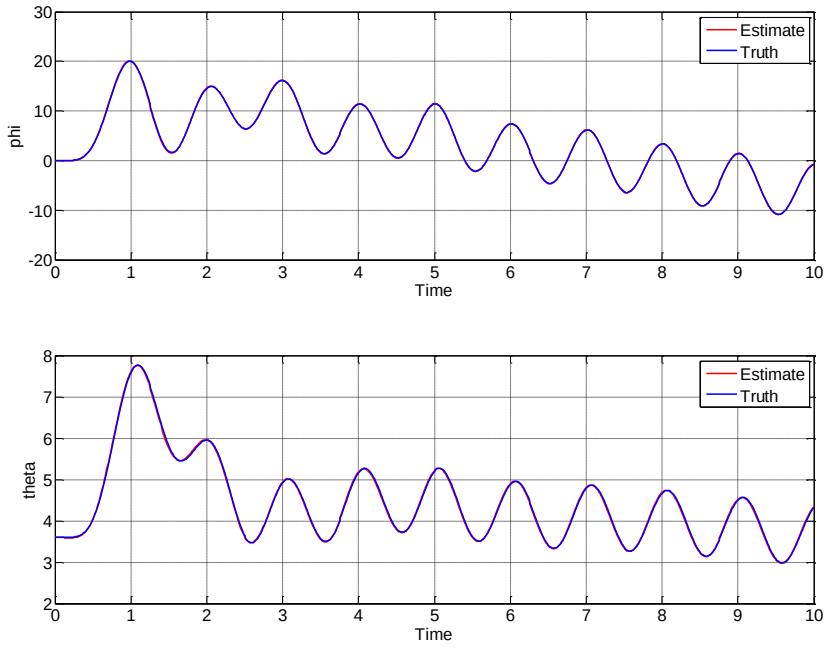

FIGURE 55: ATTITUDE, GPS AND INS, AND AIR DATA MODEL SMALL INPUT ATTITUDE COMPARISON

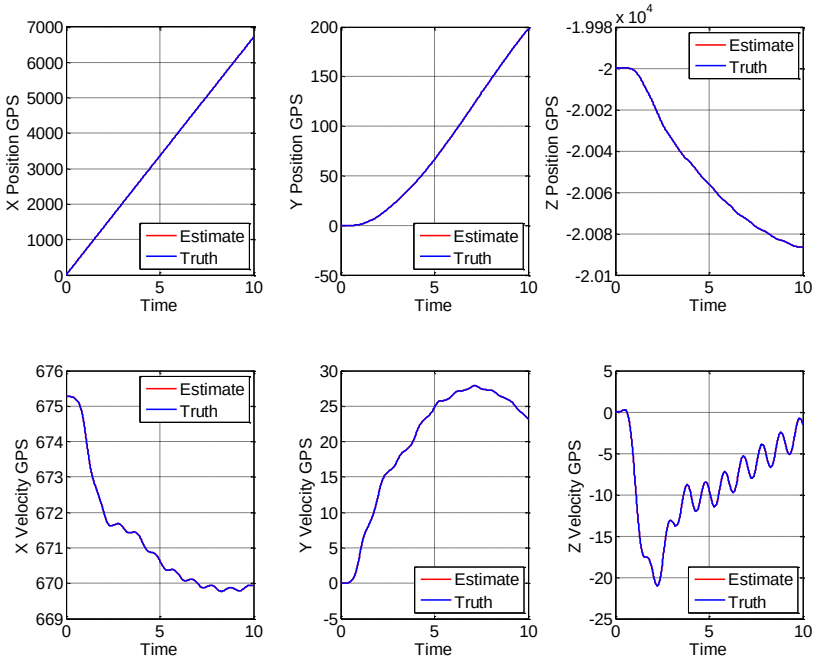

FIGURE 56: ATTITUDE, GPS AND INS, AND AIR DATA MODEL SMALL INPUT POSITION AND VELOCITY COMPARISON

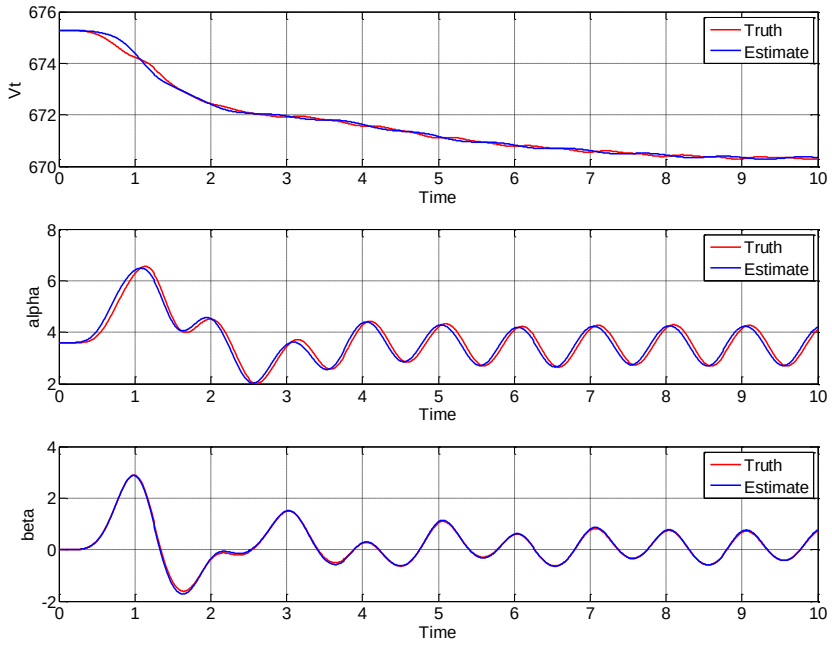

FIGURE 57: ATTITUDE, GPS AND INS, AND AIR DATA MODEL SMALL INPUT AIR DATA COMPARISON

Here as all the models are used in combination and properly weighted, each parameter shows spectacular correspondence to simulation truth values which is expected. Each of the algorithm's error signals are incorporated to the cost functions. The results indicate that the anticipated final use of the technology should be applicable to nearly all flight scenarios including those with less dynamic conditions as seen here.

4.11: Simulation Results Comparison

The comparison of performance between each studied combination and singular algorithm is important to denote the most ideal system to use. Performance in actual use may vary from plane to plane based on accuracy and collection rate of the sensors available, as well as typical conditions experienced by the aircraft. Table 12 shown portrays the accuracy of parameter estimation for the simulations conducted. Note that identical flight data, collection periods, initial estimates, and truth parameters were used in each simulation corresponding to the large and small flight response collections.

Parameter	X CG Error	Y CG Error	Z CG Error	N_x Bias Error	N_y Bias Error	N_z Bias Error
Attitude Only - Large	0.089	0.0085	-0.3711	-	-	-
Attitude Only - Small	0.1223	0.1994	-0.4559	-	-	-
Air Data Only - Large	-0.0024	0	0.0577	0	0	0.0004
Air Data Only - Small	-0.0245	0.0033	0	0	0	0
GPS and INS Only - Large	-0.0076	0	0	0	0	0
GPS and INS Only - Small	-0.0097	0.0024	-0.0004	0	0	0
Attitude and Air Data	-0.0043	0	-0.0338	0	0	-0.0002
Attitude and GPS and INS	-0.0075	0	-0.0004	0	0	0
Attitude, Air Data, and GPS and INS - Large	-0.0052	0	-0.0006	0	0	0
Attitude, Air Data, and GPS and INS - Small	-0.0145	0.0024	-0.0002	0	0	0

TABLE 12: SIMULATION RESULTS COMPARISON

As observed through this comparison of estimates of center-of-gravity produced, the combined algorithm appears to have the best performance all around in parameter estimation. It's clear that certain models contain improved estimates for different locations and biases estimated. Overall, the algorithm has proven successful through simulation testing.

CHAPTER 5: FLIGHT DATA RESULTS

The models investigated were also tested using real flight data collected from a high performance military type jet aircraft. The operation is performed similar to realistic flight situations where data is collected in batches and post processed for center-of-gravity estimates. The flight data is incorporated in a modified Matlab® code using the same processes as outlined in the simulation flight data. It should be noted that for the aircraft from which the data was collected, a precise center-of-gravity location is not known. The initial estimate used in the optimization routine is the previous location of the center-of-gravity prior to significant changes to the airframe. The addition of ballast to the front of the aircraft and an upgrade to a lighter engine in the rear significantly shifted the center-of-gravity location following determination of those previous estimates. Processing results are expected to reflect these movements.

The collection period for the vehicle spans over two minutes of various flight maneuvers. The units for all responses are standard for each plot included in the results: input control surfaces are in degrees, Euler angles are in degrees, rotational rates are in degrees per second, center-of-gravity location estimates are in feet, accelerometer measurements are in feet per second squared, and air data angles are in degrees. The control inputs for this time duration are shown in Fig. 58. Plots displaying accelerometer readings at a location near the pilot are shown in Fig. 59 for the entire flight collection.

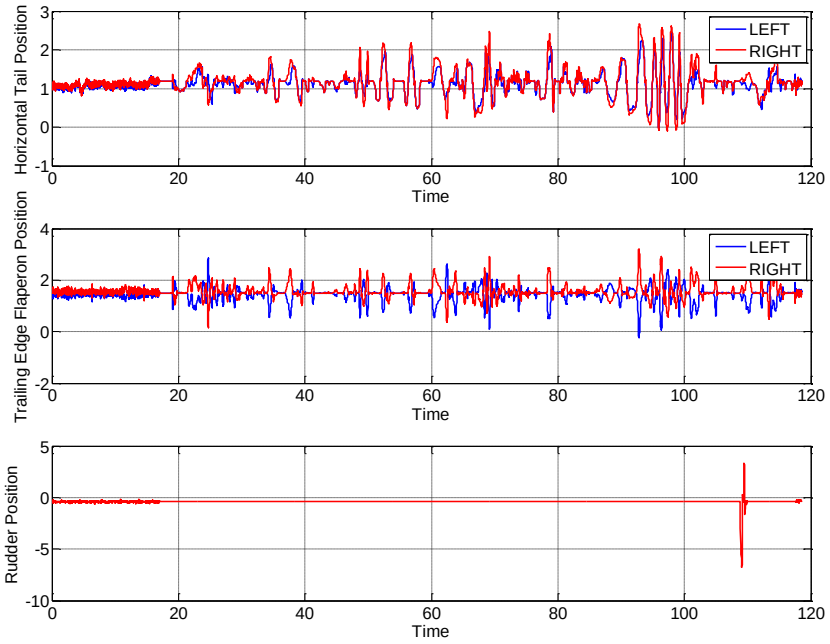

FIGURE 58: FLIGHT DATA CONTROL INPUTS

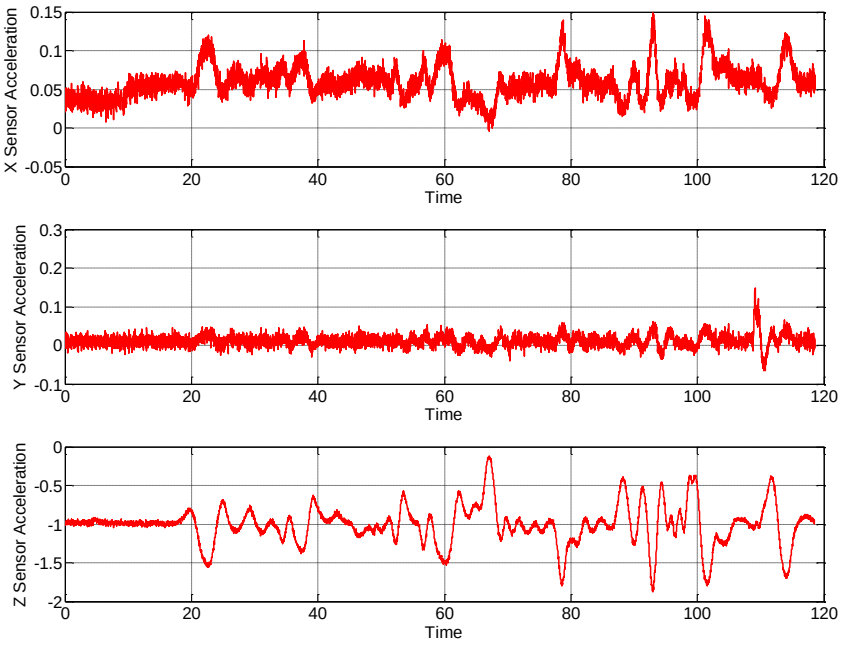

FIGURE 59: FLIGHT DATA FULL AIRCRAFT RESPONSE ACCELEROMETERS

Twenty seconds of the data is cut out and randomly selected for processing in the algorithm. Some measured parameters showing aircraft response to the conditions including accelerometer readings, Euler angles, and rotational rates are shown in Fig. 60 and Fig. 61.

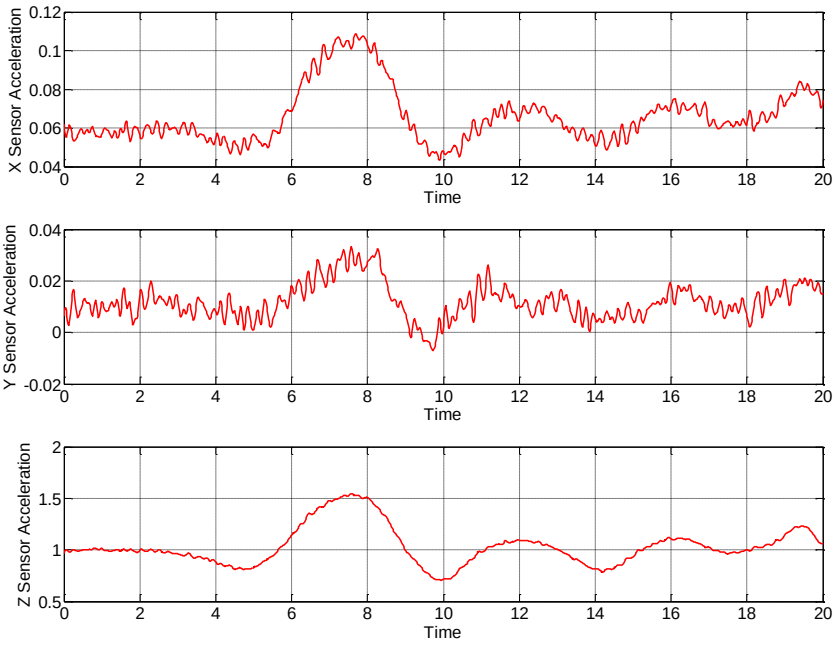

FIGURE 60: FLIGHT DATA AIRCRAFT RESPONSE ACCELEROMETERS

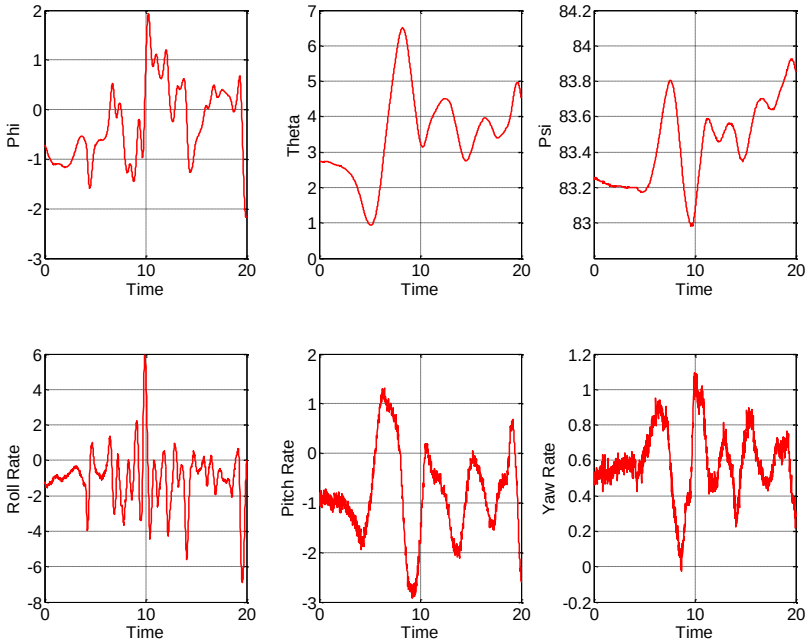

FIGURE 61: FLIGHT DATA AIRCRAFT RESPONSE

5.1: ATTITUDE MODEL FLIGHT DATA RESULTS

The first study performed using the available flight data is the Attitude Model. To perform this previous code developed is modified to incorporate the processed realistic flight data, first using the Euler Model process. Following proper preprocessing of the data to obtain truth signals and accurate roll rate estimates, the sensor data is fed through the algorithm. The primary difference between this model and the second two models is the inconsistency in accelerometer bias information. For this reason the accelerometer biases were set and not used as part of the optimization algorithm. Using the Air Data Model, it's possible to generate an accurate bias estimate and remove it from the preprocessed data if consistent. The results of the real flight data experiment are summarized in Table 13.

Parameter	Initial Estimate	Estimated Value	Offset
X CG Location Estimate	26.87311	24.8197	-2.05341
Y CG Location Estimate	0	0.1255	0.1255
Z CG Location Estimate	7.54072	7.8308	0.29008
N_x Bias	0	-	-
N_y Bias	0	-	-
N_z Bias	0	-	-

TABLE 13: ATTITUDE MODEL FLIGHT DATA RESULTS SUMMARY

The results of the algorithm indicate an expected result that the center-of-gravity location had moved forward from the previously estimated position. Once again, accelerometer biases were not estimated in the algorithm. Figure 62 displays the improvements in estimates throughout the optimization algorithm.

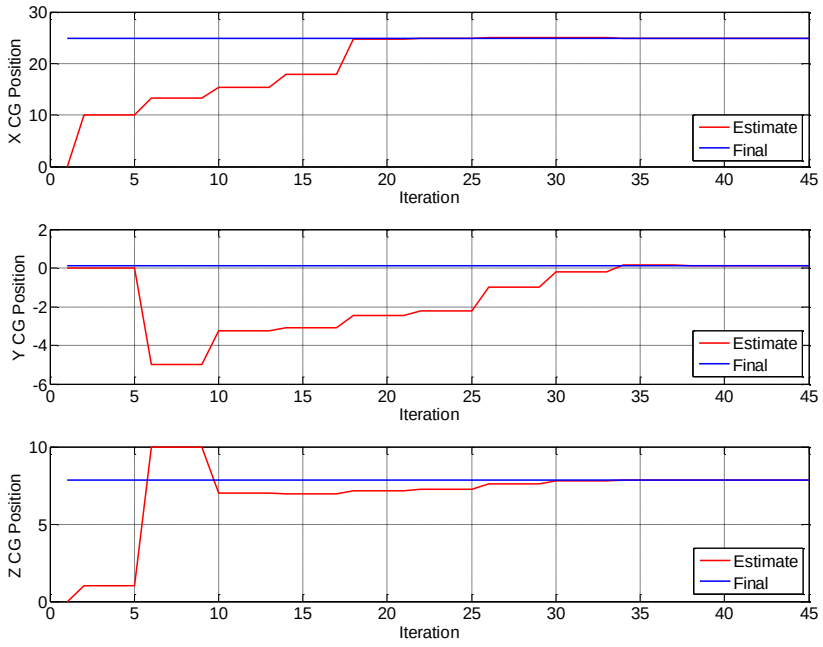

FIGURE 62: ATTITUDE MODEL FLIGHT DATA ITERATION IMPROVEMENT

The changes over iterations indicate a surprising quick conversion. To check the validity of the results, Fig. 63 and Fig. 64 show some critical estimated parameters and measurements where applicable.

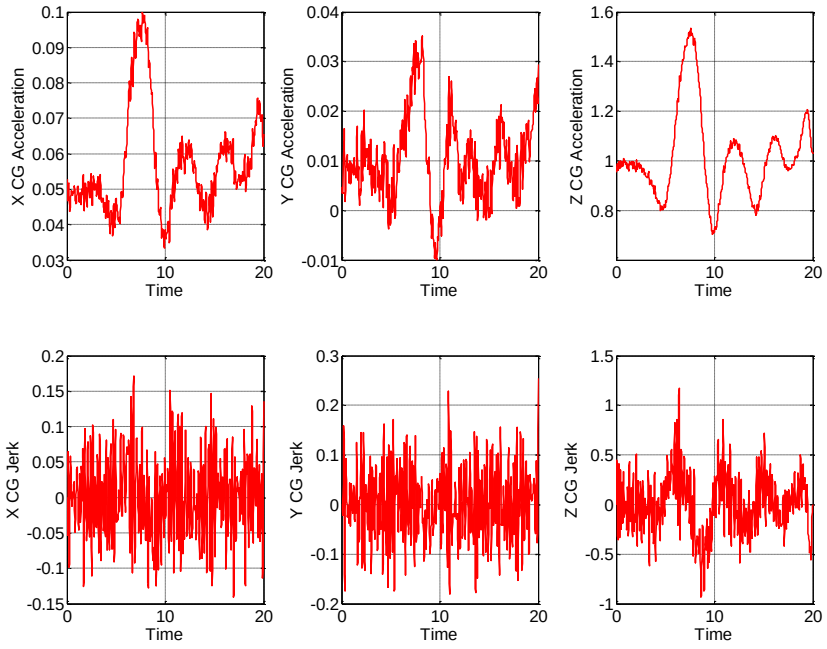

FIGURE 63: ATTITUDE MODEL FLIGHT DATA ACCELERATION AND JERK

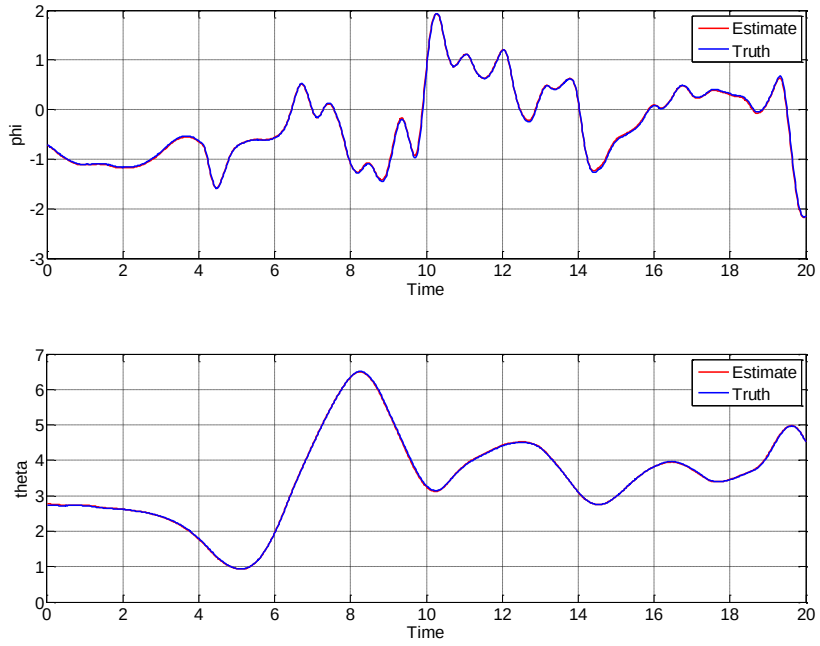

FIGURE 64: ATTITUDE MODEL FLIGHT DATA ATTITUDE COMPARISON

As expected the driving parameters of the Attitude Model, phi and theta, each indicate very good correlation to the measured values. The errors between these signals are the basic for the

cost function in the routine. Given the accuracy of the estimated parameters, the algorithm appears to have worked successfully.

5.2: Air Data Model Flight Data Results

The Air Data Model is the second algorithm programmed and incorporated for the available flight data. Identical flight data cuts were used so all aircraft responses are the same as shown in Fig. 58 through Fig. 61. Once again, an accurate center-of-gravity truth is not known for the vehicle under consideration. Table 14 shows the resulting estimates obtained from processing the flight data using the Air Data Model.

Parameter	Initial Estimate	Estimated Value	Offset
X CG Location Estimate	26.87311	23.3801	-3.49301
Y CG Location Estimate	0	0.1395	0.1395
Z CG Location Estimate	7.54072	7.2296	-0.31112
N_x Bias	0	0.0092	0.0092
N_y Bias	0	0.0016	0.0016
N_z Bias	0	0.0129	0.0129

TABLE 14: AIR DATA MODEL FLIGHT DATA RESULTS SUMMARY

The center-of-gravity location is determined to have moved forward in the plane by nearly 3.5 feet. The change is roughly the expected shift given the structural changes made since the previous center-of-gravity estimate, but slightly different from the Attitude Model estimate. On a positive note, each resulted in similar trends in center-of-gravity location changes. All the parameters estimated using the optimization routine fall well within expected values, including accelerometer biases which were small. The accelerometer biases are critical in the Air Data Model because of the algorithm dependence on the integral of related measurements. Figure 65 shown below shows the changes in center-of-gravity estimates throughout the routine.

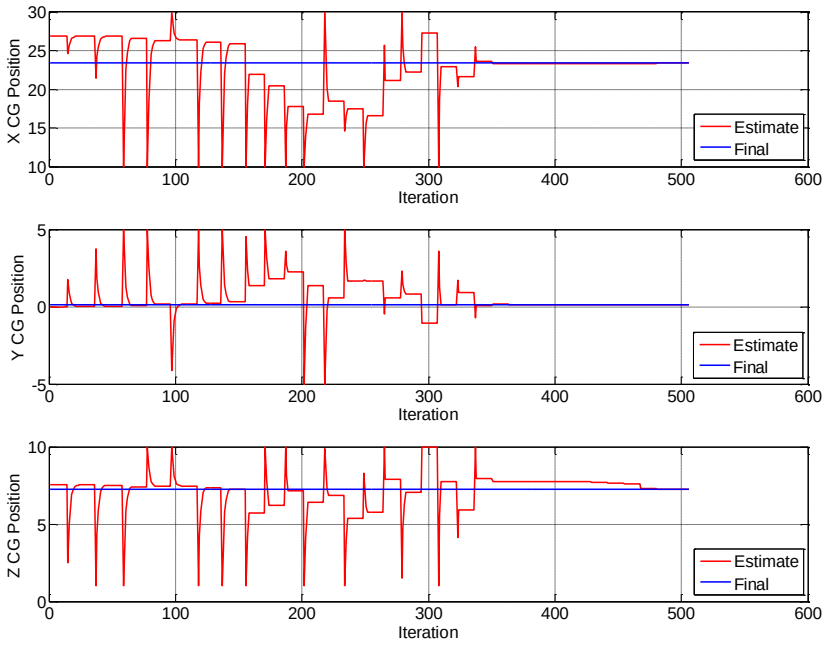

FIGURE 65: AIR DATA MODEL FLIGHT DATA ITERATION IMPROVEMENT

The plot shows the estimated positions with respect to the final estimated value. Figure 66 and Fig. 67 display key estimated parameters in the algorithm.

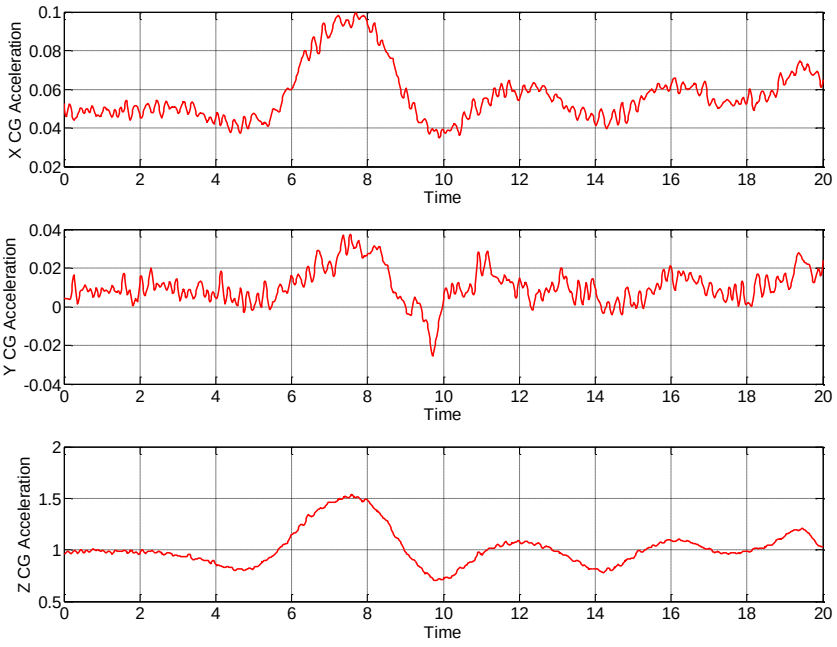

FIGURE 66: AIR DATA MODEL FLIGHT DATA ACCELERATION

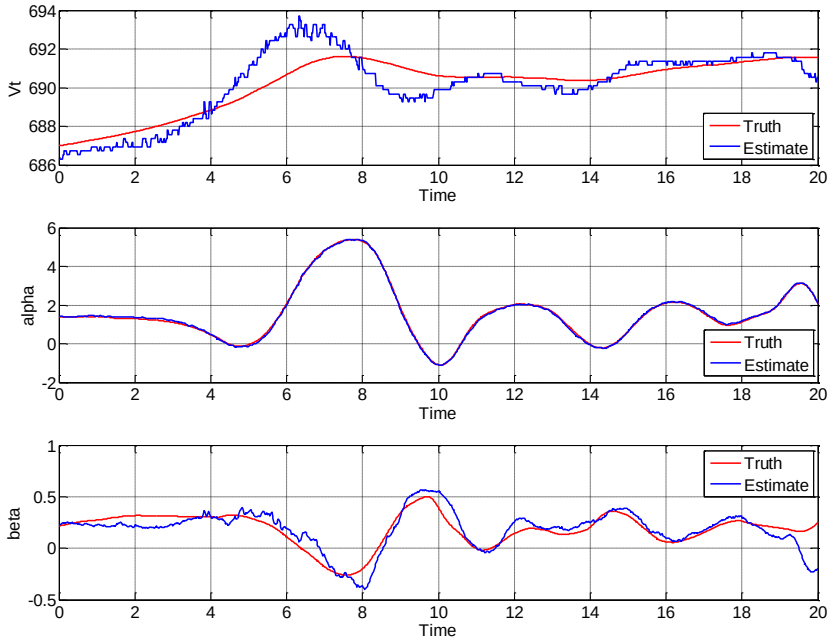

FIGURE 67: AIR DATA MODEL FLIGHT DATA AIR DATA COMPARISON

Each of the parameters incorporated in the algorithm display adequate correlation to the measurements where applicable.

5.3: Attitude and Air Data Model Flight Data Results

The Attitude Model and Air Data Model concepts were incorporated into the realistic flight data studies. The algorithm is incorporated into a modified code in Matlab® to process the available information. Proper weighting of the parameters included must be taken into heavy consideration. In any realistic application of the technology developed, it's expected that preliminary tuning of the weighting factors would be required before fully incorporating and trusting estimates produced by the algorithm. Overweighing certain parameters will cause the results to be driven by that particular measurement. Table 15 shows the results from analysis with the combined algorithm.

Parameter	Initial Estimate	Estimated Value	Offset
X CG Location Estimate	26.87311	23.3249	-3.54821
Y CG Location Estimate	0	0.145	0.145
Z CG Location Estimate	7.54072	7.869	0.32828
N_x Bias	0	0.0092	0.0092
N_y Bias	0	0.0016	0.0016
N_z Bias	0	0.0129	0.0129

TABLE 15: ATTITUDE AND AIR DATA MODEL FLIGHT DATA RESULTS SUMMARY

Here the center-of-gravity location is predicted to have shifted forward in the aircraft by roughly 3.5 feet. The shift is expected due to the noted changes made on the aircraft. No significant changes were seen in the y axis for center-of-gravity estimation, and very minor biases in accelerometers were estimated as expected. The results for processing the selected data appear successful. To further observe the performance, the step by step estimates from optimization are displayed in Fig. 68.

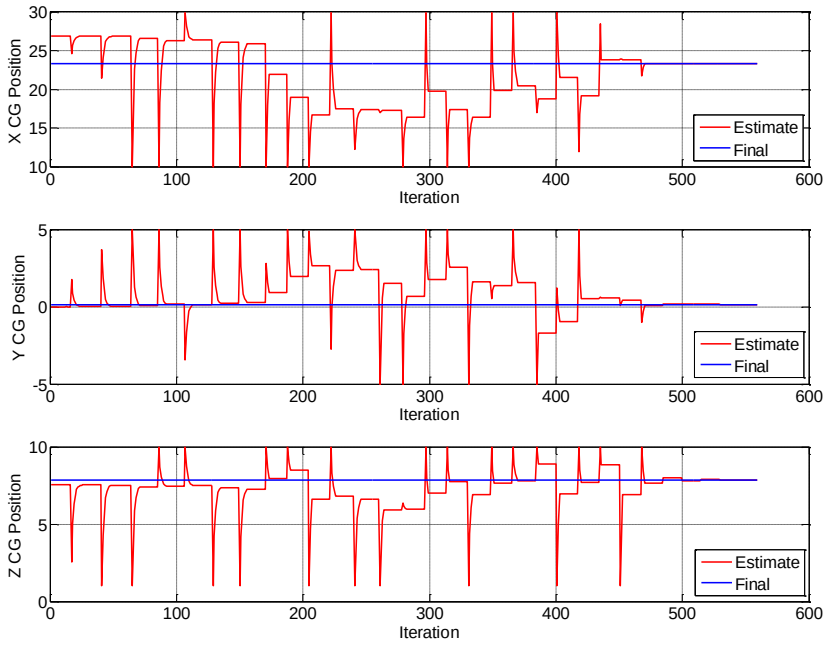

FIGURE 68: ATTITUDE MODEL FLIGHT DATA ITERATION IMPROVEMENT

Here the changes in center-of-gravity for each iteration are shown in correlation to the final estimated value. Again a significant increase in required iterations to reach a final solution is observed, expected from cases when multiple models are included with noisy realistic signals. The estimate improvement response is similar to that of the simulated results with chattering above and below the final value. Figure 69 through Fig. 71 show other aircraft parameters estimated compared to available sensors where available.

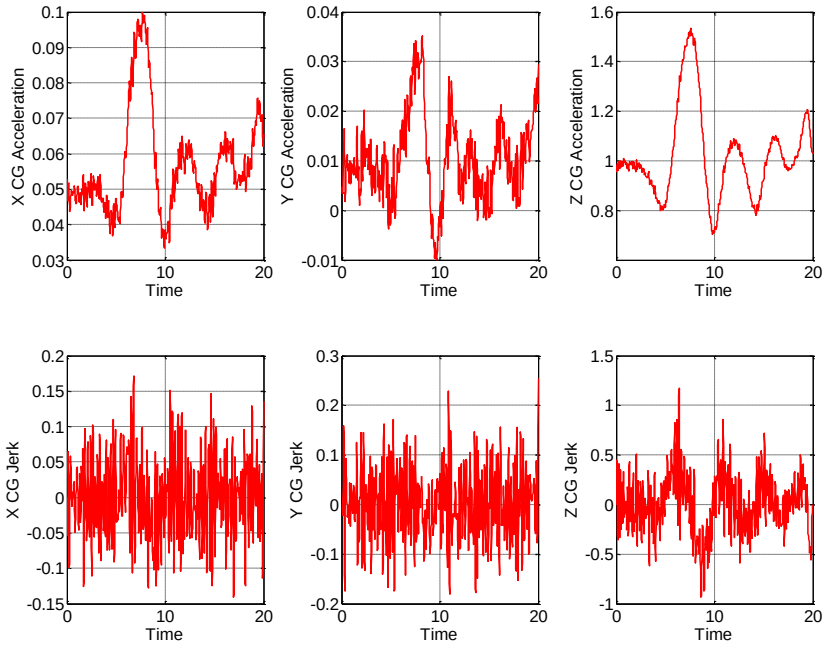

FIGURE 69: ATTITUDE MODEL FLIGHT DATA ACCELERATION RESULTS

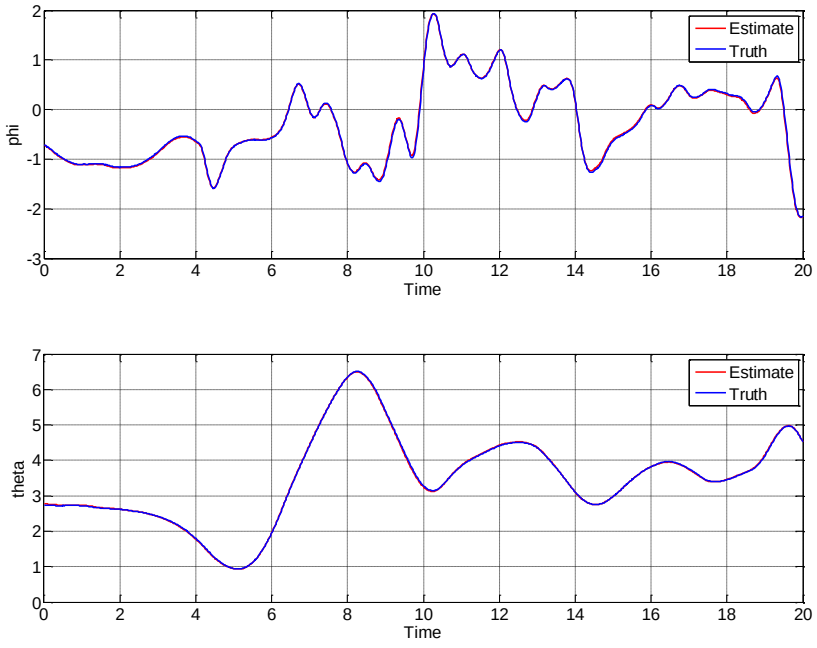

FIGURE 70: ATTITUDE MODEL FLIGHT DATA ATTITUDE COMPARISON

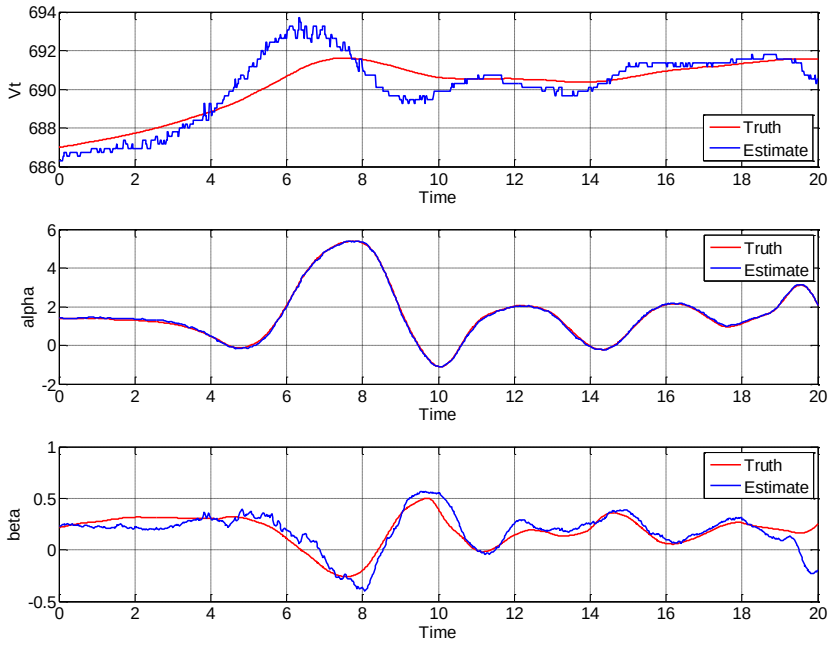

FIGURE 71: ATTITUDE MODEL FLIGHT DATA AIR DATA COMPARISON

As anticipated the estimated parameters and measurements show adequate correlation where applicable. The results from optimization are well within the expected range of potential estimates based on prior knowledge of the aircraft and the modifications made. Though a significant increase on computations is required with respect to the simulated cases, the combined algorithm successfully estimated the center-of-gravity.

5.4: Flight Data Results Comparison

It's difficult to quantify the most accurate approach to center-of-gravity estimation method without an accurate center-of-gravity location for the flight data processed. However because the different methods each reveal the similar locations and follow the expected trends it can be determined that the estimation techniques are accurate and successful. Table 16 compares the results of the three approaches incorporated with the available flight data.

Parameter	X CG Error	Y CG Error	Z CG Error	N_x Bias Error	N_y Bias Error	N_z Bias Error
Attitude Only	-2.05341	0.1255	0.29008	-	-	-
Air Data Only	-3.49301	0.1395	-0.31112	0.0092	0.0016	0.0129
Attitude and Air Data	-3.54821	0.145	0.32828	0.0092	0.0016	0.0129

TABLE 16: FLIGHT DATA RESULTS COMPARISON

Here a slight discrepancy between the Attitude Model and Air Data Model is observed. In this case, the most appropriate direction would be to lean towards the combined algorithm results. The combined algorithm allows for added repetition in measurements and can minimize errors caused by sensors with undetected biases of errors. When in doubt, adding as many models and signals to the cost function should allow for the minimization of effects from inaccurate signals.

CHAPTER 6: SUMMARY, CONCLUSIONS, AND FUTURE WORK

6.1: SUMMARY

In this work three approaches for estimating the center-of-gravity of an aircraft system were developed. These methods are an improvement over previous technology due to their independence from aerodynamic models of the vehicle and reduction of human error commonly introduced to center-of-gravity calculation. The new approach relied solely on traditional aircraft measurements and kinematic based models. The information obtained from the algorithm can be used to improve autopilot control and response, ensure safe loading conditions throughout flight, and reduce conservative calculations for frame fatigue predictions.

The technology and physics used can be applied to any rigid aircraft body over a given time interval in which the center-of-gravity location of the body is constant. Transformation of the sensory information including accelerometers and rate gyros to the estimated center-of-gravity and comparison with other available sensors allows refinement of center-of-gravity position. Three approaches including an Attitude Model, GPS and INS Model, and Air Data Model were developed. Measurements included attitude information, acceleration information, rate gyro information, air data quantities, and GPS and INS information. Using knowledge of acceleration conditions transformed to the center-of-gravity, kinematic relationships were formed to estimate predicted values of measurements that were compared to conditioned sensor measurements from the center-of-gravity location. Center-of-gravity location and sensor error parameters such as accelerometer biases were varied in an optimization scheme, minimizing a weighted cost function using a least squares method between sensor measurements and calculated parameter estimates. Realistic sensor noise, biases, and filters were included in an effort that simulated real-world measurement system effects. The algorithms were tested in a relevant simulation environment as well as using actual flight data for a high performance vehicle.

6.2: CONCLUSIONS

The Attitude Model developed here has proven feasible for center-of-gravity estimation through the simulations performed under various conditions. The Air Data Model and GPS and INS Model confirmed the functionality of the approaches used also through simulation. Each contained complete efforts to capture true conditions existent in real flight hardware. Combination of the models presented an algorithm fully capable of center-of-gravity estimation solely using traditionally available aircraft sensor systems currently available. The operation of the algorithm occurs in a batch process providing updates in non-real-time. The functionality of

the algorithm was confirmed through the processing of real flight data. Overall, the technology developed has proven to estimate center-of-gravity of an aircraft with a high degree of accuracy.

6.3: FUTURE WORK

The work performed here demonstrated the feasibility of using traditional aircraft sensor measurements to localize the center-of-gravity location. Both simulations and application with real flight data have resulted in accurate estimates of key parameters and center-of-gravity location. Improvements to the novel approach presented here can be made such as:

1. The Attitude Model can be further enhanced by including heading angle estimation in the weighted optimization cost function, to allow for determination of accelerometer biases and potentially improved center-of-gravity estimates. The heading angle parameter was not originally included in the algorithm.
2. Real-time estimation algorithms may be incorporated to update center-of-gravity locations for input to the control system, improving aircraft performance.
3. Incorporation of a gross weight estimator can be included in a similar manner, helping to reduce conservative estimates currently in place for fatigue calculations on airframes and additionally improving control system performance.
4. Although the feasibility of the algorithm was tested using actual flight data, the algorithm should be tested within an actual flight vehicle including hardware and software used for control of the aircraft.

WORKS CITED

[1]Cummins, J., Berning, A., Adams, D., and Sterkenburg, R., "Automated Estimation of an Aircraft's Center of Gravity Using Static and Dynamic Measurements," Proceedings of the IMAC-XXVII, February 9 – February 12, Orlando, Florida, 2009.

[2]Idan, M., Iosilevskii, G., and Nazarov, S., "In-Flight Weight and Balance Identification Using Neural Networks," Journal of Aircraft, Vol. 41, No. 1, pp. 137–143, 2004.

[3]Abraham, M., and Costello, M., "In-Flight Estimation of Helicopter Gross Weight and Mass Center Location," Journal of Aircraft, 46, pp. 1042-1049, 2009.

[4]Mack, R. J., "Rapid Empirical Method for Estimating the Gross Takeoff Weight of a High Speed Civil Transport," NASA TM-1999-209535, October, 1999.

[5]Nelson, N., *Flight Stability and Automatic Control*, The McGraw-Hill Companies, Inc., 1998.

[6]Crassidis, A, "Identification Update of Aerodynamic Models with Sensor Consistency Checks," AIAA Atmospheric Flight Mechanics Conference, August 16 – August 19, Providence, Rhode Island, 2004.

[7]Klein, V., and Schiess, J. R., "Compatibility Check of Measured Aircraft Responses Using Kinematic Equations and Extended Kalman Filter," NASA-TN-D-8514, Langley Research Center, Hampton, Virginia, 1977.

[8]Klein, V., and Morgan, D. R., "Estimation of Bias Errors in Measured Airplane Responses Using Maximum Likelihood Method," NASA TM-89059, Langley Research Center, Hampton, Virginia, 1987.

[9]Phillips, W., *Mechanics of Flight*, Second Edition, John Wiley and Sons, Inc., Hoboken, New Jersey, 2010.

[10]Schmidt, L., *Introduction to Aircraft Flight Dynamics*, American Institute of Aeronautics and Astronautics, Reston, Virginia, 1998.

[11]McRuer, D., Ashkenas, I., and Graham, D., *Aircraft Dynamics and Automatic Control*, Princeton University Press, Princeton, New Jersey, 1973.

[12]Hibbler, R., *Engineering Mechanics – Dynamics*, Twelfth Edition, Pearson Prentice Hall, Upper Saddle River, New Jersey, 2010.

[13]Gainer, T., and Hoffman, S., "Summary of Transformation Equations and Equations of Motion Used in Free Flight and Wind Tunnel Data Reduction and Analysis," NASA-SP-3070, NASA Langley Research Center, 1972.

[14]Weisman, R., "Robust Longitudinal Rate Gyro Bias Estimation for Reliable Pitch Attitude Observation through Utilization of a Displaced Accelerometer Array," Masters of Science in Mechanical Engineering, Rochester Institute of Technology, Rochester, New York, 2008.

[15]Scorse, W., “Two Dimensional Rate Gyro Bias Estimation for Precise Pitch and Roll Attitude Determination Utilizing a Dual Arc Accelerometer Array,” Masters of Science in Mechanical Engineering, Rochester Institute of Technology, Rochester, New York, 2011.

[16]Zimmerman, A., “State Estimation Filtering Algorithms for Vehicle Attitude Determination Using a Dual-Arc Accelerometer Array and 3-Axis Rate Gyroscopes,” Masters of Science in Mechanical Engineering, Rochester Institute of Technology, Rochester, New York, 2011.

[17]Gurbacki, P., “Feasibility Study of a Novel Method for Real-Time Aerodynamic Coefficient Estimation,” Masters of Science in Mechanical Engineering, Rochester Institute of Technology, Rochester, New York, 2010.

[18]Chheda, B., Crassidis, A., and Walter, W., "Attitude Estimation Using an Accelerometer and Rate Gyro Based Device," Proc. 2006 Atmospheric Flight Mechanics Conference, August 21 - August 24, Keystone, Colorado, pp. 659-669, 2006.

[19]Weisman, R., and Crassidis, A., "Longitudinal Rate Gyro Bias and Pitch Attitude Estimation Utilizing an Accelerometer Array," Proc. AIAA Atmospheric Flight Mechanics Conference, August 10 - August 13, Chicago, Illinois, 2009.

[20]Scorse, W., and Crassidis, A., “Two Dimensional Rate Gyro Bias Estimation for Precise Pitch and Roll Attitude Determination Utilizing a Dual Arc Accelerometer Array,” Proceedings of American Institute of Aeronautics and Astronautics Atmospheric Flight Mechanics Conference, August 2 – August 5, 2010.

[21]Crassidis, A., "A Light Weight, Mini Inertial Measurement System for Position and Attitude Estimation on Dynamic Platforms," Impact Technologies, LLC, 2010.

APPENDICES

APPENDIX A: CENTER-OF-GRAVITY ESTIMATION SIMULATION ALGORITHM

```
%Attitude CG Estimation Algorithm
%Flight Data
%Attitude Algorithm Only
%Komendat 8/12

clear, clc, close all, format compact

global cg_fs_est cg_bl_est cg_wl_est nx_bias_est ny_bias_est nz_bias_est
i_opt CG_opt n_bias_opt
global use_att_data use_air_data use_INS_GPS_data

%Define constants
d2r=pi/180;
r2d=180/pi;
g=32.172;     %ft/sec

%Initialize counter for storing of cg movement in optimization
i_opt=1;

%Flag for simulation data used
sim_data_flag=1;      %=1, use large input manuever data; =2, use small input
manuever data

%Scaling for for initial guesses of cg location
CG_sf_X0=1.0;

%Choose estimation
use_att_data=0;        %=1, turn on attitude model; =0, turn off attitude
model
use_INS_GPS_data=0;    %=1, turn on GPS/INS model; =0, turn off GPS/INS model
use_air_data=1;        %=1, turn on airdata model; =0, turn off airdata model

%Load simulated data
if( sim_data_flag<1.5 )
    load pitch_roll_sin_input_data %(large input) this is on the one I
normally used
else
    load pitch_roll_sin_input_data1 %(small input)
end

%CG estimator switch
CG_estimator_flag=1;   %=1, estimate CG; =0, turn off CG estimators

%Plot results flag
plot_results_flag=1;   %=1, plot results; =0, do not plot results

%Define signals for accelerometer signals
acc_flag=3; %=1, use upper signals; =2, use lower signals; =3, use pilot
station
```

```
aoa_flag=2; %=1, use right sensor; =2, use left sensor; =3, use cf signal
aos_flag=2; %=1, use lower sensor; =2, use upper sensor; =3, use cf signal

%Convert signals
pdot=pdot*r2d;
qdot=qdot*r2d;
rdot=rdot*r2d;

%Define IC's
Vt_0     = Vt(1);
alpha_0  = alpha(1)*d2r;
beta_0   = beta(1)*d2r;
nx_imp0  = 0;
ny_imp0  = 0;
nz_imp0  = 0;

%Define airdata IN model parameters
Vt_m_0     = 0;
Vt_m_sf    = 1;
Vt_b       = 0;
alpha_m_0  = 0;
alpha_m_sf = 1;
alpha_b    = 0;
beta_m_0   = 0;
beta_m_sf  = 1;
beta_b     = 0;

%Define start, end time and step time
t0=0;
tf=time(length(time));tf=10;
dt=time(2)-time(1);

%Determine accel parameters
pdotdot=der_filt(time,pdot);
qdotdot=der_filt(time,qdot);
rdotdot=der_filt(time,rdot);
jx_cg=der_filt(time,nx_cg);
jy_cg=der_filt(time,ny_cg);
jz_cg=der_filt(time,nz_cg);

%Define cg location truth
cg_fs=26.8731159420290;    %cg fusalage station (ft)
cg_bl=0.0;                 %cg buttline station (ft)
cg_wl=7.54072463768116;    %cg waterline station (ft)

%Define initial cg location estimates for optimization
cg_fs_est=20*CG_sf_X0;    %cg fusalage station (ft)
cg_bl_est=1;                          %cg buttline station (ft)
cg_wl_est=5*CG_sf_X0;    %cg waterline station (ft)

%Define sensor locations
if( acc_flag<1.5 )
    n_m_fs=326.5*in2ft;    %upper accels fusalage station (ft)
    n_m_bl=9.86*in2ft;     %upper accels buttline station (ft)
    n_m_wl=121.75*in2ft;   %upper accels waterline station (ft)
```

```
elseif( acc_flag<2.5 )
    n_m_fs=319.3*in2ft;     %lower accels fusalage station (ft)
    n_m_bl=1.92*in2ft;      %lower accels buttline station (ft)
    n_m_wl=68.99*in2ft;     %lower accels waterline station (ft)
elseif( acc_flag<3.5 )
    n_m_fs=152.6*in2ft;     %pilot station accels fusalage station (ft)
    n_m_bl=4.9*in2ft;       %pilot station accels buttline station (ft)
    n_m_wl=88.86*in2ft;     %pilot station accels waterline station (ft)
else
    n_m_fs=cg_fs;           %cg accels fusalage station (ft)
    n_m_bl=cg_bl;           %cg accels buttline station (ft)
    n_m_wl=cg_wl;           %cg accels waterline station (ft)
end
if( aoa_flag<1.5 )
    alpha_m_fs=59.7*in2ft;    %right angle-of-attack fusalage station (ft)
    alpha_m_bl=20.00*in2ft;   %right angle-of-attack buttline station (ft)
    alpha_m_wl=89.39*in2ft;   %right angle-of-attack waterline station (ft)
elseif( aoa_flag<2.5 )
    alpha_m_fs=59.7*in2ft;    %left angle-of-attack fusalage station (ft)
    alpha_m_bl=-20.00*in2ft;  %left angle-of-attack buttline station (ft)
    alpha_m_wl=89.39*in2ft;   %left angle-of-attack waterline station (ft)
else
    alpha_m_fs=cg_fs;         %cg angle-of-attack fusalage station (ft)
    alpha_m_bl=cg_bl;         %cg angle-of-attack buttline station (ft)
    alpha_m_wl=cg_wl;         %cg angle-of-attack waterline station (ft)
end
if( aos_flag<1.5 )
    beta_m_fs=68.7*in2ft;     %lower sideslip fusalage station (ft)
    beta_m_bl=0.0*in2ft;      %lower sideslip buttline station (ft)
    beta_m_wl=79.14*in2ft;    %lower sideslip waterline station (ft)
elseif( aos_flag<2.5 )
    beta_m_fs=69.17*in2ft;    %upper sideslip fusalage station (ft)
    beta_m_bl=0.0*in2ft;      %upper sideslip buttline station (ft)
    beta_m_wl=104.2*in2ft;    %upper sideslip waterline station (ft)
else
    beta_m_fs=cg_fs;          %cg asideslip fusalage station (ft)
    beta_m_bl=cg_bl;          %cg sideslip buttline station (ft)
    beta_m_wl=cg_wl;          %cg sideslip waterline station (ft)
end
Vt_m_fs=-10.0*in2ft;          %true velocity fusalage station (ft)
Vt_m_bl=0.0*in2ft;            %true velocity buttline station (ft)
Vt_m_wl=81.16*in2ft;          %true velocity waterline station (ft)

%Define simulated truth biases for the accelerometers
nx_bias_truth=0.03;
ny_bias_truth=0.03;
nz_bias_truth=0.03;

%Define initial guess of biases for the accelerometers
if( (use_att_data>0.5) && (use_air_data<0.5) && (use_INS_GPS_data<0.5) )
    nx_bias_est=nx_bias_truth;
    ny_bias_est=ny_bias_truth;
    nz_bias_est=nz_bias_truth;
else
    nx_bias_est=nx_bias_truth+0.01;
    ny_bias_est=ny_bias_truth+0.01;
```

```
    nz_bias_est=nz_bias_truth+0.01;
end

%Define optimization IC
if( (use_att_data>0.5) && (use_air_data<0.5) && (use_INS_GPS_data<0.5) )
    x0=[cg_fs_est cg_bl_est cg_wl_est];
else
    x0=[cg_fs_est cg_bl_est cg_wl_est nx_bias_est ny_bias_est nz_bias_est];
end


%Determine first values for stored optimization parameters
CG_opt(i_opt,1)=cg_fs_est;
CG_opt(i_opt,2)=cg_bl_est;
CG_opt(i_opt,3)=cg_wl_est;
n_bias_opt(i_opt,1)=nx_bias_est;
n_bias_opt(i_opt,2)=ny_bias_est;
n_bias_opt(i_opt,3)=nz_bias_est;

%Butterworth filter design for filter derivative of INS lat/long signal
%Used for autoland CLAW
%Comp filter time constant for GPS/INS filter
%[b_der_GPS_INS_filter,a_der_GPS_INS_filter]=butter(4,0.5);     %discrete
filter
[b_der_GPS_INS_filter,a_der_GPS_INS_filter]=butter(4,100,'low','s');
%continuous domain
tau_comp_filter_GPS_INS=1;

%x=fminsearch('cg_localizer_jerk_terms_xyzest_f',x0)
if( CG_estimator_flag>0.5 )
    if( (use_att_data>0.5) && (use_air_data<0.5) && (use_INS_GPS_data<0.5) )
        par_upp=[ 35  2  15];
        par_low=[ 10 -2   2];
    else
        par_upp=[ 35  2  15  0.1  0.1  0.1];
        par_low=[ 10 -2   2 -0.1 -0.1 -0.1];
    end
    options=optimset('Algorithm','active-set','TolFun',1e-10,'TolCon',1e-10);

x=fmincon('cg_localizer_jerk_terms_xyzest_f',x0,[],[],[],[],par_low,par_upp,[
],options) %use this one!
end


sim('cg_localizer_jerk_terms_xyzest_s')

%End algorithm
```

APPENDIX B: CENTER-OF-GRAVITY ESTIMATION SIMULATION COST FUNCTION

```
function J=cg_localizer_jerk_terms_xyzest_f(x)

global cg_fs_est cg_bl_est cg_wl_est nx_bias_est ny_bias_est nz_bias_est
i_opt CG_opt n_bias_opt
global use_att_data use_air_data use_INS_GPS_data

%Increment index for recording estimates
i_opt=i_opt+1;

%Update estimates
if( (use_att_data>0.5) && (use_air_data<0.5) && (use_INS_GPS_data<0.5) )
    cg_fs_est=abs(x(1));
    cg_bl_est=abs(x(2));
    cg_wl_est=abs(x(3));
else
    cg_fs_est=abs(x(1));
    cg_bl_est=abs(x(2));
    cg_wl_est=abs(x(3));
    nx_bias_est=x(4);
    ny_bias_est=x(5);
    nz_bias_est=x(6);
end


%Record updated estimates
CG_opt(i_opt,1)=cg_fs_est;
CG_opt(i_opt,2)=cg_bl_est;
CG_opt(i_opt,3)=cg_wl_est;
n_bias_opt(i_opt,1)=nx_bias_est;
n_bias_opt(i_opt,2)=ny_bias_est;
n_bias_opt(i_opt,3)=nz_bias_est;

%Call attitude, airdata, and GPS/INS modelss
[tout,xout,yout]=sim('cg_localizer_jerk_terms_xyzest_s');

%Define square errors for cost
theta_err=(yout(:,2)-yout(:,1)).^2;
phi_err=(yout(:,4)-yout(:,3)).^2;
xe_err=(yout(:,6)-yout(:,5)).^2;
ye_err=(yout(:,8)-yout(:,7)).^2;
ze_err=(yout(:,10)-yout(:,9)).^2;
xedot_err=(yout(:,12)-yout(:,11)).^2;
yedot_err=(yout(:,14)-yout(:,13)).^2;
zedot_err=(yout(:,16)-yout(:,15)).^2;
Vt_err=(yout(:,18)-yout(:,17)).^2;
alpha_err=(yout(:,20)-yout(:,19)).^2;
beta_err=(yout(:,22)-yout(:,21)).^2;

%Define cost
if( (use_att_data>0.5) && (use_air_data<0.5) && (use_INS_GPS_data<0.5) )
    J=trapz( use_att_data*(10*theta_err+2*phi_err) )*0.01
else
    J=trapz( use_att_data*(0.02*theta_err+0.0001*phi_err)...
```

```
+use_INS_GPS_data*(xe_err+ye_err+ze_err+xedot_err+yedot_err+zedot_err)...
             +use_air_data*(Vt_err+100*alpha_err+100*beta_err) )*0.01
end
x
end
```

APPENDIX C: CENTER-OF-GRAVITY ESTIMATION SIMULATION SIMULINK® DIAGRAMS

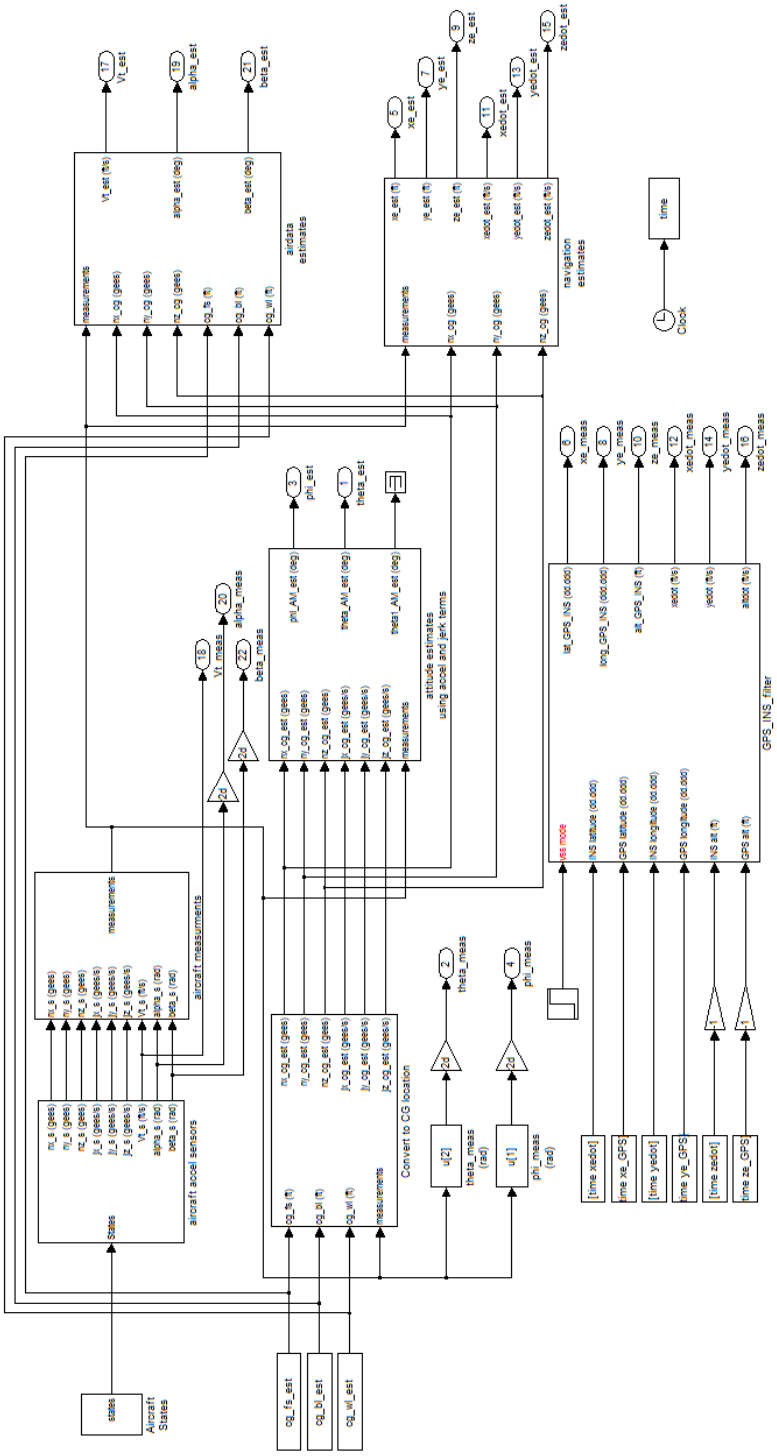

FIGURE 72: ESTIMATION ALGORITHM SIMULINK® DIAGRAM

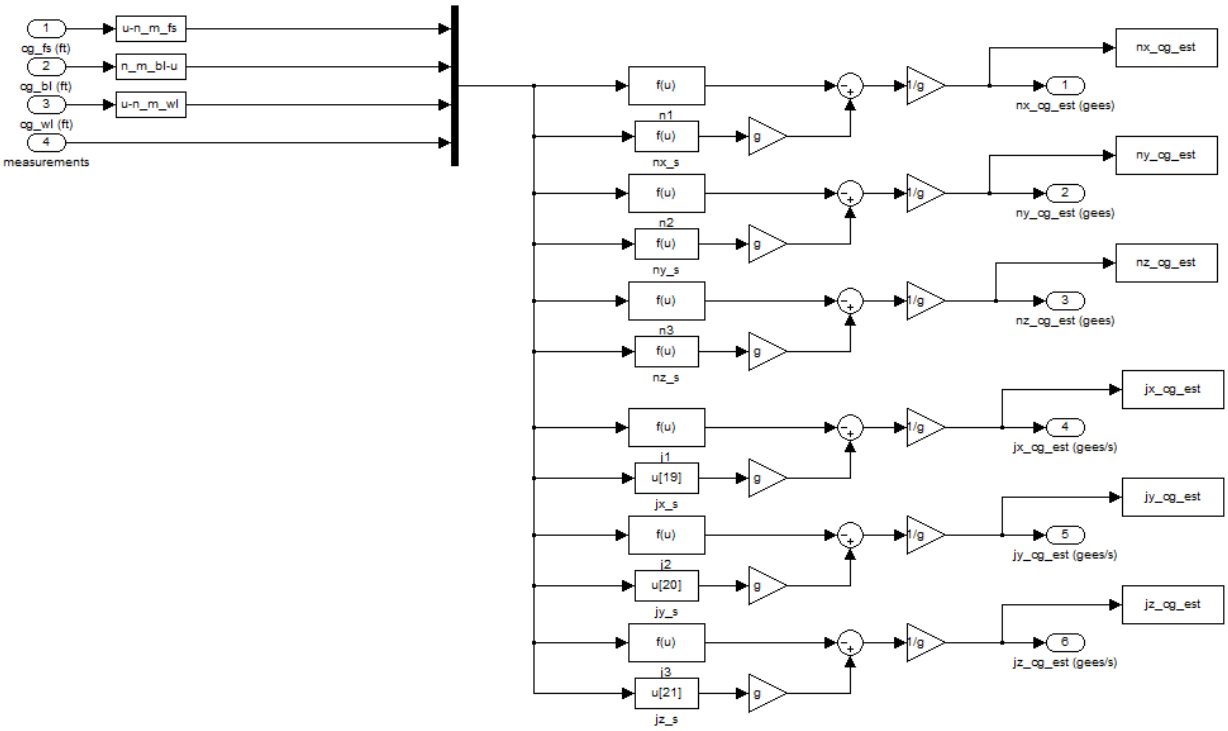

FIGURE 73: CONVERT TO CENTER-OF-GRAVITY LOCATION

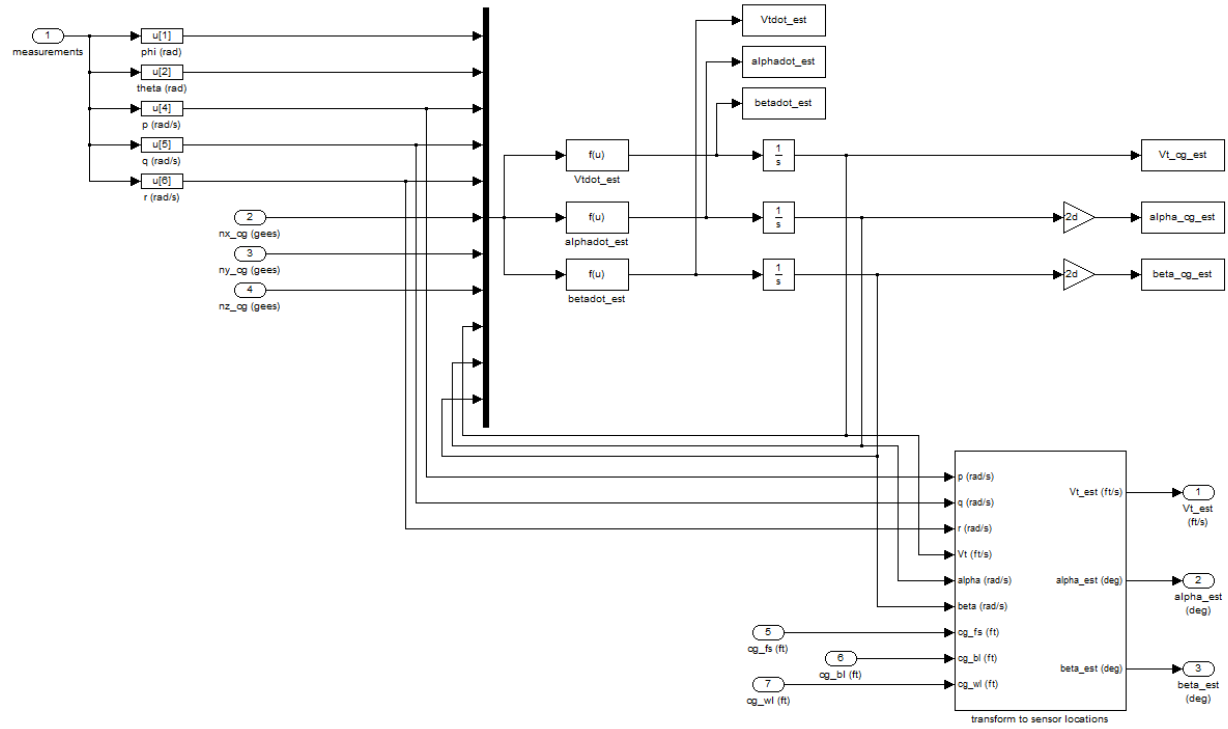

FIGURE 74: AIR DATA PARAMETER ESTIMATION

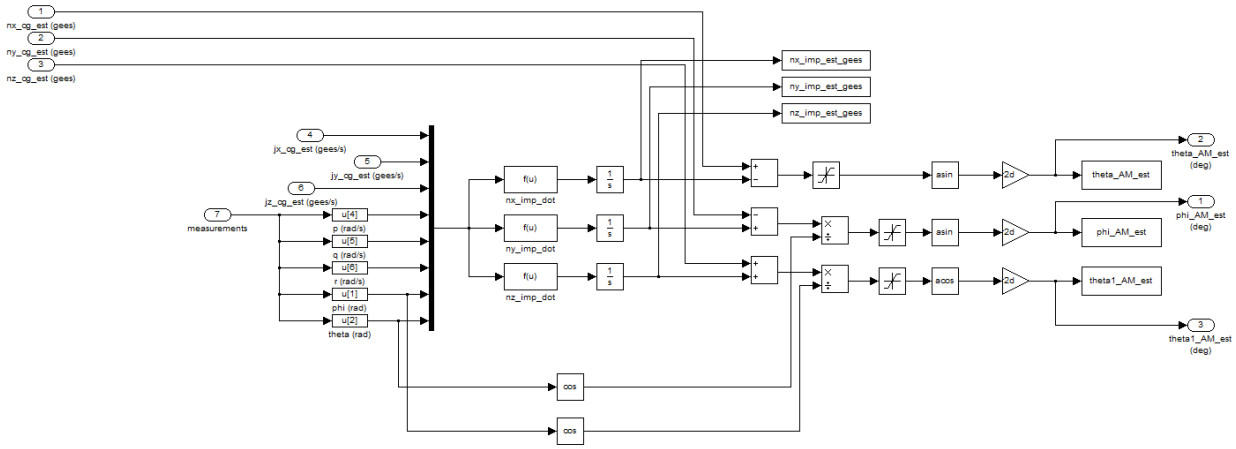

FIGURE 75: ATTITUDE PARAMETER ESTIMATION

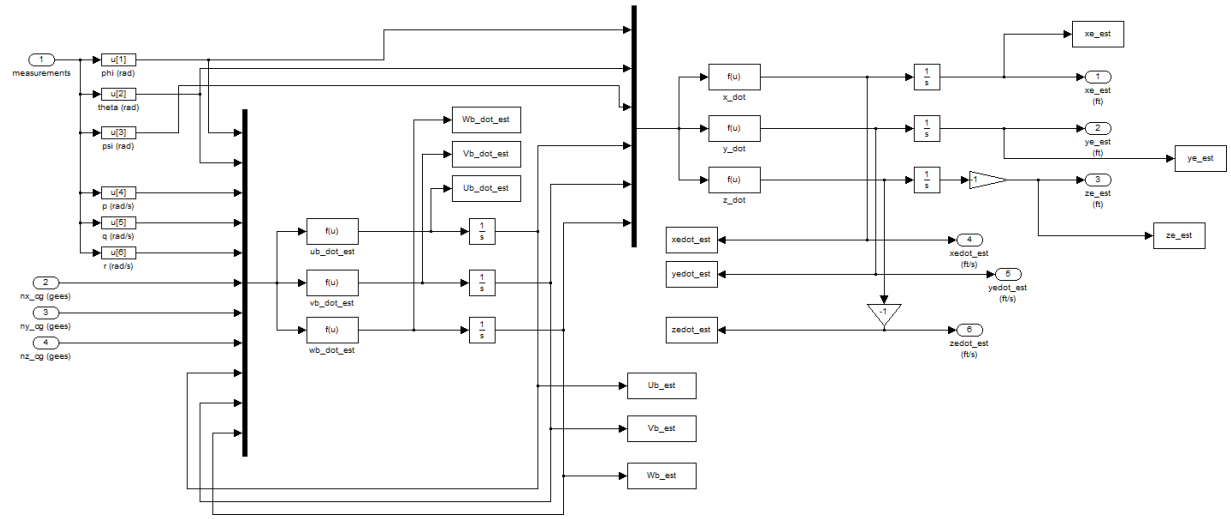

FIGURE 76: NAVIGATION PARAMETER ESTIMATION

APPENDIX D: CENTER-OF-GRAVITY ESTIMATION FLIGHT DATA ALGORITHM

```
%Combined CG Estimation Algorithm
%Flight Data
%Combined Attitude and Attitude Algorithm Only
%Komendat 8/12

clear, clc, close all, format compact, format short e

global dt Vt_0 alpha_0 beta_0 nx_bias_est ny_bias_est nz_bias_est
global Vt_m_sf alpha_m_sf beta_m_sf
global cg_fs cg_bl cg_wl i_opt CG_opt
global nx_imp0 ny_imp0

%Define constants
d2r=pi/180;
r2d=180/pi;
in2ft=1/12;
g=32.172;

%Use phi, theta, p, q, and r or EULER states
use_EULER_states_flag=1;      % =0, use measurements; =1, use EULER states

%Kinematic model estimator switch
CG_estimator_flag=1;          % =0, turn off estimators; =1, estimate CG
estimator_flag=0;             % =0, use constrained estimator; =1, use
inconstrained algorithm

load VISTA_data_r01_slice

%Define dt, intial and final simulation time
dt=time_m(2)-time_m(1);    %(sec)
t0=0;                      %(sec)
tf=time_m(length(time_m)); %(sec)

%Define measurement initial conditions
p_m_0=p_m(1)*d2r;
q_m_0=q_m(1)*d2r;
r_m_0=r_m(1)*d2r;
phi_m_0=phi_m(1)*d2r;
theta_m_0=theta_m(1)*d2r;
psi_m_0=psi_m(1)*d2r;
Vt_m_0=Vt_m(1);
alpha_m_0=alpha_m(1)*d2r;
beta_m_0=beta_m(1)*d2r;

%Define cg location
cg_fs=26.8731159420290;    %cg fusalage station (ft)
cg_bl=0.0;                 %cg buttline station (ft)
cg_wl=7.54072463768116;    %cg waterline station (ft)

%Define sensor locations
if( acc_flag<1.5 )
    n_m_fs=326.5*in2ft;    %upper accels fusalage station (ft)
    n_m_bl=9.86*in2ft;     %upper accels buttline station (ft)
```

```
    n_m_wl=121.75*in2ft;    %upper accels waterline station (ft)
elseif( acc_flag<2.5 )
    n_m_fs=319.3*in2ft;     %lower accels fusalage station (ft)
    n_m_bl=1.92*in2ft;      %lower accels buttline station (ft)
    n_m_wl=68.99*in2ft;     %lower accels waterline station (ft)
elseif( acc_flag<3.5 )
    n_m_fs=152.6*in2ft;     %pilot station accels fusalage station (ft)
    n_m_bl=4.9*in2ft;       %pilot station accels buttline station (ft)
    n_m_wl=88.86*in2ft;     %pilot station accels waterline station (ft)
else
    n_m_fs=cg_fs;           %cg accels fusalage station (ft)
    n_m_bl=cg_bl;           %cg accels buttline station (ft)
    n_m_wl=cg_wl;           %cg accels waterline station (ft)
end
if( aoa_flag<1.5 )
    alpha_m_fs=59.7*in2ft;    %right angle-of-attack fusalage station (ft)
    alpha_m_bl=20.00*in2ft;   %right angle-of-attack buttline station (ft)
    alpha_m_wl=89.39*in2ft;   %right angle-of-attack waterline station (ft)
elseif( aoa_flag<2.5 )
    alpha_m_fs=59.7*in2ft;    %left angle-of-attack fusalage station (ft)
    alpha_m_bl=-20.00*in2ft;  %left angle-of-attack buttline station (ft)
    alpha_m_wl=89.39*in2ft;   %left angle-of-attack waterline station (ft)
else
    alpha_m_fs=cg_fs;         %cg angle-of-attack fusalage station (ft)
    alpha_m_bl=cg_bl;         %cg angle-of-attack buttline station (ft)
    alpha_m_wl=cg_wl;         %cg angle-of-attack waterline station (ft)
end
if( aos_flag<1.5 )
    beta_m_fs=68.7*in2ft;     %lower sideslip fusalage station (ft)
    beta_m_bl=0.0*in2ft;      %lower sideslip buttline station (ft)
    beta_m_wl=79.14*in2ft;    %lower sideslip waterline station (ft)
elseif( aos_flag<2.5 )
    beta_m_fs=69.17*in2ft;    %upper sideslip fusalage station (ft)
    beta_m_bl=0.0*in2ft;      %upper sideslip buttline station (ft)
    beta_m_wl=104.2*in2ft;    %upper sideslip waterline station (ft)
else
    beta_m_fs=cg_fs;          %cg asideslip fusalage station (ft)
    beta_m_bl=cg_bl;          %cg sideslip buttline station (ft)
    beta_m_wl=cg_wl;          %cg sideslip waterline station (ft)
end
Vt_m_fs=-10.0*in2ft;          %true velocity fusalage station (ft)
Vt_m_bl=0.0*in2ft;            %true velocity buttline station (ft)
Vt_m_wl=81.16*in2ft;          %true velocity waterline station (ft)

%Define state initial conditions
load VISTA_data_r01_slice_EULER_run
nx_imp0= 0.0217;
ny_imp0=-0.0052;
nz_imp0= 0.0;
Vt_0=0;
alpha_0=0;
beta_0=0;
nx_bias_est=0;
ny_bias_est=0;
nz_bias_est=0;
Vt_b=0;
alpha_b=0.0;
```

```
beta_b=0.0;
Vt_m_sf=1;
alpha_m_sf=1/0.54;
beta_m_sf=1;
x0=[Vt_0 alpha_0 beta_0 nx_bias_est ny_bias_est nz_bias_est Vt_m_sf
alpha_m_sf beta_m_sf cg_fs cg_bl cg_wl nx_imp0 ny_imp0];

%Define upper and lower bounds of parameters
par_upp=[ 10  2  2  0.5  0.5  0.5 3.0 3.0 3.0 30  5  10  0.05  0.05];
par_low=[-10 -2 -2 -0.5 -0.5 -0.5 0.5 0.5 0.5 10 -5   1 -0.05 -0.05];

%Start estimation
i_opt=1;
CG_opt(i_opt,1)=cg_fs;
CG_opt(i_opt,2)=cg_bl;
CG_opt(i_opt,3)=cg_wl;
if( CG_estimator_flag>0.5 )
    if( estimator_flag<0.5 )
        options=optimset('Algorithm','active-set');
        x=fmincon('cg_estimator_f',x0,[],[],[],[],par_low,par_upp,[],options)
%use this one!
    else
        x=fminsearch('cg_estimator_f',x0)
    end
end
sim('cg_estimator_s')

%End algorithm
```

APPENDIX E: CENTER-OF-GRAVITY ESTIMATION FLIGHT DATA COST FUNCTION

```
function J=cg_estimator_f(x)

global dt Vt_0 alpha_0 beta_0 nx_bias_est ny_bias_est nz_bias_est
global Vt_m_sf alpha_m_sf beta_m_sf
global cg_fs cg_bl cg_wl i_opt CG_opt
global nx_imp0 ny_imp0

%Increment index for recording estimates
i_opt=i_opt+1;

%Update estimates
Vt_0        = x(1);
alpha_0     = x(2);
beta_0      = x(3);
nx_bias_est = x(4);
ny_bias_est = x(5);
nz_bias_est = x(6);
Vt_m_sf     = x(7);
alpha_m_sf  = x(8);
beta_m_sf   = x(9);
cg_fs       = x(10);
cg_bl       = x(11);
cg_wl       = x(12);
nx_imp0     = x(13);
ny_imp0     = x(14);

%Record updated estimates
CG_opt(i_opt,1)=cg_fs;
CG_opt(i_opt,2)=cg_bl;
CG_opt(i_opt,3)=cg_wl;

%Call kinematic model
[tout,xout,yout]=sim('cg_estimator_s');

%Define square errors for cost
phi_AM_err=(yout(:,20)-yout(:,19)).^2;
theta_AM_err=(yout(:,22)-yout(:,21)).^2;
Vt_err=(yout(:,14)-yout(:,13)).^2;
alpha_err=(yout(:,16)-yout(:,15)).^2;
beta_err=(yout(:,18)-yout(:,17)).^2;

%Define weighting functions
phi_AM_w=0.2;
theta_AM_w=1;
Vt_w=0.1;
alpha_w=50;
beta_w=260;

%Define cost
J=trapz( phi_AM_w*phi_AM_err + theta_AM_w*theta_AM_err +
Vt_w*Vt_err+alpha_w*alpha_err+beta_w*beta_err )*dt
```

APPENDIX F: CENTER-OF-GRAVITY ESTIMATION FLIGHT DATA SIMULINK® DIAGRAMS

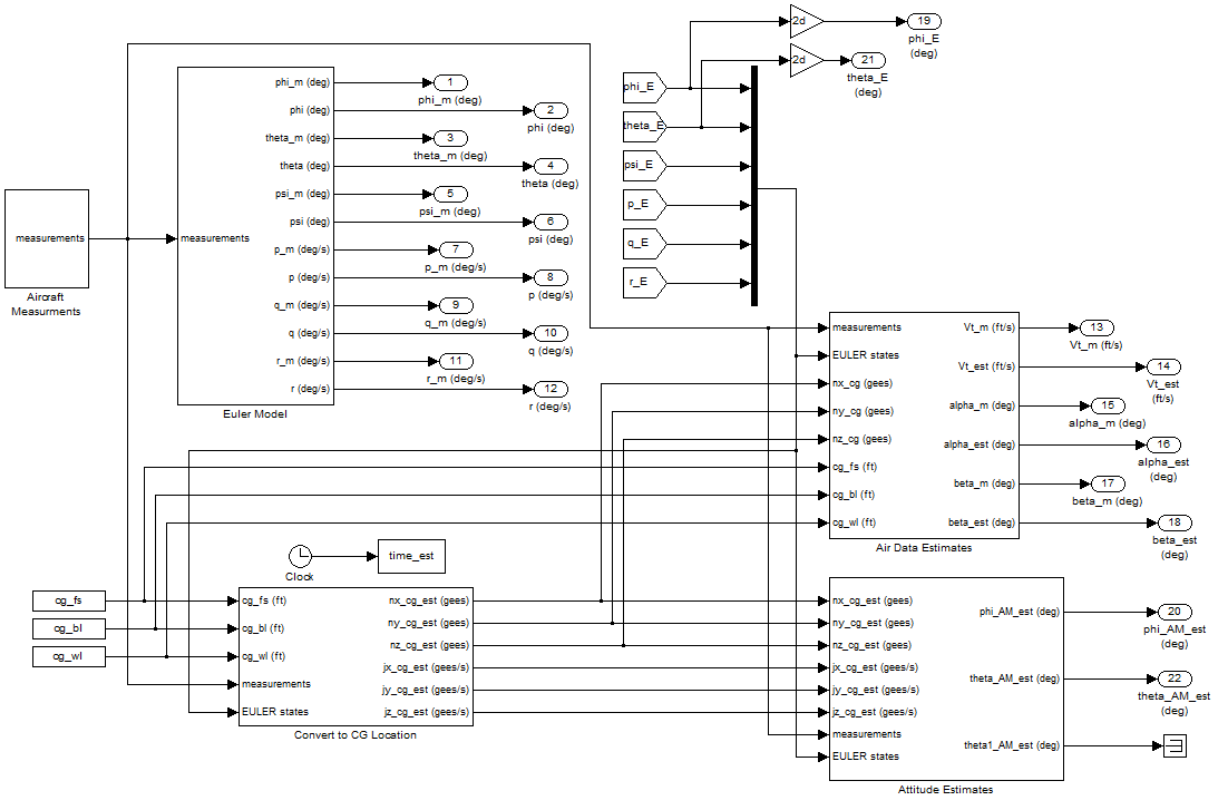

FIGURE 77: CENTER-OF-GRAVITY ESTIMATION SIMULINK® DIAGRAM

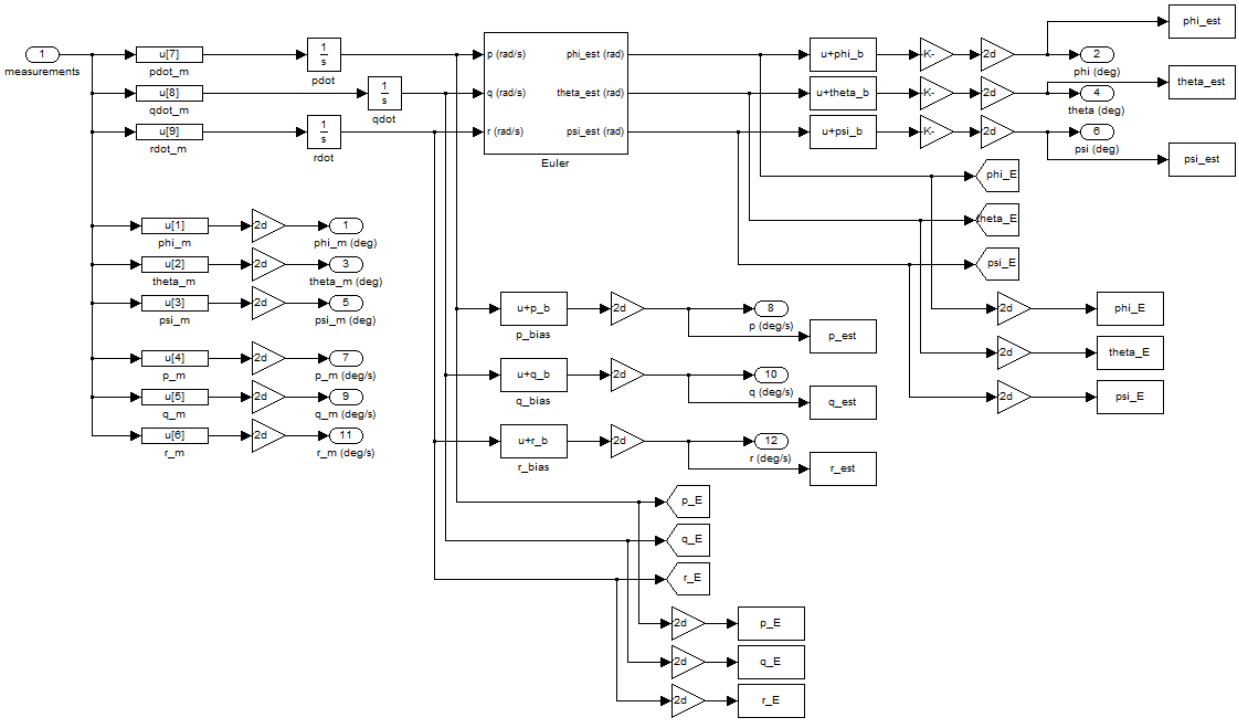

FIGURE 78: EULER MODEL